



HAL
open science

Mechanical performances of PEKK thermoplastic composites linked to their processing parameters

Tanguy Choupin

► **To cite this version:**

Tanguy Choupin. Mechanical performances of PEKK thermoplastic composites linked to their processing parameters. Mécanique des matériaux [physics.class-ph]. Ecole nationale supérieure d'arts et métiers - ENSAM, 2017. Français. NNT: 2017ENAM0043 . tel-01882121

HAL Id: tel-01882121

<https://pastel.hal.science/tel-01882121v1>

Submitted on 26 Sep 2018

HAL is a multi-disciplinary open access archive for the deposit and dissemination of scientific research documents, whether they are published or not. The documents may come from teaching and research institutions in France or abroad, or from public or private research centers.

L'archive ouverte pluridisciplinaire **HAL**, est destinée au dépôt et à la diffusion de documents scientifiques de niveau recherche, publiés ou non, émanant des établissements d'enseignement et de recherche français ou étrangers, des laboratoires publics ou privés.

École doctorale n° 432 : Sciences des Métiers de l'ingénieur

Doctorat ParisTech

THÈSE

pour obtenir le grade de docteur délivré par

l'École Nationale Supérieure d'Arts et Métiers

Spécialité “ Mécanique et Matériaux ”

présentée et soutenue publiquement par

Tanguy CHOUPIN

le 7 décembre 2017

Mechanical performances of PEKK thermoplastic composites linked to their processing parameters

Directeur de thèse : **Bruno FAYOLLE**
Co-encadrement de la thèse : **Gilles RÉGNIER**

Jury

M. Nicolas BOYARD, CNRS Researcher, Polytech Nantes
M. René FULCHIRON, Associate Professor, Université Claude Bernard
M. Philippe OLIVIER, Professor, Institut Clément Ader
Mme Ewa PIORKOWSKA, Professor, CMMS Poland
M. Jacques CINQUIN, Research Engineer, Airbus
M. Christophe PARIS, Research Engineer, Airbus Operations
M. Gilles RÉGNIER, Professor, Arts et Métiers ParisTech
M. Bruno FAYOLLE, Professor, Arts et Métiers ParisTech

Rapporteur
Rapporteur
Président
Examinateur
Examinateur
Examinateur
Examinateur
Examinateur

**T
H
È
S
E**

REMERCIEMENTS

J'ai eu beaucoup de liberté pendant cette thèse, mes 4 encadrants m'ont toujours fait confiance et je les en remercie beaucoup pour ça, c'est ce qui m'a donné confiance en moi tout au long de la thèse.

Merci à mon équipe encadrante du côté d'Airbus.

Christophe merci de m'avoir accueilli pour mon stage de fin d'étude chez Airbus et de m'avoir fait confiance pour continuer en thèse. Tu as toujours été disponible pour corriger mes rapports, présentations etc. même après ton départ chez Airbus à Toulouse.

Jacques, j'ai pu apprendre beaucoup avec toi concernant les composites, c'est aussi grâce à toi que j'ai pu continuer en thèse et je t'en remercie.

Didier Filleul de m'avoir accueilli dans ton équipe et Didier Lang de m'avoir fait prendre du recul sur ma thèse, sur le pourquoi de cette thèse et ce qu'on voulait montrer.

Du côté du PIMM, j'ai eu des managers assez différents !

Bruno la force tranquille. C'est déjà grâce à toi que j'ai eu mon stage chez Airbus. A la fin d'un cours tu nous avais annoncé en passant « à la Bruno »: « Oui il y a un petit stage disponible chez Airbus, si ça intéresse quelqu'un ». Je me suis bien sûr jeté sur l'occasion ! Tu es ensuite devenu mon maître de stage puis mon directeur de thèse. Tu es la personne qui a été la plus présente durant cette thèse, ta qualité principale est que tu es très humain et à l'écoute. Tu as été là pour toutes les étapes de la thèse, d'un grand soutien psychologique et tu es également devenu un ami. Tu es celui qui a aussi subi le plus de repet !

Gilles la force énergétique. J'ai une grande admiration pour toi. On a eu beaucoup de réunions dans ton bureau à parler de notre passion commune la cristallisation ! Je sortais en ayant compris la moitié de notre conversation avec souvent tout à modifier de ce que j'avais fait. De nombreuses fois je me disais bon là on ne va pas y arriver, je ne sais pas comment faire, ça ne marche pas et tu m'as toujours poussé pour aller plus loin et grâce à ça on a pu développer des beaux modèles de cristallisation !

J'aimerais aussi remercier l'équipe d'Arkema qui a suivi la thèse de très près.

Jérôme, que j'ai rencontré pour la première fois sur le stand d'Arkema au salon composite JEC, j'étais assez impressionné il y avait beaucoup de monde mais je voulais parler avec toi du PEKK ! On a enfin parlé de tout l'historique du PEKK et comment il était arrivé dans les mains d'Arkema. C'est un très bon souvenir pour moi.

Benoît, tu as toujours été disponible pour répondre à mes questions et tu as toujours été là pour mes présentations d'avancement de thèse et pour corriger mes divers livrables.

Henri Alexandre, qui m'a accueilli au CERDATO pour fabriquer mes premières plaques composites, je me rappelle encore de mon excitation à la fabrication de la première !

Je remercie également mes 2 stagiaires, Louis et Romain, c'était un réel plaisir de travailler avec vous, vous m'avez permis de sortir le nez de ce que je faisais et regarder d'autres aspects de mon sujet. C'est grâce à vous deux qu'une grosse partie des essais mécaniques

a été faite. Je remercie aussi les 4 PFE ENSAM qui m'ont également aidé à développer la partie mécanique de la thèse.

Je remercie les techniciens du PIMM, Paulo, Gaëlle, Anne, Alain et d'Airbus Group Innovation à Suresnes notamment Pascal Nef et Alain Renoncourt.

Mes collègues du PIMM : Sara et Fatima mes collègues de bureau qui m'ont supporté 3 ans ! Maxime Sagnard, Nicolas Gay, Justine, Sébastien.

Mes collègues chez Airbus : Basile et Pierre, Tanguy Bize, Thibaut, Marco, Alain Mesinele, Fernand, François Marie, Christian Lardière, Ana Isabel, Patrick, Isabelle, François

Je finis par remercier les deux femmes de ma vie :

Maman, même si je sais qu'Arthur me dirait qu'au festival de Cannes on a l'interdiction de remercier ses parents. Je voulais t'exprimer l'admiration que j'ai pour toi. Tu es mon inspiration dans ton travail et dans ta vie personnelle. Tu as toujours été d'un grand soutien pour tes trois enfants, toujours derrière nous à nous faire confiance. C'est en grande partie grâce à toi que je suis là.

Samira, nous nous sommes rencontrés grâce au PIMM, cette thèse est associée à beaucoup de bons souvenirs avec toi, tu m'as apporté beaucoup de sérénité durant les moments difficiles et je t'en remercie.

TABLE OF CONTENTS

TABLE OF CONTENTS..... 1

INTRODUCTION 3

Industrial Context..... 3

Objectives 4

1. MATERIALS..... 7

1.1 Prepregs..... 7

1.2 PEKK matrices..... 8

 1.2.1 PAEK polymer family 8

 1.2.2 PEKK copolymers..... 10

 1.2.3 Crystalline morphology 13

 1.2.4 Secondary crystallization..... 16

 1.2.5 Nucleation and growth..... 17

1.3 Conclusion..... 18

2. IMPACT OF THERMAL CYCLES ON PEKK MATRICES MECHANICAL PROPERTIES..... 19

2.1 Experimental..... 19

 2.1.1 Differential Scanning Calorimetry (DSC) 19

 2.1.2 Wide angle X-ray diffraction..... 20

 2.1.3 Optical microscopy..... 20

 2.1.4 Mechanical tests 20

2.2 Crystalline morphologies 23

 2.2.1 Crystalline structure 23

 2.2.2 Nucleation and growth..... 23

2.3 Crystallization kinetics 25

 2.3.1 Crystallization kinetic comparison 25

 2.3.2 Isothermal crystallization kinetics..... 27

 2.3.3 Non-isothermal crystallization kinetics 43

2.4 Influence of crystallization on The matrix mechanical properties 50

 2.4.1 Crystallinity measurement of PEKK plates 50

 2.4.2 Influence of crystallinity on PEKK matrix mechanical properties..... 51

 2.4.3 Influence of crystalline morphologies on PEKK 6002 mechanical properties 56

2.5 Conclusion..... 58

3. IMPACT OF TIME/TEMPERATURE PARAMETERS ON THE PROCESSING WINDOW..... 61

3.1 Experimental..... 61

 3.1.1 Thermo-Gravimetric Analysis (TGA)..... 61

 3.1.2 Rheological measurements 61

 3.1.3 Differential Scanning Calorimetry (DSC) 61

 3.1.4 Gel Permeation Chromatography (GPC) 62

 3.1.5 Mechanical tests 62

3.2	Macromolecular modification mechanisms	62
3.3	Crosslinking kinetics	63
3.3.1	Weight changes	63
3.3.2	Gel Permeation Chromatography (GPC) analysis	65
3.3.3	Rheological analysis.....	67
3.3.4	DSC measurements	75
3.4	Crosslinking kinetics Modelling	76
3.5	Impact of macromolecular changes on crystallization kinetics.....	79
3.5.1	Crystallization peak analysis.....	79
3.5.2	Modification of the Hillier crystallization kinetic parameters.....	81
3.6	Impact of macromolecular changes on mechanical properties	83
3.7	Conclusion.....	85
4.	<i>APPLICATION TO PEKK STRUCTURAL COMPOSITES</i>	<i>87</i>
4.1	Experimental	87
4.1.1	Differential Scanning Calorimetry (DSC)	87
4.1.2	Optical microscopy	87
4.1.3	Scanning Electron Microscope (SEM).....	88
4.1.4	Composite manufacturing processes	88
4.1.5	Tensile tests.....	88
4.2	PEKK prepregs	90
4.3	Impact of carbon fibers on crystallization	91
4.3.1	Impact of carbon fibers on crystalline morphologies.....	91
4.3.2	Impact of carbon fibers on crystallization kinetics.....	92
4.4	PEKK COMPOSITE MANUFACTURING	98
4.4.1	Protocol	98
4.4.2	Composite plates quality control	100
4.4.3	DSC analysis.....	101
4.5	Mechanical properties of PEKK composites	101
4.5.1	Unidirectional composites	101
4.5.2	$\pm 45^\circ$ composites	102
4.6	Conclusion.....	106
	<i>CONCLUSION AND PROSPECTS</i>	<i>109</i>
	<i>REFERENCES</i>	<i>113</i>
	<i>RÉSUMÉ ÉTENDU</i>	<i>119</i>
	<i>ABSTRACT.....</i>	<i>136</i>

INTRODUCTION

INDUSTRIAL CONTEXT

The aeronautic industry uses more and more composite materials to lighten its structures and enhance their performances. This weight saving also allows the aeronautic industry to limit their environmental impact by significantly decreasing aircraft kerosene consuming and consequently decreasing greenhouse gases emissions such as CO₂ and NO_x. Nowadays, composite materials constitute more than 50% of the latest generation civil aircraft structure weight (Airbus A350 and Boeing B787).



Fig. 1: Airbus A350 XWB with more than 50% by weight of composite in the structure

Even if most of those composite materials are thermosetting composites, the use of thermoplastic composites is gaining ground due to many benefits. In fact, they have good damage tolerance, they are weldable, recyclable, they are especially suitable for automated fiber placement and they can be consolidated out of autoclave. Those two last features would help to increase the aircraft production rate which is currently a major issue for aircraft manufacturers.

Among those thermoplastics, Poly Aryl Ether Ketone (PAEK) polymer family would be the best candidate as matrix for composite structural parts. Indeed, they have high temperature performances, high chemical and oxidation resistance. The most well-known thermoplastic belonging to the PAEK family is PEEK which is already used as matrix for composite structural parts as for the A400M cockpit floor consolidated out of autoclave and produced by Daher Company. However, this material is still much expensive than epoxy resins and its processing is made difficult by the high melting temperature (around 400°C) leading to high processing times and costs and potential degradation of the matrix during processing.

In this industrial context, new range of high performance thermoplastics PAEK matrices have been recently developed such as Arkema PEKK KEPSTAN™. PEKK are nowadays much studied in the aircraft industry to compete with PEEK as matrix for composite structural parts. Indeed, for equivalent mechanical performances, PEKK matrices have lower processing temperatures (around 360°C) simplifying the manufacturing of composite parts.

OBJECTIVES

The final mechanical performances of composite parts are closely linked to their processing. In fact, depending on the thermal processing cycle, the matrix properties as well as the interaction between the matrix and the carbon fibres are modified. The first composite manufacturing part step is the consolidation associated to the heating of the composite part above the matrix melting temperature to obtain a viscosity decrease of the matrix in order to evacuate all porosities under pressure. As PEKK melting temperature remains above 300°C, the matrix could be modified or degraded during this step and the final mechanical performances of the composite part could be thus potentially altered [1,2]. Secondly, after the consolidation step, the composite part is cooled down to the room temperature. During this step, the matrix may crystallize with different crystallinity ratio and crystalline morphologies depending on the cooling conditions which could also impact the final mechanical performances of the composite part [3–8]. This is why, those phenomena must be understood and controlled to be able to predict and then optimize processing parameters regarding composite parts mechanical performances and processing times.

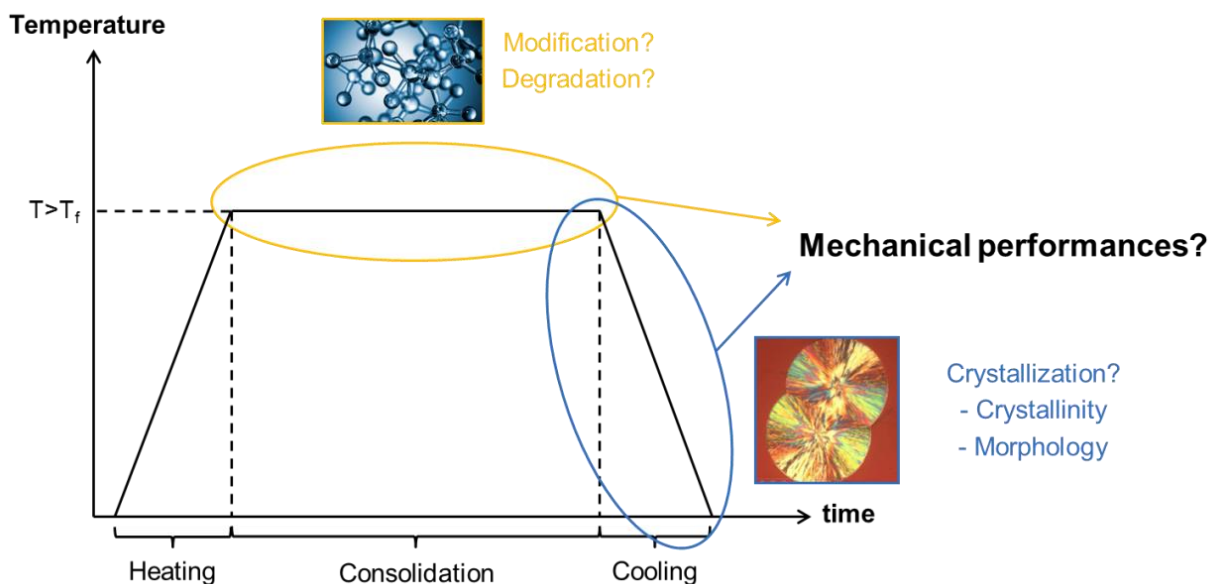


Fig. 2: Processing thermal cycle of a thermoplastic composite part

In collaboration with the PIMM laboratory of Arts et Métiers ParisTech and the material provider Arkema, Airbus Group Innovations (AGI) aims to explore the capacities of those new high performances thermoplastic PEKK composites for the manufacturing of aeronautical structural parts. To answer to this problematic, the manuscript is divided in four chapters:

This first chapter deals with a bibliographic review on the studied materials in the Phd. The main properties of the tape preregs used for the composite manufacturing as well as carbon fiber reinforcements and PEKK matrices used in the preregs are presented.

The second chapter investigates the crystallization kinetics modelling of PEKK matrices and the influence of crystallinity and crystalline morphologies on PEKK matrix mechanical properties.

The third chapter focuses on the macromolecular modifications of PEKK matrices at high processing temperatures under nitrogen and their impact on PEKK matrices crystallization and mechanical properties.

The last chapter presents the influence of carbon fibers on crystalline morphologies and crystallization kinetics, the manufacturing of unidirectional and $\pm 45^\circ$ PEKK composites under press and autoclave and finally the impact of crystallinity and crystalline morphologies on PEKK composite mechanical properties.

CHAPTER I. MATERIALS

This first chapter deals with a bibliographic review on the studied materials. It is introduced the main properties of the provided tape preregs used for the composite manufacturing and their impregnation way, the main properties of carbon fibers used for the preregs manufacturing, the chemical structure of PEKK copolymers matrices, their thermal properties and finally their crystalline behaviors.

I.1 PREPREGS

Composite materials were provided for the project as unidirectional tape preregs of 50 mm width and 140 μm thick with 60% by volume of carbon fiber and 40% by volume of PEKK matrix.

Carbon fibers used for manufacturing unidirectional tape preregs are high strength non-sized HexTow[®] AS4 carbon fiber provided by Hexcel. AS4 carbon fibers are continuous high strength, high strain, PAN based fiber with 12,000 (12K) filament count tows. Main properties from the product data sheet are listed in Table I.1.

Density ($\text{g}\cdot\text{cm}^{-3}$)	Tensile Modulus (GPa)	Tensile Strength (MPa)	Strain at Break (%)
1.79	231	4,413	1,7

Table I.1 : Properties of Hexcel AS4 12K carbon fibers

Two different tapes were studied, PEKK 6002 and PEKK 7002 preregs. Data taken from the control certificate of tapes provided by the material supplier are summarized in Table I.2. Details for PEKK matrices are presented in paragraph I.2 respectively. From those data different characteristics were calculated as the matrix mass content which is necessary for the calculation of the crystallinity of the matrix in the preregs, the matrix and the fiber area weight and the theoretical ply thickness which can give information of the quality of the composite after consolidation. In fact, if the average of the ply thickness in the composite after consolidation is higher than the theoretical value, this could be due to some porosities trapped in the composite, which will be discussed later by microscopic observations.

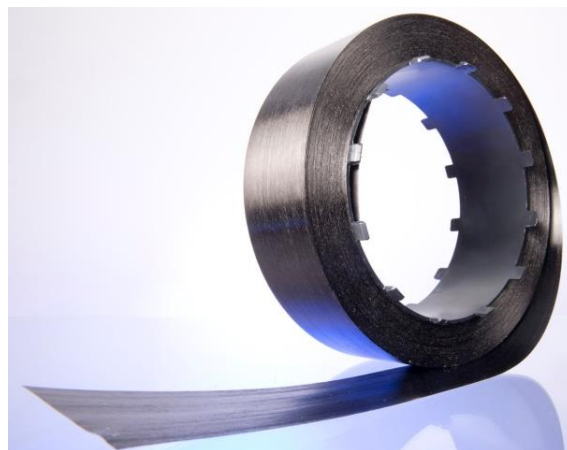


Fig. I.1 : Roll of PEKK tape preregs

Carbon fibers were impregnated with PEKK by passing them through a bath where PEKK powder is suspended. Carbon fiber tows are then heated up to melt the PEKK polymer and calendared at the dimension of the tape.

Data	PEKK 6002 preregs	PEKK 7002 preregs
Matrix density (g.cm ⁻³)	1,27	1,29
Fiber density (g.cm ⁻³)	1,79	
Fiber volume content (%)	60	
Preregs surface mass (g.m ⁻²)	228,2	230,3
Theoretical calculations		
Matrix mass content (%)	32,11	32,45
Matrix area weight (g.m ⁻²)	73,29	74,74
Fiber area weight (g.m ⁻²)	154,95	155,56
Ply thickness (μm)	144,3	144,8

Table I.2 : Properties of PEKK preregs tapes

I.2 PEKK MATRICES

I.2.1 PAEK polymer family

PAEK are semi-crystalline thermoplastic polymers made from ether and ketone molecules (Fig. I.2):

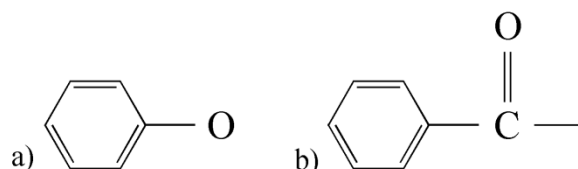


Fig. I.2 : Ether a) and ketone b) molecules

With a high glass transition temperature (Table I.4) and a high modulus and strength at yield (Table I.5), PAEK matrices have the best thermo-mechanical properties among existing thermoplastics (Fig. I.3):

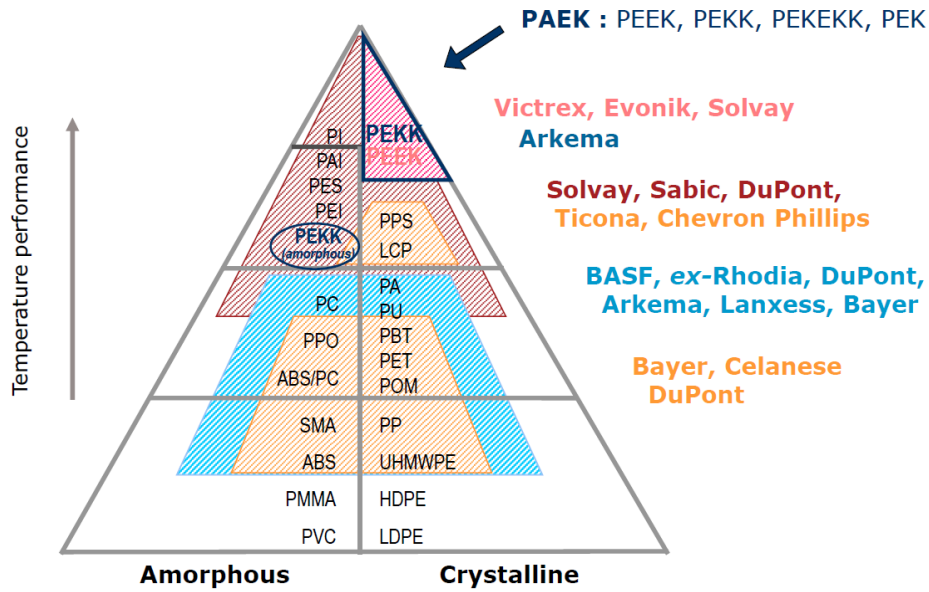


Fig. I.3 : Classification of thermoplastic polymers as a function of their thermo-mechanical properties [9]

PAEK are different from each other depending on the number of ether and ketone molecules of their monomer (Table I.3):

Structure	Name	Ketone (%)
	PPO	0
	PEK	50
	PEEK	33
	PEKK	67

Table I.3 : Chemical structure of different PAEK with their ratio of ketone entities [10]

The influence of ketone entities on PAEK properties has been studied by different authors [11–14]. They showed that the melting temperature (T_m) and the glass transition temperature (T_g) increase with the ratio of ketone entities (Fig. I.4). In fact, ketone bonds are less flexible than ether one which increases the macromolecular chains rigidity and thus T_g . They also increase the compactness of the crystalline structure which increases the intermolecular energy bonds and thus melting temperature T_m .

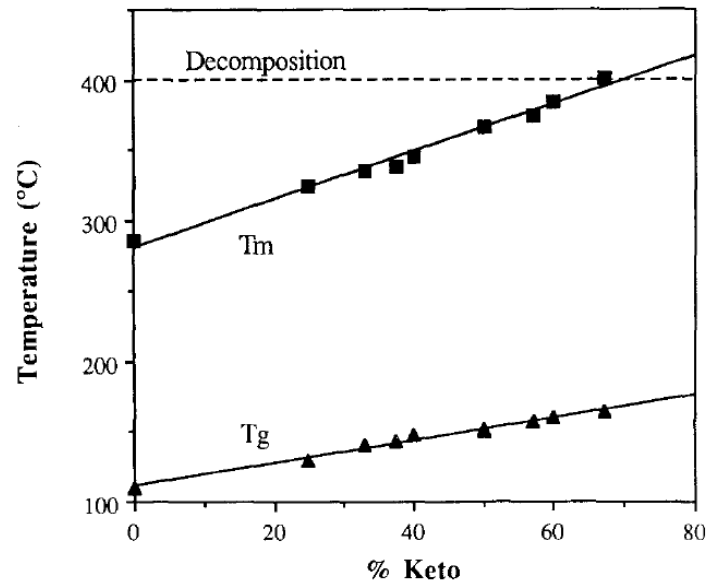


Fig. I.4 : Evolution of T_g and T_m as a function of the ketone ratio [10]

The PEKK homopolymer has the highest ratio of ketone entities (% Keto=67%) and thus the highest T_g and T_m . Its T_g is very interesting for high temperature applications (below T_g) however its T_m involves high processing temperatures which could lead to degradation during composite parts manufacturing. To address this problem, PEKK chemical structure can be modified to decrease its T_m [10].

I.2.2 PEKK copolymers

The PEKK homopolymer is prepared from diphenyl ether (DPE) and terephthalic acid (T) (Fig. I.5.a). Terephthalic acid (T) with para phenyl links can be substituted by isophthalic acid (I) with meta phenyl links (Fig. I.5.b) and form copolymers constituted with two different isomers, the terephthaloyle (Fig. I.5.a) and the isophthaloyle isomers (Fig. I.5.b). Those isomers can form two different diads, the TT diads compounded by two terephthaloyle isomers (Fig. I.6.a) and the TI diads compounded by one terephthaloyle isomer and one isophthaloyle isomer (Fig. I.6.b). The introduction of isophthaloyle isomers decreases the T_m (Fig. I.7) which makes PEKK very interesting for composite parts manufacturing.

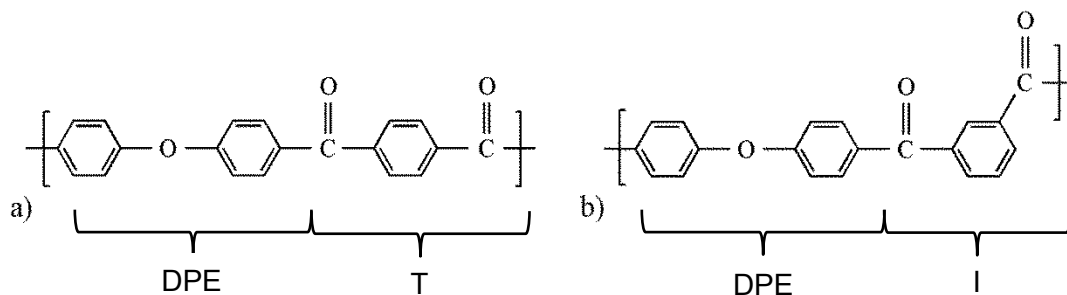


Fig. I.5 : PEKK terephthaloyle a) and isophthaloyle b) isomers

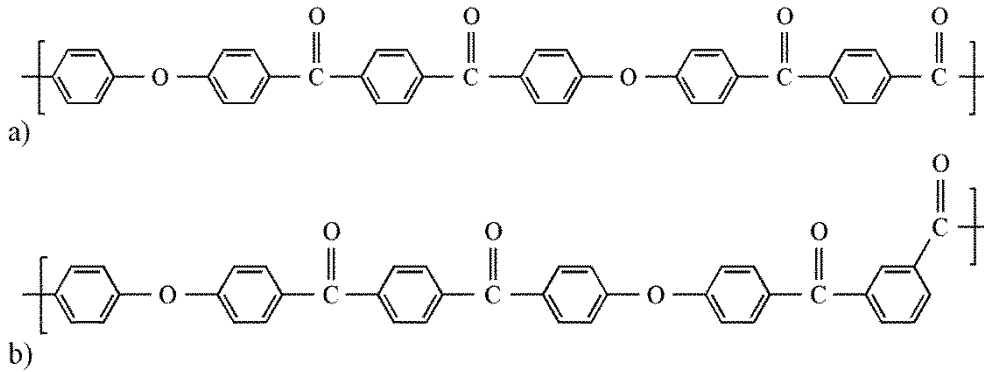
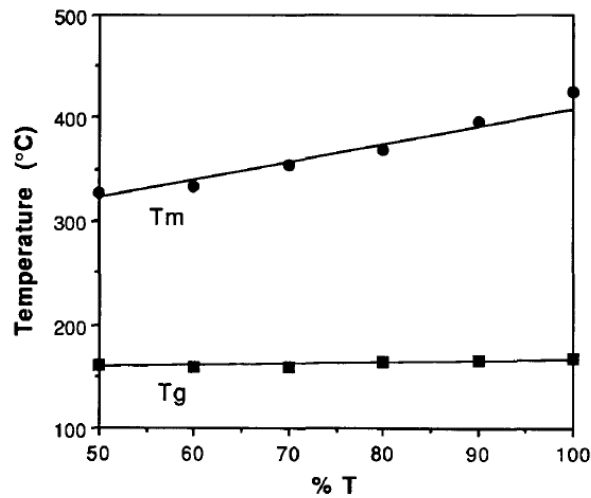


Fig. I.6 : PEKK TT a) and TI b) diads

Fig. I.7 : Evolution of the equilibrium melting temperature T_m^0 measured with the Hoffman-Weeks method and T_g as a function of the terephthaloyl ratio (T) [10]

The decrease of the T_m is due to meta linkages of isophthaloyl isomers which decreases the macromolecular chain regularity and thus the compactness of the crystalline phase. As we will see, they also induce lower crystallization kinetics (Fig. I.8) and lower maximum crystallinity ratios. However, it can be noticed that there is no significant impact on T_g which is a strong advantage.

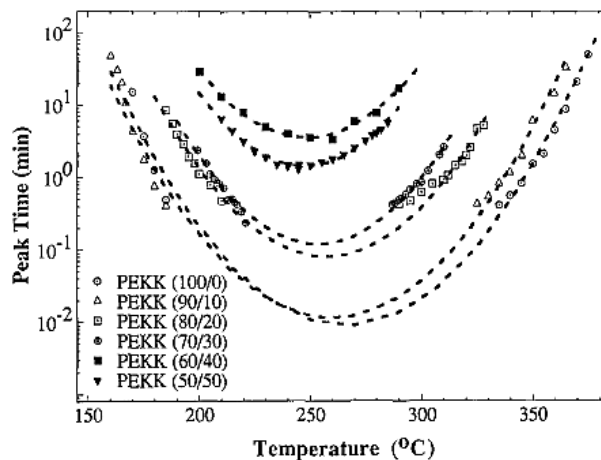


Fig. I.8 : Plot of isothermal crystallization peak time vs temperature for PEKK copolymers crystallized from the melt [10]

Our study focus on PEKK matrices provided by Arkema Company referenced as PEKK 8002, PEKK 7002 and PEKK 6002 with T/I ratios of 80/20, 70/30 and 60/40 respectively. The last digit is linked to the melt volume flow index of the polymer, the more important it is the more the melt volume flow index is important. In our case, the melt volume flow index is equal to $35\text{cm}^3 \cdot 10\text{min}^{-1}$ (ISO 1133). The thermal and mechanical properties of those three matrices compared to Victrex PEEK 450G are described in Table I.4 and Table I.5.

Grade	Ratio T/I	T _g (°C)	T _m (°C)
PEKK 8002	80/20	165	358
PEKK 7002	70/30	162	332
PEKK 6002	60/40	160	305
PEEK 450G		143	343

Table I.4 : Thermal properties of PEKK copolymers from Arkema company [15–17] and PEEK 450G from Victrex Company [18]

It can be observed that PEKK 8002 has a higher T_m than PEEK which makes it less interesting for its processing however it has the highest mechanical properties. PEKK 7002 has a lower T_m than PEEK with similar mechanical properties which makes it a good candidate as matrix for structural composite part. Finally, PEKK 6002 has the lowest T_m with about 50°C less than PEEK one which is very interesting for its processing. However, it has lower mechanical properties than the others. It can be added that mechanical tests have been done on injected tensile samples and due to very low crystallization kinetics PEKK 6002 is at a quasi-amorphous state which explains much lower Young modulus and stress at yield compared to PEKK 8002 and 7002 however its strain at break is much more important. At room temperature, PEKK 6002 do not have a brittle behavior which shows that it is tested above its brittle-ductile transition temperature.

Grade	Young modulus (GPa)	Stress at yield (MPa)	Strain at yield (%)	Strain at break (%)
PEKK 8002	3.8	105-125	5.2	20-30
PEKK 7002	3.8	70-110	5.2	2-20
PEKK 6002*	2.9	88	5.4	>80
PEEK 450G	3.7	100	5.5.	45

Table I.5 : Mechanical properties of PEKK copolymers from Arkema company [15–17] and PEEK 450G from Victrex Company [18] tested at room temperature (*PEKK 6000 is at the amorphous state compared to the others which are fully crystallized)

I.2.3 Crystalline morphology

As the others PAEK, it has been shown in the literature [10,19–21] that PEKK copolymers crystallizes with a two-chain orthorhombic unit cell with the following dimensions: lamellae growing direction $a=0.767\text{nm}$, $b=0.606\text{nm}$ and chain axis $c=1.008\text{nm}$ [22] (Fig. I.10). This unit cell has been identified from a Cu $K\alpha$ X-ray diffraction pattern with the (110) peak at $2\theta=18.7^\circ$, the (111) peak at $2\theta=20.6^\circ$ and the (200) peak at $2\theta=22.7^\circ$ (Fig. I.9). This unit cell will be called “form I” throughout the manuscript.

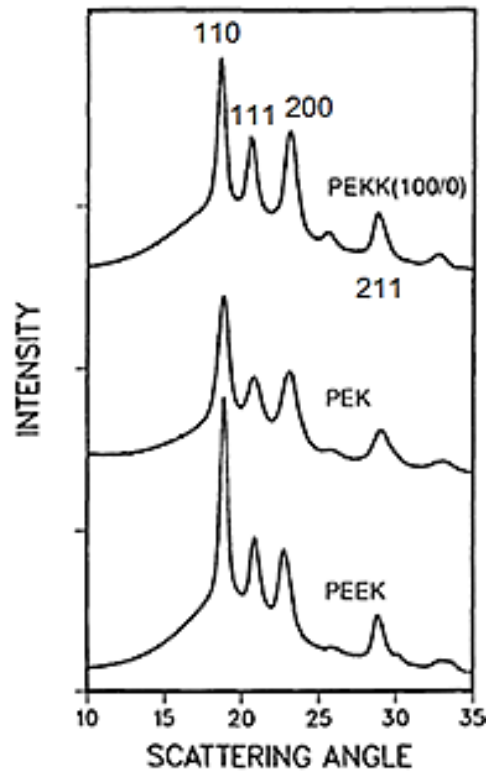


Fig. I.9 : WAXS measurement for three different PAEK [10]

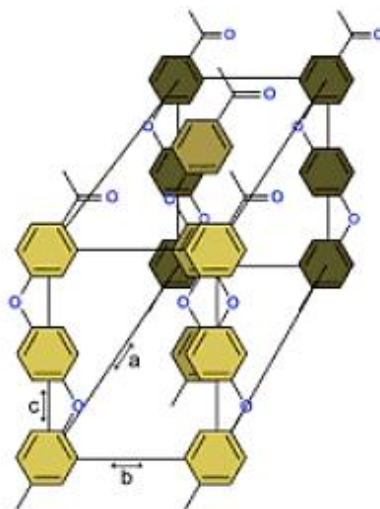


Fig. I.10 : Two-chain orthorhombic unit cell of PEEK [23]

In addition to form I, it has been reported that depending on the crystallization conditions and the T/I ratio PEKK can crystallize with two additional forms called form II and III [22,24–28]. Form II has been identified by Blundell et al. [28] and DuPont and ICI research group [22,24–27] from X-ray measurements with the apparition of an additional peak (020)^{II} at $2\theta=16^\circ$ (Fig. I.11) and indexed by a one or two-chain orthorhombic lattice depending on the authors (Fig. I.12). The ability to form this second crystalline phase is significantly favored for high chain stiffness and low molecular mobility. PEKK copolymers have a high ratio of ketone linkages which increases the stiffness of the molecule and enhances the apparition of form II. More precisely, ketone linkages have high rotational conformation energy barriers which enhance chain stiffness.

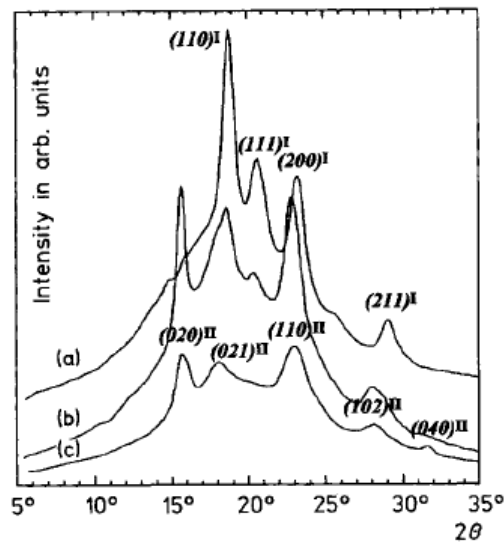


Fig. I.11 : X-ray diffraction scans of PEKK 100/0 crystallized at 340°C during 1h from the melting state (a), at 180°C for 1h from the glassy state (b) and crystallized from solvent-induced crystallization (c) [22]

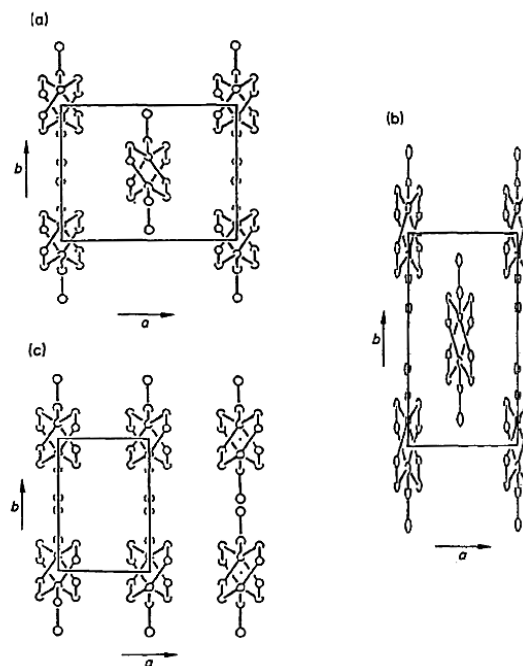


Fig. I.12 : Polymorphism with different crystal unit cells in PEKK : form I (a), form II suggested by Blundell et al. [28] (b) and by Gardner et al. [10,25] (c) [22]

The apparition of form II for PEKK is strongly linked to the crystallization conditions and the ratio T/I. A phase diagram proposed by Gardner et al. [25] summarizing the apparition conditions of form I and II is presented in Fig. I.13. Firstly, it can be observed that form II appears for high T/I ratio. In fact, as ketone linkages, terephthaloyl entities have a high chain stiffness favoring the apparition of form II. Secondly, form II apparition seems to be enhanced for solvent crystallization or low mobility crystallization conditions such as cold crystallization which is consistent with Fig. I.11 whereas only form I was observed for crystallization from the melting state corresponding high chain mobility crystallization.

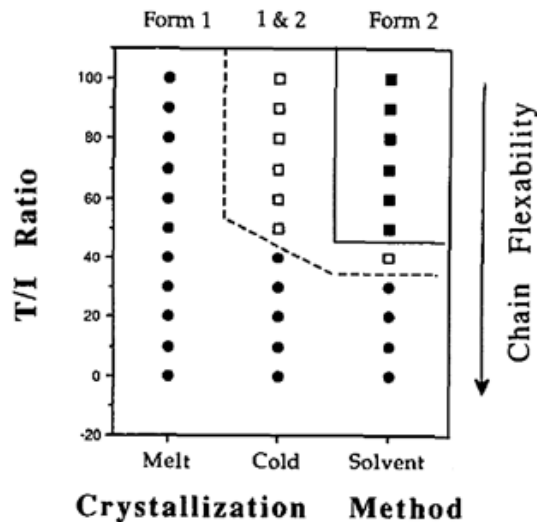


Fig. I.13 : Phase diagram of the two crystalline polymorphism in PEKK as a function of the T/I ratio and the crystallization conditions [25]

In addition to form I and II, an intermediate morphology called form III was reported in the literature by Gardner et al. [10], Cheng et al. [22] and Ho et al. [26] with the apparition of the peak (113) at 20° (Fig. I.14) indexed to an orthorhombic unit cell. This subsidiary form was observed for high annealing temperatures and assumed to correspond to a recrystallization process of form II to a more stable form.

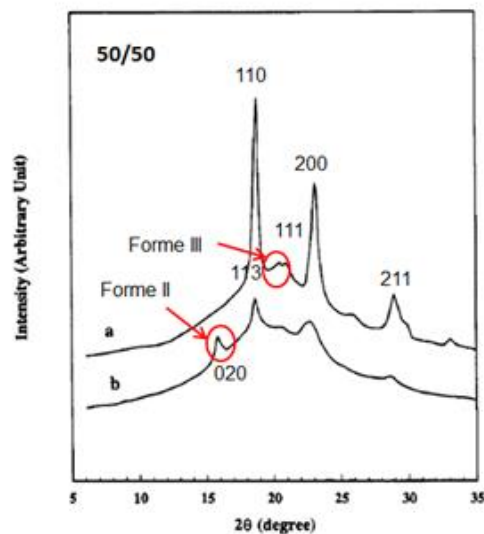


Fig. I.14 : X-ray diffraction scans of PEKK 50/50 crystallized at 260°C for 60 min from the melting state before annealing (a) and after annealing at 310°C for 10 min

I.2.4 Secondary crystallization

Isothermal crystallization mechanisms of PEKK have been studied by Gardner et al. [10] and Cortés et al. [29]. After annealing, they observed an additional endotherm during the melting which occurs about 10°C above the annealing temperature (Fig. I.15). Such behavior has also been observed for PEEK [20,30,31] and other semi-crystalline polymers as poly(ethyleneterephthalate) [32–34] and is called the double-melting behavior. This additional endotherm is attributed to the melting of a secondary crystallization associated to the growth of an interlamellar crystalline structure within lamellae [35]. This subsidiary crystallization appears after long annealing or slow cooling rates.

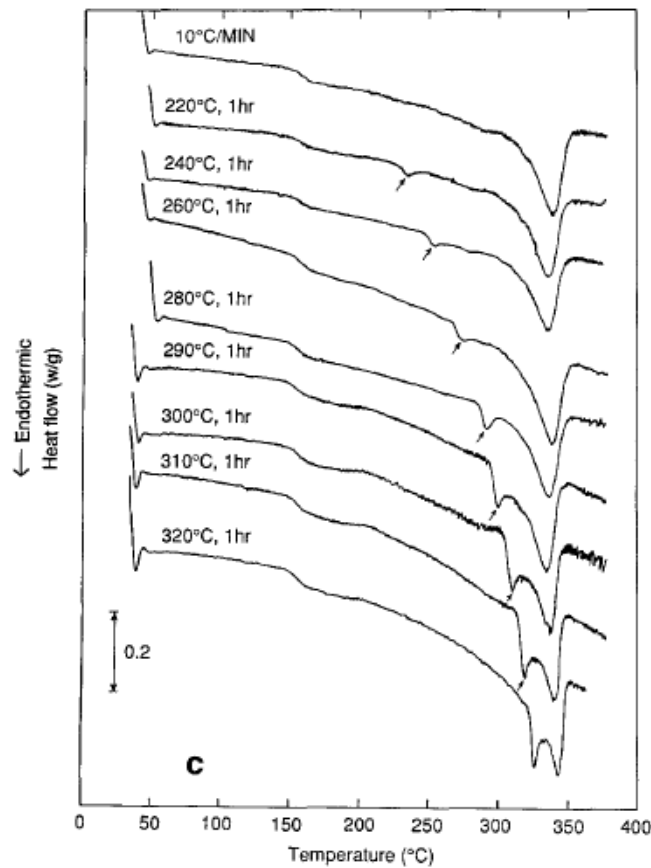


Fig. I.15 : DSC heating scans at $10^{\circ}\text{C}\cdot\text{min}^{-1}$ of PEKK 80/20 crystallized at different temperatures from the melt [10]

I.2.5 Nucleation and growth

As for most of thermoplastic polymers, PEKK crystallizes with a spherulitic growth by chain layovers and deposits.

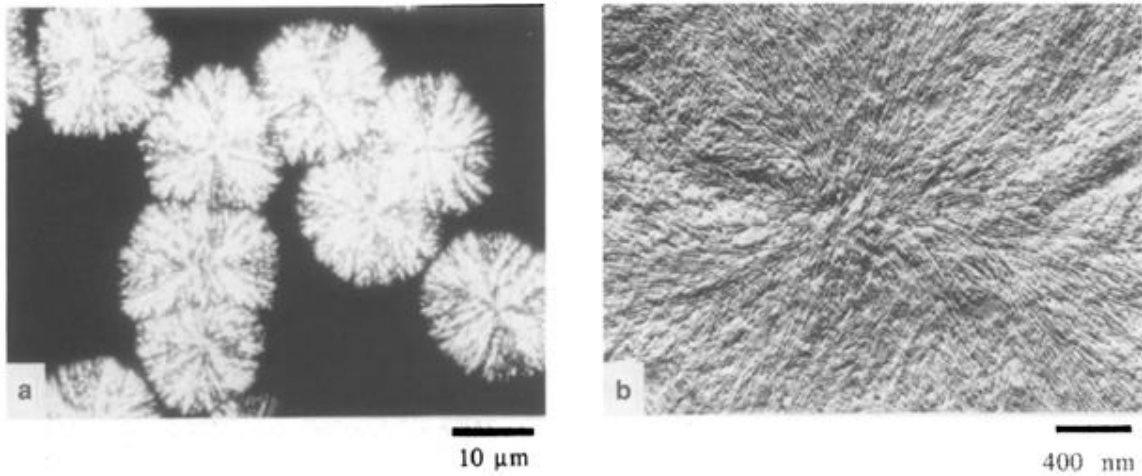


Fig. I.16 : Polarized optical microscopy (a) and TEM (b) observations of PEKK spherulites after isothermal crystallization at 280°C for 30 min [10]

Crystalline lamellae are separated by amorphous zone which includes end of chains, chain segments belonging to two adjacent crystalline lamellae and entangled chain segments. The lamellae thickness depends on the crystallization conditions. It has been shown for PEEK [36] that the motif {crystalline lamellae + amorphous zone} is about 15 nm with a crystalline lamellae thickness of 10 nm corresponding to 7 consecutive crystalline unit cells

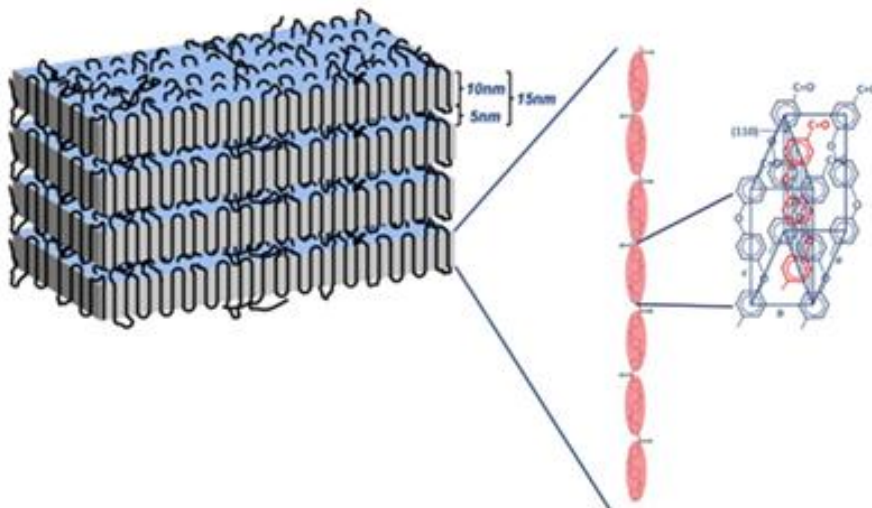


Fig. I.17 : Crystalline morphology model of PEEK [36]

I.3 CONCLUSION

Tape preregs used for the composite manufacturing are prepared with 40% by volume of PEKK matrix and 60% by volume of carbon fibers volume. PEKK matrices are copolymers containing isophthaloyle (I) and terephthaloyle isomers (T) with different ratios depending on the copolymer. Three different PEKK are studied, PEKK 8002, PEKK 7002 and PEKK 6002 with T/I ratios of 80\20, 70\30 and 60\40 respectively. They have the same glass transition temperature whereas their melting temperature decreases with the number of isophthaloyle entities until 305°C for PEKK 6002. PEKK matrices crystallize with spherulitic growth and depending on the ratio T/I and the processing thermal conditions they can crystallize with two different crystalline morphologies with different unit cell dimensions. In addition, a secondary crystallization associated to the growth of an interlamellar crystalline structure within lamellae can occur after long annealing or slow cooling rates. Each PEKK copolymer crystallizes differently with different crystallization kinetics and crystallinity. PEKK 6002 crystallizes more slowly than PEKK 7002 and 8002 and has a lower crystallinity.

CHAPTER II. IMPACT OF THERMAL CYCLES ON PEKK MATRICES MECHANICAL PROPERTIES

In this chapter, we investigated the isothermal and non-isothermal crystallization kinetics modelling of neat PEKK resins. Crystalline structure and morphologies were first identified by X-ray measurements and optical microscopy. A new methodology was developed to identify the parameters of the isothermal crystallization kinetics Hillier model directly from the heat flow measured by DSC. Isothermal Time Transformation Temperature (TTT) diagrams of the crystallinity were built providing a useful tool for PEKK processing. A new non-isothermal crystallization kinetics model established from the derivative of the isothermal crystallization kinetics Hillier model is presented allowing the prediction of the non-isothermal crystallization behavior of neat PEKK. Finally, we studied the impact of crystallinity and crystalline morphologies on the mechanical properties of neat PEKK at room temperature and above the glass transition.

II.1 EXPERIMENTAL

II.1.1 Differential Scanning Calorimetry (DSC)

Isothermal and non-isothermal crystallization analyses were carried out on a TA Instruments Q2000 on granules of about 7-8 mg. For cold and melt crystallization, all specimens were first heated at $10^{\circ}\text{C}\cdot\text{min}^{-1}$ from room temperature to 360°C for PEKK 6002, 380°C for PEKK 7002 and 400°C for PEKK 8002 during 5 minutes (T_m in Fig. II.1). Those temperatures are above PEKK equilibrium melting temperatures [10] to erase the thermal history.

For isothermal crystallization from the melt, specimens were then cooled at $40^{\circ}\text{C}\cdot\text{min}^{-1}$ to annealing temperatures (T_c in Fig. II.1). Annealing temperatures were maintained during 240 minutes and specimens were finally cooled to room temperature at $40^{\circ}\text{C}\cdot\text{min}^{-1}$. For isothermal cold crystallization, the polymer is cooled from the melt at $60^{\circ}\text{C}\cdot\text{min}^{-1}$ to room temperature and then heated at $60^{\circ}\text{C}\cdot\text{min}^{-1}$ to the isothermal temperature which was maintained during 240 minutes. Finally, specimens were cooled at $40^{\circ}\text{C}\cdot\text{min}^{-1}$ to room temperature. The chosen cooling and heating rates were high enough to make sure that the polymer does not crystallizes before annealing and the annealing time was long enough to allow the polymer to fully crystallize.

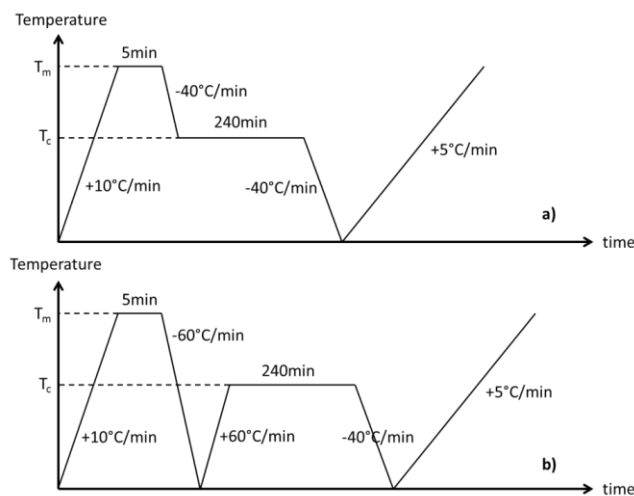


Fig. II.1 : Isothermal melt (a) and cold (b) crystallization thermal cycles for DSC measurements

For non-isothermal crystallization, specimens were cooled at cooling rates between 1°C/min to 30°C/min to room temperature.

For all specimens, a heat scan at 10°C.min⁻¹ to 400°C was carried out after crystallization to measure the glass transition, the melting temperature and the melting enthalpy induced by the crystallization cycle.

II.1.2 Wide angle X-ray diffraction

The X-ray data were collected by performing wide angle X-ray scattering (WAXS) patterns at room temperature on samples with a thickness of 2mm thanks to the SAXS/WAXS system from Xenocs. The apparatus consists of an X-ray source using a Cu-K_α anode radiation with a wavelength of a 1.54 Å delivering a parallel beam. The X-ray patterns were recorded with a MAR300 2D detector piloted with the MAR300 software. The sample to detector distance was 168 mm. Silver behenate standard reference material was used for sample-to-detector distance calibration. The exposure time was 15h. The 2D patterns were treated using Fit2D software developed by the European Synchrotron (ESRF). The 2D X-ray diffraction patterns were integrated along the azimuthal direction from isotropic samples.

II.1.3 Optical microscopy

The optical microscope used was a polarizing Nikon Eclipse LV100 model equipped with a Nikon DS Digital Sight DS-Fi1 camera and a hot stage Linkam LTS-420. Observations were carried out with an ocular lens of 30x on PEKK film with a thickness of 5 μm prepared with a Leica RM-2235 microtom. Films were first heated at 10°C.min⁻¹ from room temperature to 360°C during 5 minutes to erase the thermal history of the specimen and then cooled down at 40°C.min⁻¹ to 270°C. The annealing temperature of 270°C was maintained during two hours and corresponds to a low supercooling i.e. to a low nucleation rate allowing the formation of large spherulites.

II.1.4 Mechanical tests

II.1.4.1 Tensile tests

Mechanical tests were carried out with a tensile test machine Instron 5966 equipped with a laser extensometer and an oven to make tests at high temperature. Tests were done on normalized 1BA tensile samples (ISO 527) with length of 75 mm, width of 5 mm for the fitting length and a thickness of 2 mm machined from amorphous plates of 100x100x2 mm³ crystallized in an oven (Fig. II.5). Plates were first dried at 120°C during 48h and crystallized from the glassy state at 200°C, 230°C and 260°C (T_c) (Fig. II.2.b.) and from the melting state (360°C during 5 minutes) at 260°C during different times to obtain different crystallinities (Fig. II.2.b.). For PEKK 8002 and 7002 only amorphous or fully crystallized from the glassy state plates could be compared due to their fast crystallization rates (Fig. II.2.b.).

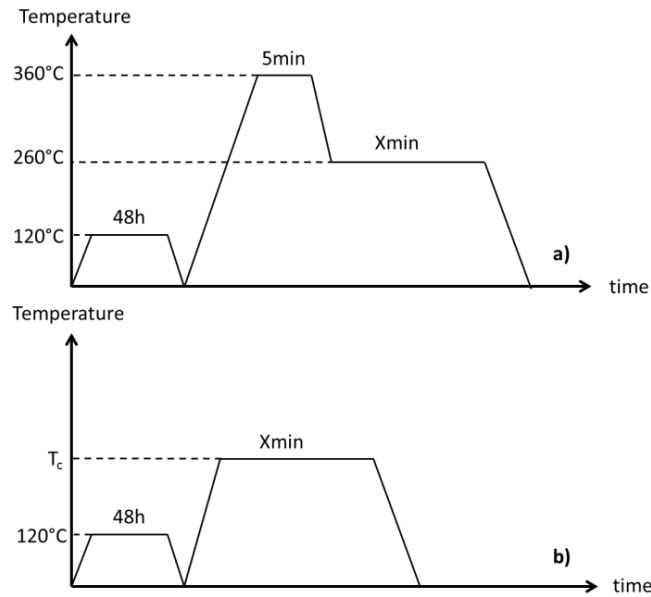


Fig. II.2 : Isothermal melt (a) and cold (b) crystallization thermal cycles for PEKK crystallization plates

A casing was used during the crystallization to keep the plat flat with the same dimensions (Fig. II.3). Plates were put between Teflon films for crystallization from the glassy state and a more complex environment described in Fig. II.4 was carried out for crystallization from the melt due to a problem of bubbles apparition on the surface of plates. More precisely, superposition of thermalimide strips and woven fiber glass of 300 g.m^{-2} has shown good results to evacuate bubbles on the surface of plates. After crystallization, DSC scans from room temperature to 400°C at 5°C.min^{-1} were carried out on pieces cut from the crystallized plates to measure the crystallinity. Specimens were tested at room temperature and 180°C (above T_g) with testing speed of 1 mm.min^{-1} and 100 mm.min^{-1} that is 0.033 s^{-1} and 3.3 s^{-1} respectively. At 180°C , PEKK matrices are at the rubbery state and the testing speed must be high enough to measure entanglements network properties and not chain flow due to disentanglement. At this temperature, the crystallization kinetics is low enough to assume that the polymer do not crystallize during the test.

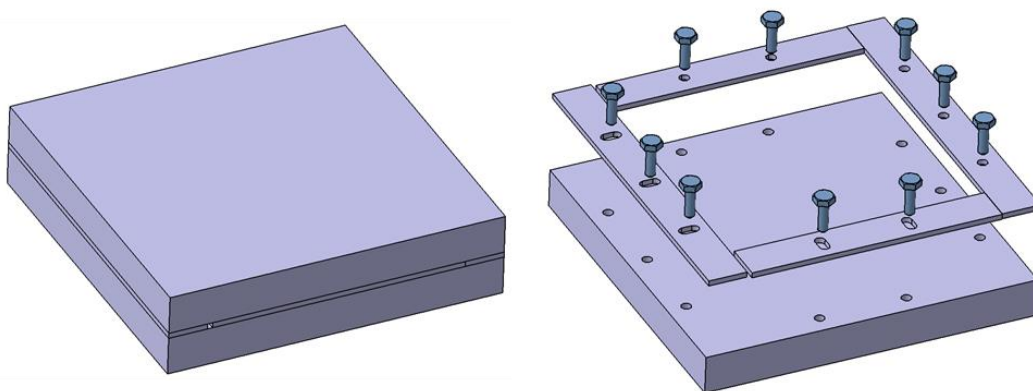




Fig. II.3 : Casing for the PEKK plates crystallization

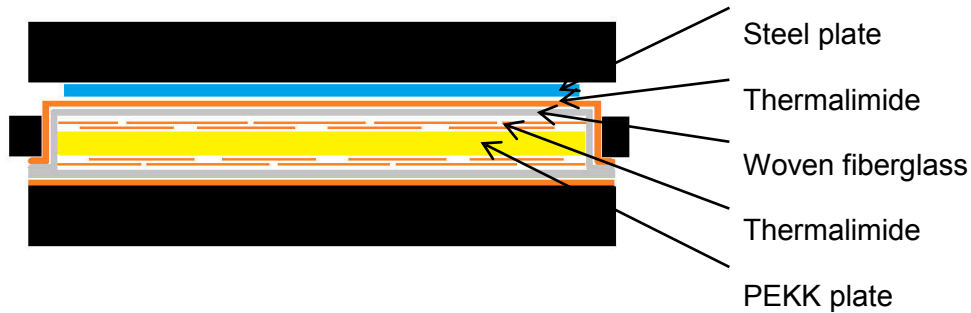


Fig. II.4 : PEKK plates environment for crystallization from the melt

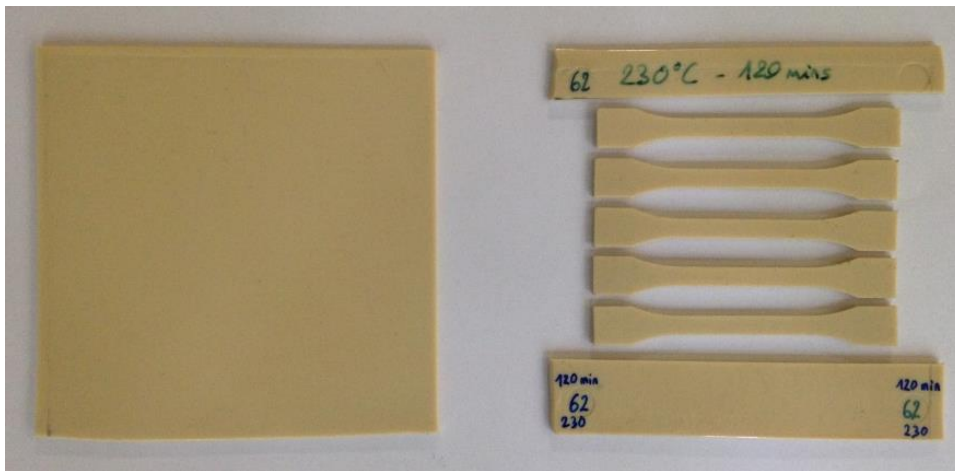


Fig. II.5 : PEKK plate crystallized with the machined 1BA tensile samples

II.1.4.2 Dynamic Mechanical Analysis (DMA)

A DMA Q800 of TA Instruments has been used to characterize the viscoelastic behavior of PEKK. The bending mode chosen was a “Single Cantilever” mode which is the most relevant mode for rubbery state polymers and thermoplastics (AITM 1-0003). The calibration of both clamps has been made with a standard sample of steel 17.5 x 12.77 mm² with a thickness of 3.16 mm. For every sample, the working length was 17.5 mm corresponding to the distance between the two clamps. The atmosphere was the room air. DMA tests were done on rectangular samples with length of 50 mm, width of 10 mm and thickness of 2 mm machined from fully crystallized plates at 230°C from the glassy state with the protocol describe in the previous paragraph. Fully crystallized samples were tested from 40°C to 300°C with a

heating rate of 3°C/min which is low enough to consider the thermal inertia of the material negligible. A strain of 0.5% at a frequency of 1 Hz were determined to stay in the linear viscoelastic domain and to consider that dynamical mechanical properties do not depend on strain.

II.2 CRYSTALLINE MORPHOLOGIES

II.2.1 Crystalline structure

WAXS measurements have been carried out on a PEKK 6002 sample crystallized from the melt and from the glassy state at 230°C during 2 hours (Fig. II.6). It has been observed for crystallization from the melting state a diffraction pattern with the (110) peak at $2\theta=18.7^\circ$, the (111) peak at $2\theta=20.6^\circ$ and the (200) peak at $2\theta=22.7^\circ$. This pattern is similar to the other PAEK and is attributed the crystalline morphology form I presented in paragraph I.2.3. An additional pattern with the (020) peak at $2\theta=16^\circ$ has been observed for both crystallization conditions which corresponds to form II reported in paragraph I.2.3. For PEKK 6002 crystallized from the glassy state, a more important (020) peak has been observed compared to crystallization from the melting state and the (111) peak is non-existent. This is consistent with the fact that cold crystallization induces low chain mobility enhancing the growth of the form II. The disappearing of the (111) peak highlights that PEKK 6002 crystallized from the glassy state presents only pure form II.

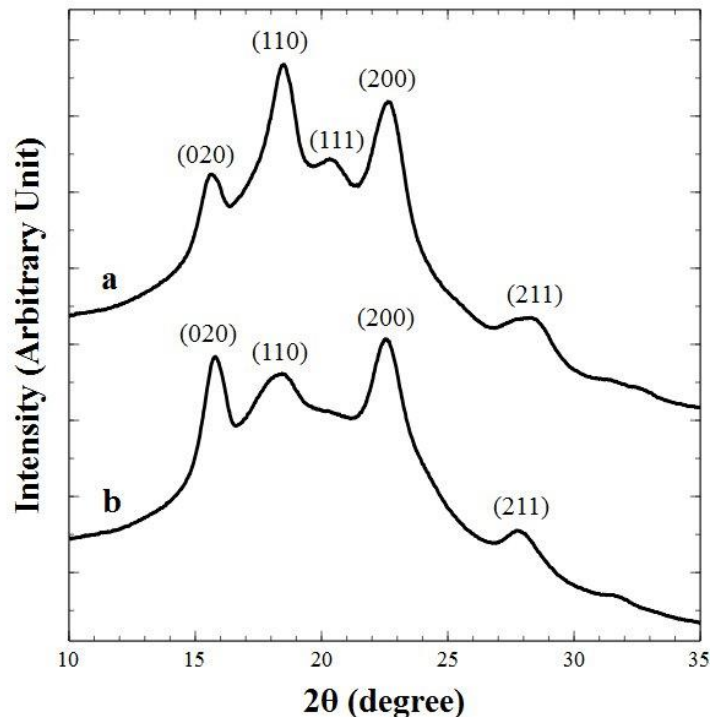


Fig. II.6 : X-ray diffraction scans of neat PEKK 6002 crystallized at 230°C during 2h from the melting state (a) and from the glassy state (b)

II.2.2 Nucleation and growth

Fig. II.7 shows the crystal growth of a PEKK 6002 sample crystallized from the melt at 270°C during 20 minutes (Fig. II.7.a), 30 minutes (Fig. II.7.b) and 40 minutes (Fig. II.7.c). Radial growths of crystalline entities similar to spherulites were observed. During the first step of crystallization, the crystalline entities grow independently to each other with the same size

until impingement which is typical to an instantaneous nucleation. The initial number of potential nuclei N_0 has been calculated and is equal to about $0.0014 \mu\text{m}^{-3}$. It is equal to the number of nuclei at the early beginning of the crystallization divided by the volume containing the nuclei which have been both measured with an image processing program. At the end of the crystallization process, the crystalline entities diameters have been measured from $18\mu\text{m}$ to $33\mu\text{m}$.

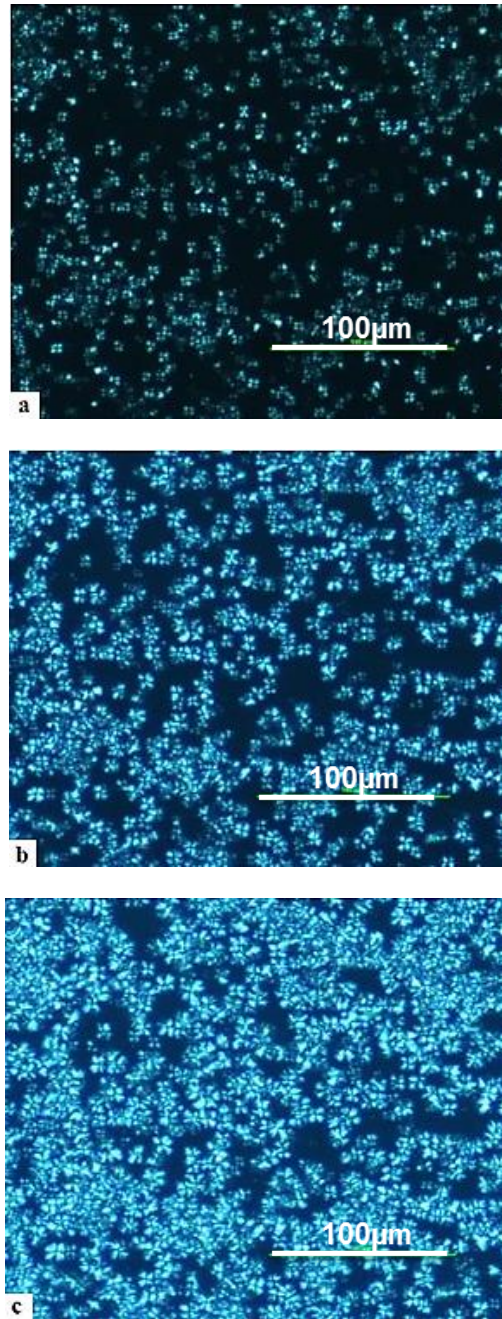


Fig. II.7 : Micrographs of PEKK 6002 crystallized from the melt at 270°C during 20min (a), 30min (b) and 40min (c)

The evolution of the radius of a spherulite during the crystallization process as a function of time at 270°C from the melting state has been followed in Fig. II.8. In order to better assess the crystalline growth rate, the followed spherulite has been chosen to be the most far as possible from the others to collect enough data before impingement. Three different steps

can be observed during the crystallization process. The first step is related to the crystallization initiation where the spherulite studied was first observed after 8 minutes of crystallization with a radius of 2 μm . This time depends on the device resolution. After this initiation step, the spherulite grows constantly until it impinges on another spherulite. The growth rate G is independent of the size of the spherulite and calculated from the slope of the line by $G=dR/dt$. The growth rate of spherulites at 270°C from the melt has been measured of about 0.2 $\mu\text{m}\cdot\text{min}^{-1}$. At the end of the crystallization growth, the radius has been observed of about 16.5 μm . Those results will be compared later with the following DSC study.

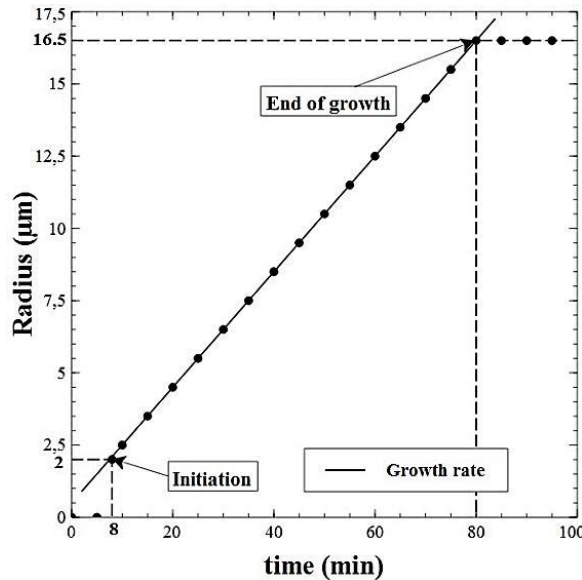


Fig. II.8 : Spherulite radius vs time during crystallization at 270°C from the melting state

II.3 CRYSTALLIZATION KINETICS

II.3.1 Crystallization kinetic comparison

In a first approach, PEKK 8002, 7002 and 6002 matrices were cooled from the melt at three different cooling rates (1°C.min⁻¹, 5°C.min⁻¹ and 10°C.min⁻¹) to compare their crystallization kinetics. For each cooling condition, the melting enthalpy was measured by DSC during a heat scan at 5°C.min⁻¹ after crystallization and the crystallinity (X_c) was calculated with Equation II.1:

$$X_c = \frac{\Delta H_m - \Delta H_{cc}}{\Delta H_{100\%}} \quad \text{Equation II.1}$$

with ΔH_m the melting enthalpy (J.g⁻¹), ΔH_{cc} the cold crystallization enthalpy (J.g⁻¹) and $\Delta H_{100\%}$ the fully crystallized polymer enthalpy which was taken the same as for PEEK equal to 130 J.g⁻¹ [20]. Results are presented in Table II.1. DSC heating scans at 5°C.min⁻¹ of PEKK 8002, 7002 and 6002 cooled from the melt at 10°C.min⁻¹ are presented in Fig. II.9.

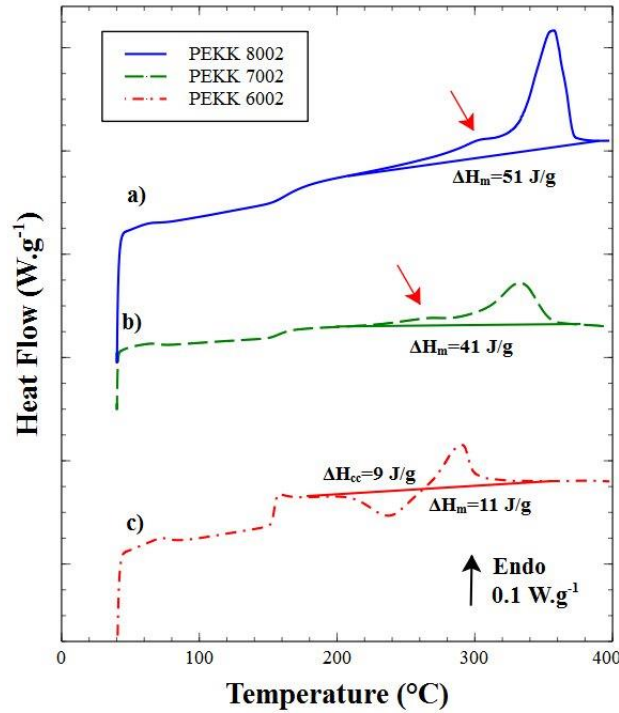


Fig. II.9 : DSC heating scans at $5^{\circ}\text{C}\cdot\text{min}^{-1}$ of PEKK 8002, 7002 and 6002 cooled from the melt at $10^{\circ}\text{C}\cdot\text{min}^{-1}$

It can be observed in Fig. II.9 that PEKK 8002 crystallizes more than PEKK 7002 with melting enthalpies of $51 \text{ J}\cdot\text{g}^{-1}$ and $41 \text{ J}\cdot\text{g}^{-1}$ respectively. A cold crystallization peak appears for PEKK 6002 scan with an enthalpy of $9 \text{ J}\cdot\text{g}^{-1}$ closed to the melting enthalpy equal to $11 \text{ J}\cdot\text{g}^{-1}$. This shows that PEKK 6002 hardly crystallizes for a cooling rate of $10^{\circ}\text{C}\cdot\text{min}^{-1}$ from the melt due to a low crystallization kinetics. Additional endothermic peaks were noticed at around 300°C and 260°C for PEKK 8002 and 7002 respectively which are associated to the melting of a secondary crystallization (see CHAPTER I).

Grade	X_c (%) at $V=10^{\circ}\text{C}\cdot\text{min}^{-1}$	X_c (%) at $V=5^{\circ}\text{C}\cdot\text{min}^{-1}$	X_c (%) at $V=1^{\circ}\text{C}\cdot\text{min}^{-1}$
PEKK 8002	39	39	40
PEKK 7002	31	32	33
PEKK 6002	2	14	28

Table II.1 : Crystallinity X_c (%) vs cooling rate for PEKK crystallized from the melt

In Table II.1, we can observe that PEKK 8002 and 7002 crystallinities are quasi-independent of the cooling rate between $1^{\circ}\text{C}/\text{min}$ and $10^{\circ}\text{C}/\text{min}$ showing a high crystallization rate. On the contrary, the final crystallinity of PEKK 6002 is very sensitive to the cooling rate. In fact, its crystallinity drops down with the increase of the cooling rate until almost not crystallizing at $10^{\circ}\text{C}/\text{min}$ (see Fig. II.9). Thus, PEKK 6002 matrix may not fully crystallize during the composite processing which could be a problem because we can assume that mechanical properties are linked to the crystallinity. It is thus essential to be able to predict crystallization depending on the thermal cycle.

II.3.2 Isothermal crystallization kinetics

II.3.2.1 Modified Hillier model

The isothermal crystallization kinetics of PEKK was already studied by Gardner et al. [10] with a peak-time method (time for which the crystallization exothermic peak is maximum) but they did not use a crystallization kinetic model taking into account the secondary crystallization (see CHAPTER I). This subsidiary crystallization makes the crystallization kinetics modeling more difficult.

Different isothermal crystallization models have been developed to incorporate the secondary crystallization, the most relevant reported are the Velisaris Seferis [37] and the Hillier models [35]. The former postulates that two Avrami type crystallization processes [38] occur in parallel independently whereas the second assumes that a primary Avrami type crystallization process occurs followed by a first order crystallization process which grows from the primary crystallization. Hsiao et al. [39] investigated the isothermal crystallization kinetics of a PEKK 70/30 with a modified Hillier model which postulates that the secondary crystallization is not necessarily a first order process and compared it to the Velisaris Seferis model. They concluded that the modified Hillier model has a better physical meaning than the Velisaris Seferis one because it is more suitable to describe the growth of a second crystalline structure within lamellae. In this modified Hillier model, the primary crystallization is expressed by an Avrami equation:

$$\alpha_1(t) = 1 - \exp(-K_1 t^{n_1}) \quad \text{Equation II.2}$$

where $\alpha_1(t)$ is the relative volume fraction crystallinity at time t , K_1 is the crystallization rate constant depending on the annealing temperature and n_1 the Avrami exponent depending on the nucleation and the growth geometry, for the first mechanism.

The secondary crystallization process which occurs once a volume element has been included in the lamellae at time θ is expressed in the modified Hillier model by an Avrami equation:

$$\alpha_2(t) = \int_0^t \alpha_1(\theta) \times \frac{d}{d\theta} (\alpha_2(t-\theta)) d\theta \quad \text{Equation II.3}$$

where $\alpha_2(t)$ is the relative volume fraction crystallinity at time t , K_2 is the crystallization rate constant depending on the annealing temperature and n_2 the Avrami exponent depending on the nucleation and the growth geometry, for the second mechanism. The Avrami exponent n_2 is not necessarily equal to 1 according to Hsiao et al. [39]. The total crystallinity at time t arising from those two consecutive crystallization processes is equal to:

$$\alpha(t) = w_1 \alpha_1(t) + w_2 \alpha_2(t) \quad \text{Equation II.4}$$

where w_1 and w_2 are the weight factor between the primary and the secondary crystallization with $w_1 + w_2 = 1$, indicating that the relative crystallinity at infinite time is unity which corresponds to the Avrami model hypotheses [38]. Values of weight factors provide the relative importance between both crystallizations. Consequently, From Equation II.2, Equation

II.3 and Equation II.4, total crystallinity at time t can be expressed by the modified Hillier model:

$$\alpha(t) = w_1 \left[1 - \exp(-K_1 t^{n_1}) \right] + w_2 K_2 n_2 \int_0^t \left[1 - \exp(-K_1 \theta^{n_1}) \right] (t - \theta)^{n_2 - 1} \exp[-K_2 (t - \theta)^{n_2}] d\theta \quad \text{Equation II.5}$$

It can be noticed that Equation II.5 differs from Hsiao et al. [39] model which could be due to a misprint in their article for the derivative of the secondary crystallization in Equation II.3.

If $n_2=1$, then the simplified Equation II.5 gives the Hillier model:

$$\alpha(t) = w_1 \left[1 - \exp(-K_1 t^{n_1}) \right] + w_2 K_2 \int_0^t \left[1 - \exp(-K_1 \theta^{n_1}) \right] \exp[-K_2 (t - \theta)] d\theta \quad \text{Equation II.6}$$

II.3.2.2 DSC thermogram analysis

Isothermal DSC scans of PEKK 6002 samples at 200°C and 230°C cooled at 40°C.min⁻¹ from the melt are reported in Fig. II.10. It can be witnessed that the beginning of the crystallization exothermic peaks are truncated corresponding to a gap between the beginning of the crystallization peak and the baseline (double arrow in Fig. II.10). This phenomenon has been observed by different authors [39,40] and was attributed to the instrumental thermal inertia switching from the cooling to the isothermal step. It can be observed that this gap is more important for isothermal at 230°C than 200°C due to higher crystallization kinetics at 230°C.

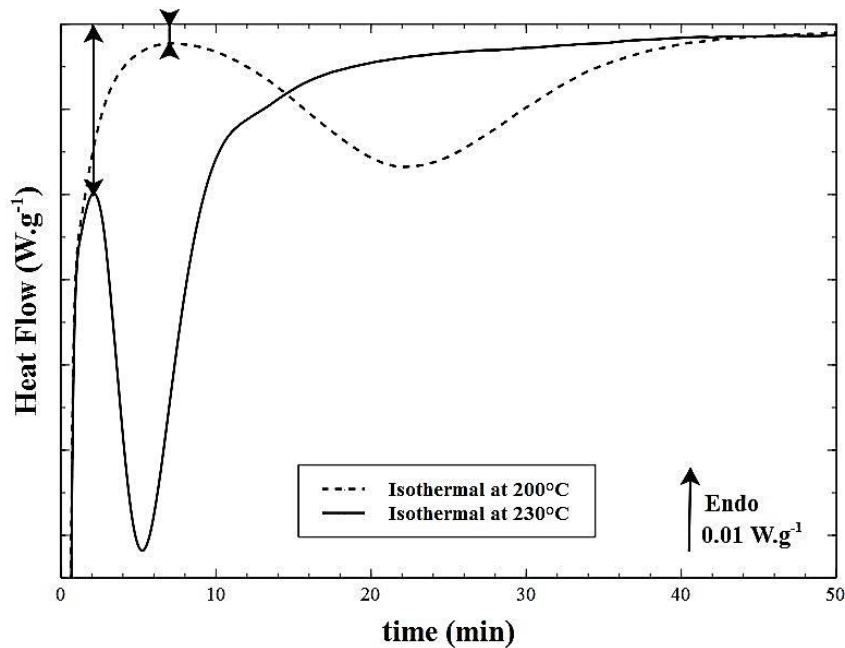


Fig. II.10 : DSC thermograms of neat PEKK 6002 crystallized from the melt during isothermal crystallization at 230°C (solid line) and 200°C (dashed line)

The absence of the crystallization peak beginning involves a problem to determine the evolution of the relative volume crystallinity because it is calculated from the area above the heat flow curve with Equation II.7:

$$\alpha(t) = \frac{\int_0^t Q(t) dt}{\int_0^{t_\infty} Q(t) dt} \quad \text{Equation II.7}$$

Where $Q(t)$ is the heat flow measured at time t and t_∞ is the time when the polymer is fully crystallized. It was thus necessary to extrapolate the beginning of the crystallization peak until the baseline to take into account the overall crystallization process. Two different approaches have been investigated to rebuild the crystallization peak.

II.3.2.3 First approach: modified Hillier model fitting on the relative crystallinity

The first approach was to extrapolate the beginning of the crystallization peak by a linear curve (dashed line in Fig. II.11) until the base line.

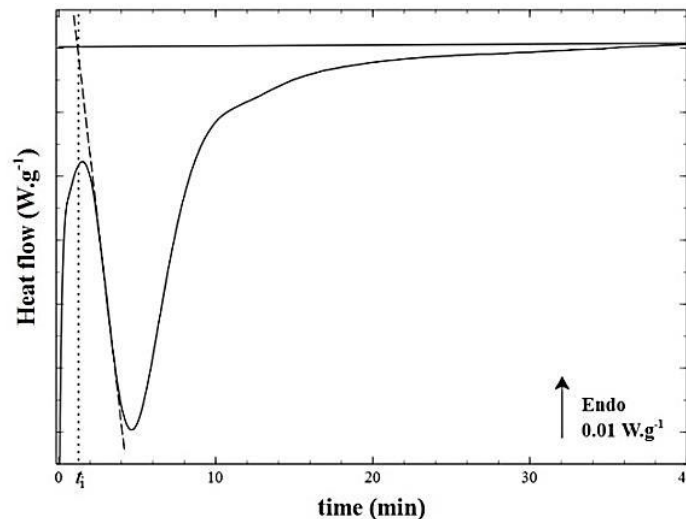


Fig. II.11 : DSC thermograms of PEKK 6002 crystallized from the melt during isothermal crystallization at 230°C with the linear extrapolation of the crystallization peak beginning (dashed line) with the crystallization induction time t_i (dotted line)

In this case, a delay can be detected between the beginning of the extrapolated crystallization peak and the isothermal scan. This delay has also been observed for other polymers with low crystallization kinetics and modelled as a crystallization induction time (t_i) [33,41]. It would correspond to the time to reach a steady state of nucleation i.e. the time to reach enough critical nuclei in the bulk to initiate crystallization. Indeed, the increase in number of critical nuclei which leads into the steady state linear would be initially slow [42]. In this work, the induction time t_i has been defined by the intersection of the baseline and the extrapolation line of the crystallization peak beginning (Fig. II.11).

For each isothermal crystallization, the relative crystallinity $\alpha(t)$ has been calculated with Equation II.7 (Fig. II.12) and its double logarithm has been plotted in Fig. II.13. Straight line trends have been observed for the double logarithm plot in Fig. II.13 during the beginning of

the crystallization which is consistent with the Avrami theory. For every crystallization, the slopes of the lines corresponding to the Avrami exponent have been measured of about 2.05 ± 0.01 (dashed lines in Fig. II.13). The corresponding Avrami model (Equation II.2) has been plotted in Fig. II.12 (dashed lines) with an Avrami exponent n_1 fixed by 2. It can be observed that the Avrami model fits well with experiments for relative crystallinity below 0.6. According to the Avrami theory, a value of 2 for the Avrami exponent would be associated either to a two dimensional crystallization growth with an instantaneous nucleation or to a one dimensional crystallization growth with a sporadic nucleation. Since the microscopic study has shown previously that the nucleation process is instantaneous (Fig. II.7), it can be assumed that the first crystallization mechanism would be a two dimensional disk-like crystallization. However, this assumption does not seem to be consistent with the microscopic observations where growing crystalline entities behave like spherulites.

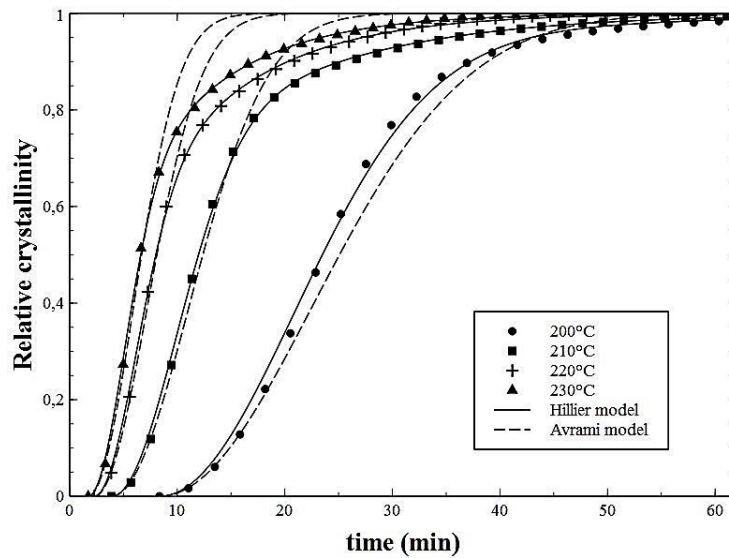


Fig. II.12 : Relative crystallinity $\alpha(t)$ vs time, the Avrami model (dashed curves) and the modified Hillier model (solid curves) plots for PEKK 6002 isothermal crystallization from the melt

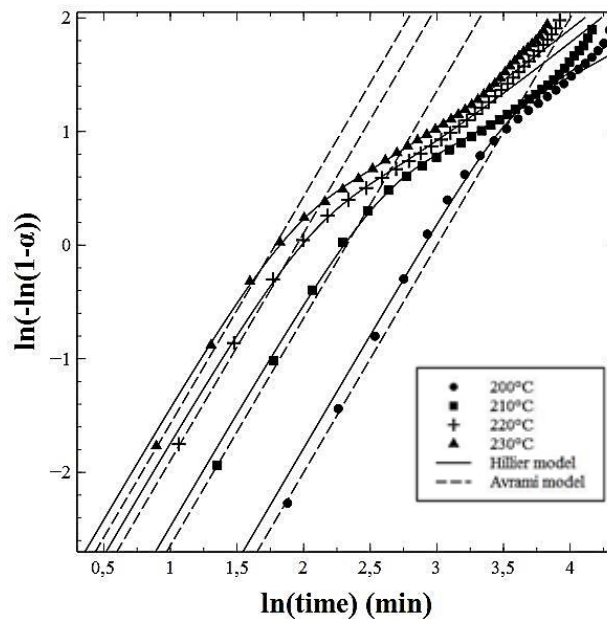


Fig. II.13 : Double logarithm vs $\ln(\text{time})$, the Avrami model (dashed curves) and the modified Hillier model (solid curves) plots for PEKK 6002 isothermal crystallization from the melt

For values of relative crystallinity above 0.6, crystallization kinetics become slower than the Avrami model which corresponds to a bending of the double logarithm plots in Fig. II.13. This phenomenon is typical of the formation of a secondary crystallization process within the primary crystallization with a slower crystallization kinetics [37,39]. The modified Hillier model previously presented (Equation II.5) has been used to take into account this secondary crystallization and fit with experiments during the overall crystallization process. The best fit of the modified Hillier model determined with a multi linear regression fitting has been found for a secondary crystallization Avrami exponent $n_2=1$. It is associated to a one dimensional crystallization growth with an instantaneous nucleation. This value is the same as reported by Hillier for polymethylene [35] and attributed to a first-order crystallization law within the crystalline lamellae. Consequently, the used crystallization kinetics model corresponds to the Hillier model presented in Equation II.6.

To conclude, this first approach gives good results regarding the fitting of the modified Hillier model with experiments [43]. However the value of 2 found for the primary crystallization Avrami exponent seems not to be consistent with microscopic observations. This could be due to the linear extrapolation of the crystallization peak beginning.

II.3.2.4 Second approach: Derivative Hillier model fitting on the heat flow

Due to inconsistent results regarding the primary crystallization Avrami exponent presented in paragraph II.3.2.3 another approach has been investigated to extrapolate the crystallization peak beginning. Instead of fitting the Hillier model with the relative crystallinity calculated from the extrapolated crystallization peak by a straight line, this approach consists of fitting directly the Hillier model with the heat flow measured by DSC. In fact by deriving Equation II.7, it can be written:

$$\frac{d\alpha}{dt} = \frac{Q(t)}{\int_0^{t_\infty} Q(t)dt} = \frac{Q(t)}{\Delta H_c} = \frac{Q(t)}{\Delta H_m} \quad \text{Equation II.8}$$

where ΔH_c is the crystallization enthalpy and ΔH_m is the melting enthalpy after crystallization. According to Equation II.4, the derivative of the Hillier model can be expressed by:

$$\frac{d\alpha}{dt} = w_1 \frac{d\alpha_1}{dt} + w_2 \frac{d\alpha_2}{dt} \quad \text{Equation II.9}$$

where the derivative of the primary and the secondary crystallization kinetics equations (Equation II.2 and Equation II.3 respectively) can be expressed by:

$$\frac{d\alpha_1}{dt} = K_1 n_1 t^{n_1-1} \exp(-K_1 t^{n_1}) \quad \text{Equation II.10}$$

$$\frac{d\alpha_2}{dt} = 0^{n_2-1} K_2 n_2 [1 - \exp(-K_1 t^{n_1})] \quad \text{Equation II.11}$$

$$+ K_2 n_2 \int_0^t [1 - \exp(-K_1 \theta^{n_1})] \exp[-K_2 (t - \theta)^{n_2}] \left\{ (n_2 - 1)(t - \theta)^{n_2-2} - K_2 n_2 (t - \theta)^{2n_2-2} \right\} d\theta$$

It can be observed that for time close to 0, the derivative of the primary crystallization kinetics equation (Equation II.10) becomes:

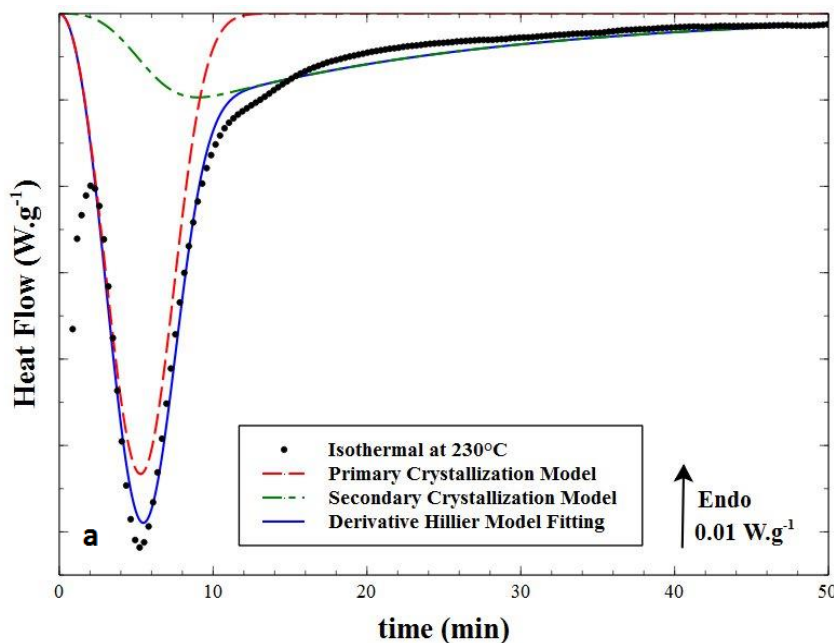
$$\frac{d\alpha_1}{dt} \propto K_1 n_1 t^{n_1-1} \quad \text{Equation II.12}$$

In this case, if n_1 is equal to 2, the expression of the derivative of the primary crystallization corresponds to the equation of a linear curve with a slope equal to $K_1 n_1$. This observation is very interesting because if we assume that only primary crystallization occurs during the beginning of the crystallization, this explains the value of 2 of the Avrami exponent for the primary crystallization found in the first approach where the crystallization peak beginning was extrapolated by a linear curve.

According to the microscopic observations, the primary crystallization Avrami exponents n_1 has been fixed with a value of 3 corresponding to a three dimensional growth with an instantaneous nucleation [38]. As for the first approach, the best fit of the derivative Hillier model determined with a multi linear regression fitting has been found for a secondary crystallization Avrami exponent $n_2=1$. Thus, by simplifying with $n_2=1$, the derivative of the secondary crystallization kinetic equation (Equation II.11) becomes:

$$\frac{d\alpha_2}{dt} = K_2 [1 - \exp(-K_1 t^{n_1})] - K_2 \int_0^t [1 - \exp(-K_1 \theta^{n_1})] \exp[-K_2(t - \theta)] d\theta \quad \text{Equation II.13}$$

The fitting of the derivative Hillier model (Equation II.9) with the heat flow measured by DSC divided by the melting enthalpy ΔH_m (Equation II.8) for isothermal crystallization at 230°C and 200°C are presented in Fig. II.14. Heat flows for the primary crystallization (Equation II.10) and secondary crystallization mechanisms (Equation II.13) determined from the derivative Hillier model fitting have also been plotted. It can be noticed that no induction times were found for this approach compared to the first one assuming that the crystallization process begins at the same time as the isothermal scan.



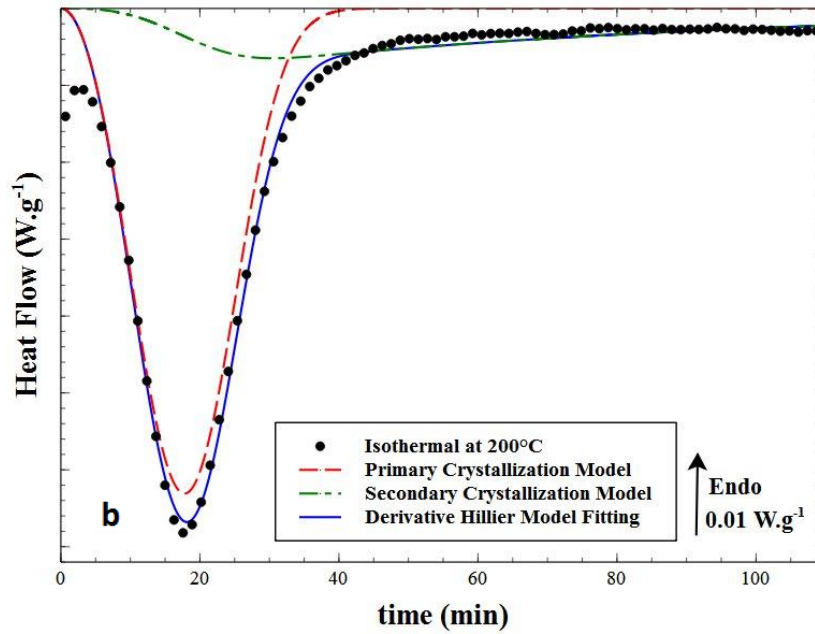


Fig. II.14 : DSC thermograms of neat PEKK 6002 crystallized from the melt at 230°C (a) and 200°C (b) with the fitting of the derivative Hillier model (solid line) and the primary (dash curves) and secondary crystallization (dash-dot curves) modeling

We can observe that the model fits well with the heat flow and allows building the beginning of the crystallization peak truncated by the DSC. The beginning of the model fitting is cofounded with primary crystallization plot which shows that the early beginning of the crystallization process corresponds only to the growth of the primary crystallization. It is then followed by the growth of the secondary crystallization related to the enhancement of the first crystallization stage.

II.3.2.5 Hillier parameter modelling

Following the general approach reported in literature for nucleation and crystallization growth, crystallization rate constants (K_1 and K_2) can be expressed as a function of the initial number of potential nuclei (N_0) and the crystal growth rate (G) depending on the dimensionality of crystallization and the nucleation mode. For the primary crystallization which has been shown to have a three dimensional crystallization growth with an instantaneous nucleation, the crystallization rate constant can be written:

$$K_1 = \frac{4}{3} \pi N_{01} G_1^3 \quad \text{Equation II.14}$$

with N_{01} the initial number of potential nuclei and G_1 the crystallization growth rate for the primary crystallization.

For the secondary crystallization which has been shown to have a one dimensional crystallization growth with an instantaneous nucleation, the crystallization rate constant can be written:

$$K_2 = N_{02} G_2 \quad \text{Equation II.15}$$

with N_{02} the initial number of potential nuclei and G_2 the crystallization growth rate for the secondary crystallization.

According to the Hoffmann and Lauritzen theory [44–46], the crystal growth can be expressed by:

$$G_i(T) = G_{0i} \exp\left(-\frac{U^*}{R(T-T_\infty)}\right) \exp\left(-\frac{K_{gi}}{T\Delta T f}\right) \quad \text{Equation II.16}$$

where G_{0i} is a pre-exponential factor independent of the temperature. The first exponential term contains the contribution of the diffusion process to the growth rate, where U^* is the activation energy of the molecular transferring through the melt crystal interface, T_∞ is the temperature below which diffusion stops ($T_\infty = T_g - 30K$) with $T_g = 155^\circ C$ and R is the gas constant.

The second exponential term is the contribution of the nucleation process, where K_{gi} is the activation energy of nucleation for a crystal with a critical size, ΔT is the degree of supercooling ($\Delta T = T_{m0} - T$) with T_{m0} the equilibrium melting temperature and f is a correction coefficient for the temperature dependence of the melting enthalpy ($f = 2T/(T_{m0} + T)$). The index i for G_i , G_{0i} and K_{gi} is equal to 1 for primary crystallization and 2 for secondary crystallization.

Finally, the primary crystallization rate constant can be written:

$$K_1(T) = K_{01} \exp\left(-\frac{3U^*}{R(T-T_\infty)}\right) \exp\left(-\frac{3K_{g1}}{T\Delta T f}\right) \quad \text{Equation II.17}$$

And the secondary crystallization rate constant can be written:

$$K_2(T) = K_{02} \exp\left(-\frac{U^*}{R(T-T_\infty)}\right) \exp\left(-\frac{K_{g2}}{T\Delta T f}\right) \quad \text{Equation II.18}$$

with the pre-exponential factors $K_{01} = \frac{4}{3} \pi N_{01} G_{01}^3$ and $K_{02} = N_{02} G_{02}$ independent of temperature. Regarding the evolution of the primary crystallization weight factor w_1 with the crystallization temperature (Fig. II.16), it was chosen to model w_1 by a linear equation:

$$w_1(T) = a_1 T + b_1 \quad \text{Equation II.19}$$

where a_1 and b_1 are two constants independent of the temperature.

II.3.2.6 Comparison of crystallization kinetics between cold and melt crystallization

The logarithm of K_1 and K_2 determined from the derivative Hillier model fitting have been plotted in Fig. II.15 and fitted with the Hoffman and Lauritzen model (respectively Equation II.17 and Equation II.18) for crystallization from the melt and cold crystallization of neat resin samples. Results for K_{0i} , K_{gi} and U^* are presented in Table II.2. As expected, we observed that both plots have typical bell shapes regarding the Hoffman and Lauritzen growth theory [45]. Crystallization kinetics are the most important around $240^\circ C$ and very low close to the T_g and T_m corresponding to low diffusion and nucleation kinetics respectively. Interestingly, it appears that crystallization rate constants for cold crystallization are slightly higher than those for crystallization from the melt. We attributed that to a lower final degree of crystallinity

for cold crystallization ($\Delta H_c \approx 26 \text{ J.g}^{-1}$) than for crystallization from the melt ($\Delta H_c \approx 31 \text{ J.g}^{-1}$). Values of K_{gi} are similar to those reported in the literature for other PAEKs [47,48]. Since, the crystallization rate constant K_1 is linked to G_1 with Equation II.14, we propose to crosscheck K_1 value with the previous microscopic study assuming that the spherulite growth rate is equal to the crystalline lamellae growth rate. Thanks to this study, the growth rate G at 270°C from the melt and the initial number of potential nuclei N_0 were measured about $0.2 \mu\text{m.min}^{-1}$ and $0.0014 \mu\text{m}^{-3}$ respectively. By assuming that the growth rate is associated to the primary crystallization process, the crystallization rate constant $\ln(K_1)$ was calculated about -8.37 min^{-1} with Equation II.14 (square in Fig. II.15). This value is consistent with the $\ln(K_1)$ value calculated with the Hillier model at 270°C from the melt of about -9.3 min^{-1} (Fig. II.15). It is noteworthy that the value of $\ln(K_1)$ calculated with the microscope study is slightly higher than the one calculated from the DSC measurements with the Hillier model which could be partly attributed to an heterogeneous nucleation taking place on the surface of the film which is between two glass slides.

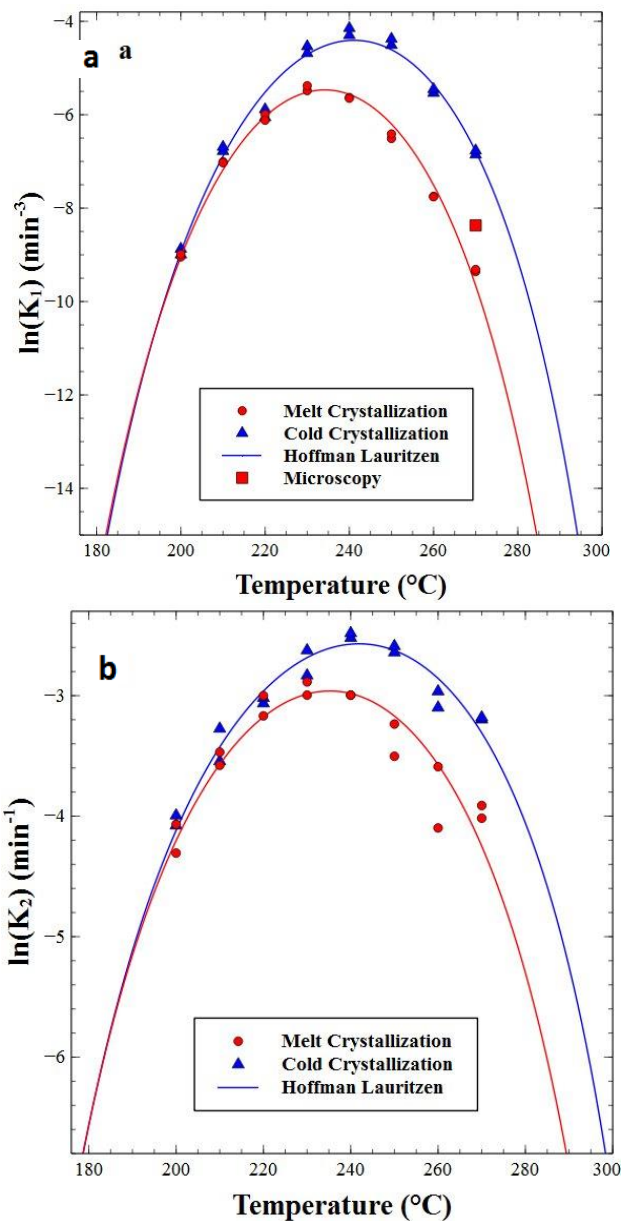


Fig. II.15 : Logarithmic plot of the primary (a) and the secondary crystallization (b) rate constants vs temperature for isothermal crystallization from the melt and cold crystallization of neat PEKK 6002 with the Hoffman and Lauritzen model fitting

The primary crystallization weight factor (w_1) for crystallization from the melt and cold crystallization has been plotted as a function of temperature in Fig. II.16 with the fitting of the linear model (Equation II.19). Results for a_1 and b_1 are presented in Table II.2. We observed that w_1 decreases with temperature showing that the formation of the secondary crystallization is promoted for low degree of supercooling. This observation has also been reported by few authors [29,49] with the increase of a first endothermic peak which occurs 10°C above the annealing temperature attributed to the melting of the secondary crystallization. In fact, for high annealing temperatures, the diffusion process is very important with a high mobility of the chains allowing the enhancement of the crystalline phase.

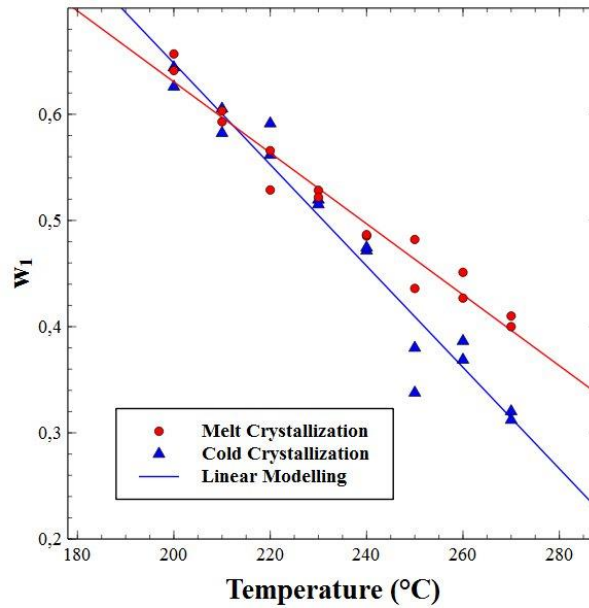
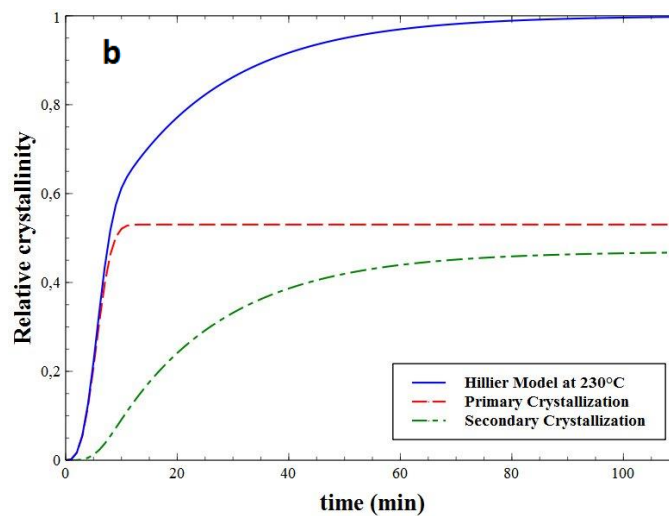
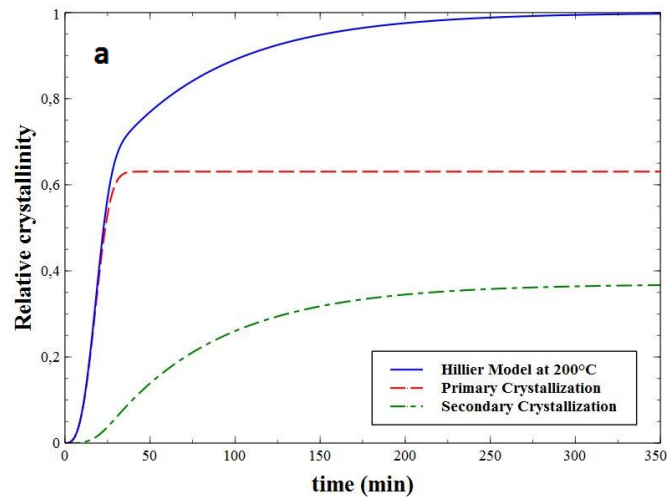


Fig. II.16 : Weight factor of the primary crystallization vs temperature for isothermal crystallization from the melt and cold crystallization of neat PEKK 6002 with the linear model fitting

Kinetics paramaters	Melt crystallization	Cold crystallization
T_{m0} (°C)	340	340
K_{01} (min ⁻³)	$1.1 \cdot 10^{14}$	$1.3 \cdot 10^{12}$
K_{02} (min ⁻¹)	$1.1 \cdot 10^4$	$3.0 \cdot 10^3$
K_{g1} (K ²)	$3.6 \cdot 10^5$	$2.7 \cdot 10^5$
K_{g2} (K ²)	$3.5 \cdot 10^5$	$2.7 \cdot 10^5$
U^* (J.mol ⁻¹)	$4.7 \cdot 10^3$	$4.7 \cdot 10^3$
a_1 (K ⁻¹)	$-3.3 \cdot 10^{-3}$	$-4.8 \cdot 10^{-3}$
b_1	2.2	2.9

Table II.2 : Parameters of the kinetic models for the crystallization rate constants (K_1 and K_2) and the weight factor (w_1) for neat PEKK 6002 crystallization from the melt and cold crystallization

From modelling of the kinetic constants K_1 and K_2 (Fig. II.15) and the weight factors w_1 (Fig. II.16) depending on temperature, the evolution of the relative crystallinity depending on time for any crystallization temperature can be plotted with the modified Hillier model (Equation II.5) for the overall crystallization process as well as for the separated primary and secondary crystallizations. Fig. II.17 shows the plot of the modified Hillier model for the overall crystallization, the primary and secondary crystallizations at 200°C, 230°C and 260°C for crystallization from the melt. It can be observed that at the beginning of crystallization, the curves of overall crystallization and primary crystallization are confounded which shows that crystallization starts with the primary crystallization growth. Then, the secondary crystallization occurs with a lower crystallization kinetics corresponding to the enhancement of the primary crystallization with the growth of a second crystalline structure within lamellae. As it was observed for the crystallization weight factor, the proportion of the secondary crystallization process increases with the annealing temperature which shows that the secondary crystallization is favored for high crystallization temperatures. We can notice that at 260°C the proportion of the secondary crystallization is more important than for the primary crystallization ($w_1 < w_2$).



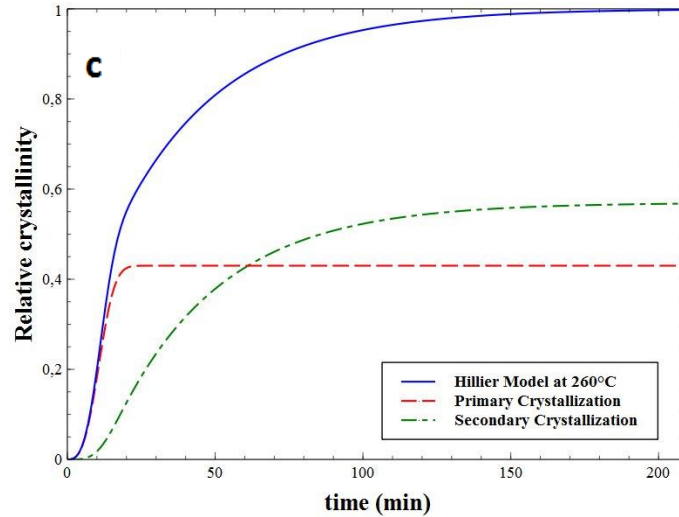
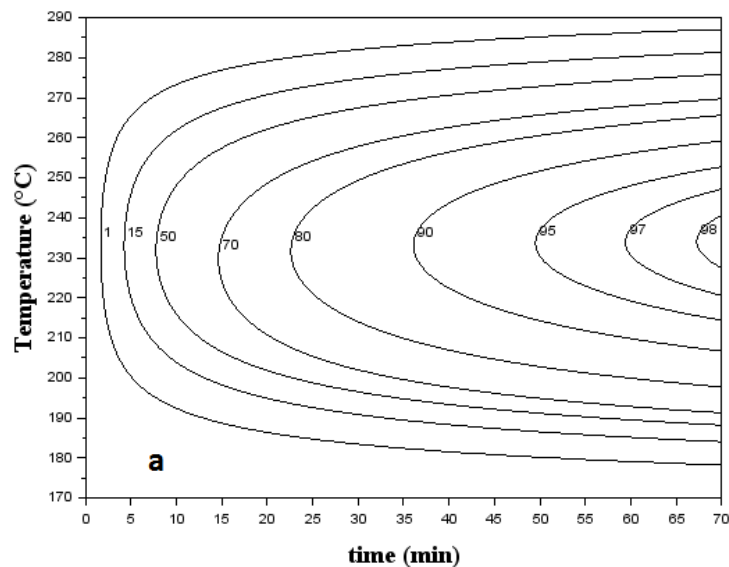


Fig. II.17 : Relative fraction crystallinity $\alpha(t)$ vs time with the Hillier model for the overall crystallization (solid curves), the primary (dashed curves) and the secondary crystallization (dashed dotted curves) at 200°C (a), 230°C (b) and 260°C (c) for neat PEKK 6002 crystallized from the melt

As the relative crystallinity of PEKK 6002 depending on time can be determined for any temperatures with the modified Hillier model, Time Transformation Temperature diagrams of the relative volume fraction crystallinity for the overall crystallization (Fig. II.18.a), for the separated primary (Fig. II.18.b) and the secondary crystallization (Fig. II.18.c) have been built. This kind of representation allows determining the crystallinity of the material for any isothermal crystallization process as well as corresponding crystallinity ratios of each crystallization mechanism. As expected, crystallization kinetics are the most important for temperatures around 240°C and become very slow close to the glass transition and the melting temperature. For instance, Fig. II.18.a shows that around 240°C, it takes approximately 55 minutes to reach 95% of the relative crystallinity whereas the last 5% takes more than 45 minutes to be achieved. This is consistent with the fact that the first crystallization mechanism is fast compared to the secondary stage. As it has been shown previously, the secondary crystallization process is promoted for high annealing temperatures (Fig. II.18.c) which is the opposite for the primary crystallization (Fig. II.18.b).



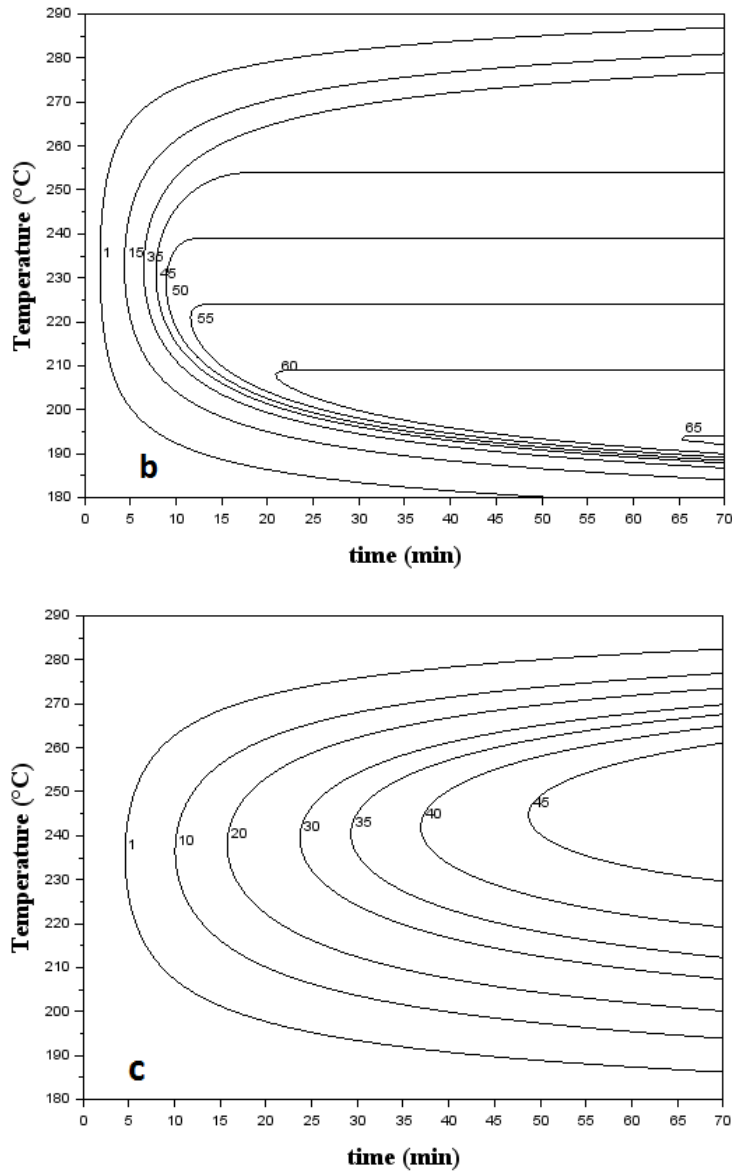


Fig. II.18: TTT diagram of the relative crystallinity for the overall crystallization (a), the primary crystallization (b) and the secondary crystallization (c) for neat PEKK 6002 crystallized from the melt

As for crystallization from the melt, the Time Temperature Transformation diagram of PEKK 6002 crystallized from the glassy state has been built and plotted in Fig. II.19. As expected, it can be noticed that the crystallization kinetics of PEKK 6002 crystallized from the glassy state is higher than for crystallization from the melting state.

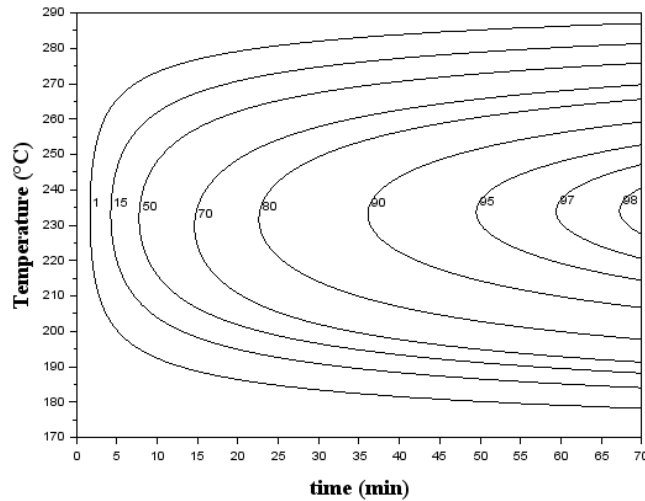


Fig. II.19 : TTT diagram of the relative crystallinity for the overall crystallization for neat PEKK 6002 crystallized from the glassy state

II.3.2.7 Comparison of crystallization kinetics between PEKK 6002 and PEKK 7002

The crystallization kinetics of PEKK 7002 has also been studied to validate the derivative Hillier model on a PEKK copolymer which crystallizes faster than PEKK 6002 (Table II.1). The result of the fitting of the derivative Hillier model (Equation II.9) with the heat flow measured by DSC for PEKK 7002 isothermal crystallization at 250°C is presented in Fig. II.20. The same primary crystallization Avrami exponent ($n_1=3$) as PEKK 6002 has been chosen for PEKK 7002 regarding optical microscopy observations. The same secondary crystallization Avrami exponent ($n_2=1$) as PEKK 6002 has also been used corresponding to the best fit of the derivative Hillier model with a multi linear regression fitting.

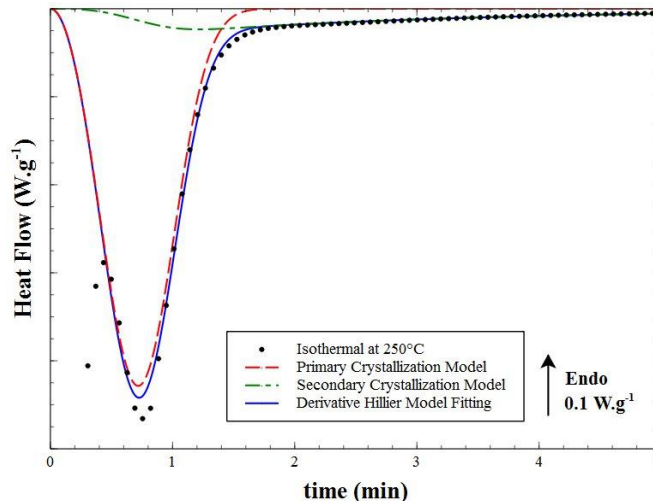


Fig. II.20 : DSC thermograms of neat PEKK 7002 crystallized from the melt at 250°C with the fitting of the derivative Hillier model (solid line) and the primary (dash curves) and secondary crystallization (dash-dot curves) modeling

In Fig. II.21 is compared the fitting of the derivative Hillier model with the heat flow measured by DSC for PEKK 6002 crystallized at 230°C and PEKK 7002 at 250°C. These temperatures correspond to the temperatures where the crystallization kinetics of PEKK 6002 and 7002 are the highest. It can be observed that even if the crystallization peak for PEKK 7002 is very

narrow compared to PEKK 6002 (Fig. II.21), the derivative Hillier model fits well with experiments and allows rebuilding the crystallization peak beginning.

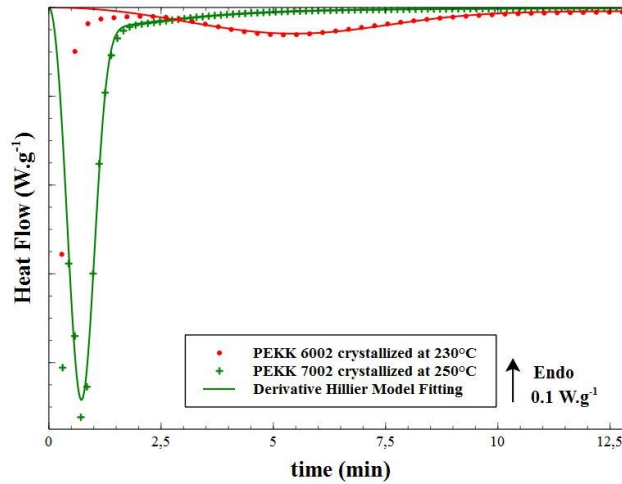
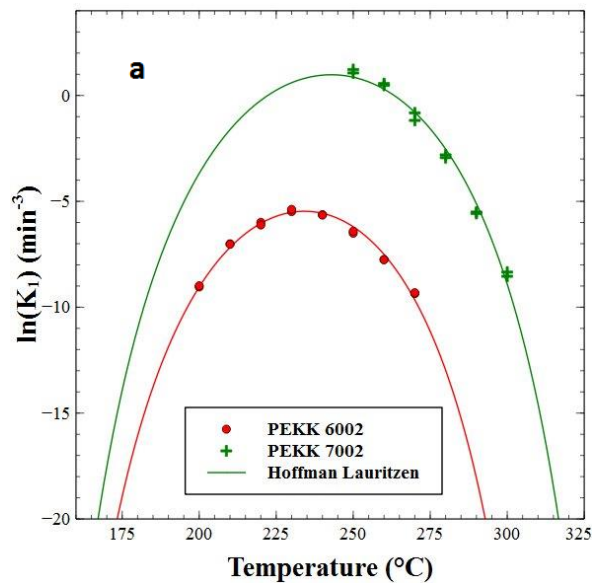


Fig. II.21 : Comparison of the fitting of the derivative Hillier model for neat PEKK 6002 and PEKK 7002

The comparison of the logarithm of the Hillier parameters K_1 and K_2 for PEKK 6002 and PEKK 7002 have been plotted in Fig. II.22 and fitted with the Hoffman and Lauritzen model (respectively Equation II.17 and Equation II.18). Compared to PEKK 6002, it was not possible to carry out isothermal crystallization measurements over a large temperature range but only until 260°C. As PEKK 7002 crystallizes very fast, below this temperature the polymer crystallizes before the crystallization temperature. A solution could have been to use a flash DSC to reach lower crystallization temperatures as it was done by Tardif et al. [50] for PEEK (although this tool implies very small samples which could not be representative for a crystallization process in volume). Results for K_{0i} and K_{gi} are presented in Table II.3. As expected crystallization kinetics parameters K_1 and K_2 are much higher for PEKK 7002 than for PEKK 6002. PEKK 7002 crystallization kinetics is the most important around 245°C.



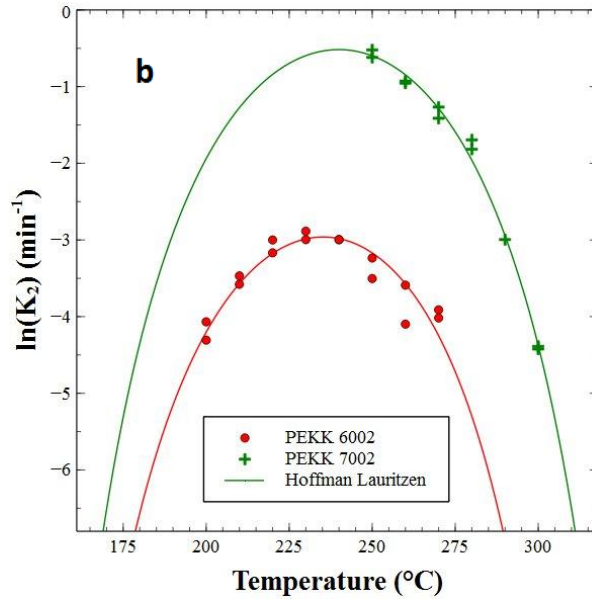


Fig. II.22 : Logarithmic plot of the primary (a) and the secondary crystallization (b) rate constants vs temperature for neat PEKK 6002 and 7002 isothermal crystallization from the melt with the Hoffman and Lauritzen model fitting

The primary crystallization weight factor (w_1) for PEKK 6002 and 7002 has been plotted as a function of temperature in Fig. II.23 with the fitting of the linear model (Equation II.19). Results for a_1 and b_1 are presented in Table II.3. We observed that PEKK 7002 weight factor seems to be quasi constant as a function of temperature with a value of about 0,78. PEKK 7002 weight factors are higher than for PEKK 6002 which could be attributed to a more organized crystallization leaving less room to the growth of the secondary crystallization.

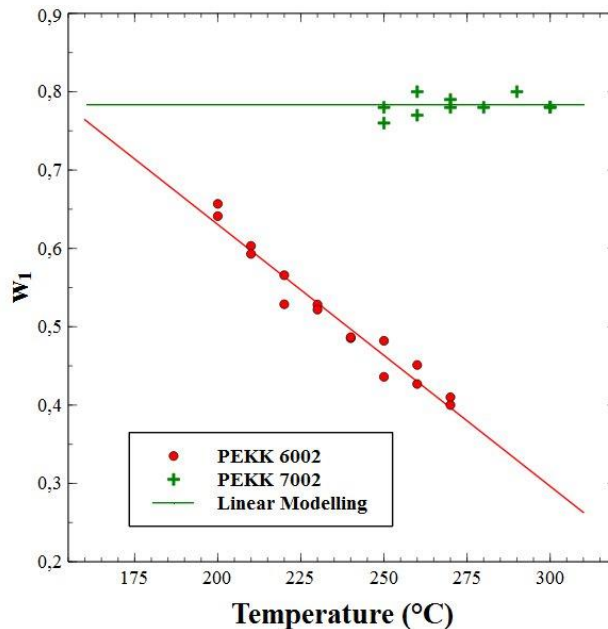


Fig. II.23 : Weight factor of the primary crystallization vs temperature for PEKK 6002 and 7002 isothermal crystallization from the melt with the linear model fitting

Kinetic parameters	PEKK 6002	PEKK 7002
T_{m0} (°C)	340	360
K_{01} (min ⁻³)	$1.1 \cdot 10^{14}$	$1.79 \cdot 10^{16}$
K_{02} (min ⁻¹)	$1.1 \cdot 10^4$	$2.6 \cdot 10^5$
K_{g1} (K ²)	$3.6 \cdot 10^5$	$4.0 \cdot 10^5$
K_{g2} (K ²)	$3.5 \cdot 10^5$	$4.4 \cdot 10^5$
U^* (J.mol ⁻¹)	$4.7 \cdot 10^3$	$4.7 \cdot 10^3$
a_1 (K ⁻¹)	$-3.3 \cdot 10^{-3}$	0
b_1	2.2	0.78

Table II.3 : Parameters of the kinetic models for the crystallization rate constants (K_1 and K_2) and the weight factor (w_1) for PEKK 6002 and 7002 crystallized from the melt

As for PEKK 6002, the TTT diagram of PEKK 7002 has been built and plotted in Fig. II.24. This TTT diagram shows the very fast crystallization kinetics of PEKK 7002. For example, it takes 10 minutes at 240°C for PEKK 7002 to fully crystallized.

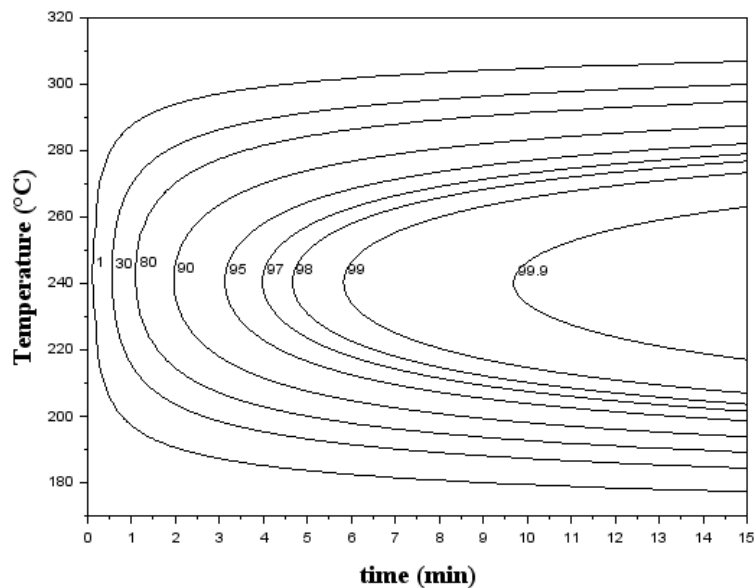


Fig. II.24 : TTT diagram of the relative crystallinity for the overall crystallization for PEKK 7002 crystallized from the melt

II.3.3 Non-isothermal crystallization kinetics

II.3.3.1 Extended derivative of Avrami model

The non-isothermal crystallization kinetics of PEKK has also been investigated to be able to predict the crystallinity for any processing cycle. Different models have been developed to model the non-isothermal crystallization kinetics of thermoplastics. All are extended from the Avrami equation (Equation II.2). The most widespread in the literature are the Ozawa [51] and the Nakamura [52] models. However, those two models don't take into account the

secondary crystallization. Velisaris and Seferis [37] and Cebe [53,54] used an integral Avrami expression to model the non-isothermal crystallization kinetics of PEEK taking into account the secondary crystallization. Nevertheless, those models are based on different empirical parameters which depend on the material. In this study, we propose a non-isothermal crystallization kinetics model based on the Hillier model taking into account primary and secondary crystallization applicable for any thermoplastics.

Non-isothermal crystallization cycles can be considered as a succession of small isotherms occurring at a temperature T as described in Fig. II.25. It is thus possible to determine the relative crystallinity for non-isothermal crystallization by summing up the relative crystallinity formed during each isotherm [41,55,56].

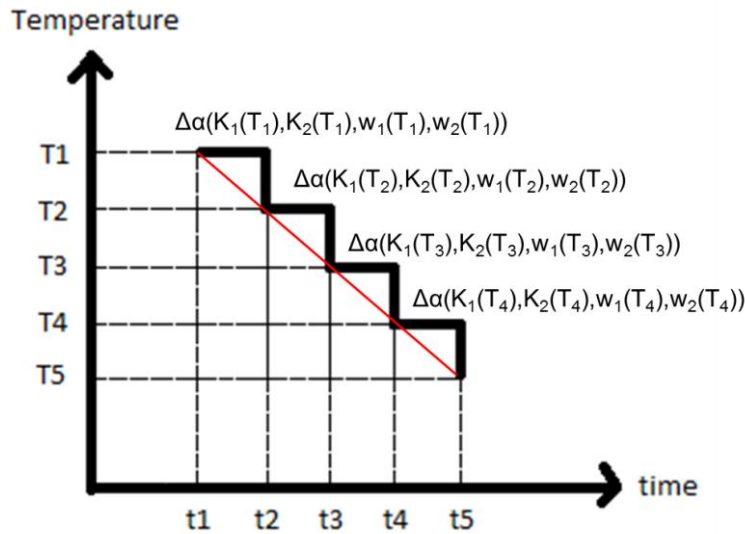


Fig. II.25 : Diagram of the decomposition of a non-isothermal crystallization cycle by small isotherms

For isothermal crystallization conditions, the transformation rate for the primary crystallization (Equation II.2) can be expressed by:

$$\frac{d\alpha_1}{dt} = K_1 n_1 t^{n_1-1} \exp(-K_1 t^{n_1}) \quad \text{Equation II.20}$$

From Equation II.2, it comes:

$$t = \left(-\frac{\ln(1-\alpha_1)}{K_1(T)} \right)^{\frac{1}{n_1}} \quad \text{Equation II.21}$$

By replacing t from Equation II.21, the derivative of $\alpha_1(t)$ can be written:

$$\frac{d\alpha_1}{dt} = n_1 K_1^{\frac{1}{n_1}} \left\{ -\ln[1-\alpha_1(t)] \right\}^{\frac{n_1-1}{n_1}} [1-\alpha_1(t)] \quad \text{Equation II.22}$$

Equation II.22 corresponds to the Avrami derivative model proposed by Patel and Spruiell [55] for any cooling rate.

As well as for the primary crystallization, the derivative of the secondary crystallization kinetics equation α_2 (Equation II.3) with $n_2=1$ can be expressed by:

$$\frac{d\alpha_2}{dt} = K_2 \left[1 - \exp(-K_1 t^{n_1}) \right] - K_2^2 \int_0^t \left[1 - \exp(-K_1 \theta^{n_1}) \right] \exp[-K_2(t-\theta)] d\theta \quad \text{Equation II.23}$$

By using Equation II.2 and Equation II.3, Equation II.23 can be simplified by:

$$\frac{d\alpha_2}{dt} = K_2 [\alpha_1(t) - \alpha_2(t)] \quad \text{Equation II.24}$$

Finally, from Equation II.4, Equation II.22 and Equation II.24, the derivative model proposed by Patel and Spruiell extended to the secondary crystallization from the Hillier model can be expressed by:

$$\frac{d\alpha}{dt} = w_1 n_1 K_1 \frac{1}{n_1} \left\{ -\ln[1 - \alpha_1(t)] \right\}^{\frac{n_1-1}{n_1}} [1 - \alpha_1(t)] + w_2 K_2 [\alpha_1(t) - \alpha_2(t)] \quad \text{Equation II.25}$$

with $w_1 + w_2 = 1$.

II.3.3.2 Numerical scheme for non-isothermal crystallization

According to the non-isothermal crystallization kinetic principle (Fig. II.25), the relative crystallinity is determined by solving Equation II.25 for each isotherm at a temperature T. A first approach is to use the explicit Euler method expressed by:

$$\alpha(t + \Delta t, T) = \alpha(t, T) + f(\alpha(t, T)) \Delta t \quad \text{Equation II.26}$$

where $\alpha(t, T)$ is the relative crystallinity at time t, $\alpha(t + \Delta t, T)$ is the relative crystallinity at time t + Δt , $f(\alpha(t, T)) = \frac{d\alpha}{dt}$ and Δt is the time between t and t + Δt which has to be small enough to ensure Euler hypotheses.

However, if we consider a crystallization process without initial crystallinity, $\alpha_1(t=0, T) = 0$ and $\alpha_2(t=0, T) = 0$, $f(\alpha(t=0, T)) = 0$ and thus Equation II.26 cannot be solved. Another method is to solve Equation II.25 with the implicate Euler method expressed by:

$$\alpha(t + \Delta t, T) = \alpha(t, T) + f(\alpha(t + \Delta t, T)) \Delta t \quad \text{Equation II.27}$$

It is in this case, it is necessary to solve an equation to determine $\alpha_1(t + \Delta t, T)$ expressed by:

$$\alpha(t + \Delta t, T) - \alpha(t, T) - f(\alpha(t + \Delta t, T)) \Delta t = 0 \quad \text{Equation II.28}$$

Applicate to primary crystallization (Equation II.22), Equation II.28 is expressed by:

$$\alpha_1(t + \Delta t, T) - \alpha_1(t, T) - n_1 K_1(T) \frac{1}{n_1} \left\{ -\ln[1 - \alpha_1(t + \Delta t, T)] \right\}^{\frac{n_1-1}{n_1}} [1 - \alpha_1(t + \Delta t, T)] \Delta t = 0 \quad \text{Equation II.29}$$

where $K_1(T)$ is calculated with Equation II.17.

For the secondary crystallization (Equation II.24), Equation II.28 becomes:

$$\alpha_2(t + \Delta t, T) - \alpha_2(t, T) - K_2(T) [\alpha_1(t + \Delta t, T) - \alpha_2(t + \Delta t, T)] \Delta t = 0 \quad \text{Equation II.30}$$

where $K_1(T)$ and $K_2(T)$ are calculated with Equation II.17 and Equation II.18 respectively and $\alpha_1(t+\Delta t)$ is the relative crystallinity determined by solving Equation II.29.

Finally, the total crystallinity for each isotherm at a temperature T is equal to:

$$\alpha(t + \Delta t, T) = w_1(T) \alpha_1(t + \Delta t, T) + w_2(T) \alpha_2(t + \Delta t, T) \quad \text{Equation II.31}$$

where $\alpha_1(t+\Delta t, T)$ and $\alpha_2(t+\Delta t, T)$ are determined by solving Equation II.29 and Equation II.30 respectively and $w_1(T)$ and $w_2(T)$ are calculated with Equation II.19.

To pass from a temperature T_1 to a very close temperature T_2 , the continuity equations for the primary and the secondary crystallization as followed respectively have to be used:

$$w_1(T_1) \alpha_1(t, T_1) = w_1(T_2) \alpha_1(t, T_2) \quad \text{Equation II.32}$$

$$w_2(T_1) \alpha_2(t, T_1) = w_2(T_2) \alpha_2(t, T_2) \quad \text{Equation II.33}$$

Form Equation II.32, $\alpha_1(t+\Delta t, T_2)$ is calculated by replacing $\alpha_1(t, T)$ in Equation II.29 with:

$$\alpha_1(t, T_2) = \frac{w_1(T_1) \alpha_1(t, T_1)}{w_1(T_2)} \quad \text{Equation II.34}$$

From Equation II.33, $\alpha_2(t+\Delta t, T_2)$ is calculated by replacing $\alpha_2(t, T)$ in Equation II.30 with:

$$\alpha_2(t, T_2) = \frac{w_2(T_1) \alpha_2(t, T_1)}{w_2(T_2)} \quad \text{Equation II.35}$$

Finally, the total relative crystallinity $\alpha(t+\Delta t, T_2)$ is calculated with Equation II.31 with $T=T_2$.

II.3.3.3 Comparison of the non-isothermal crystallization kinetics of PEKK 6002 and PEKK 7002

From the non-isothermal kinetic modelling presented in paragraph II.3.3.2 applicate to PEKK 6002 and PEKK 7002 and with isothermal crystallization kinetics parameters identified in Table II.3, the evolution of the relative crystallinity modelling as function of temperature for different cooling rates compared to experimental measurements carried out by DSC are presented in Fig. II.26.

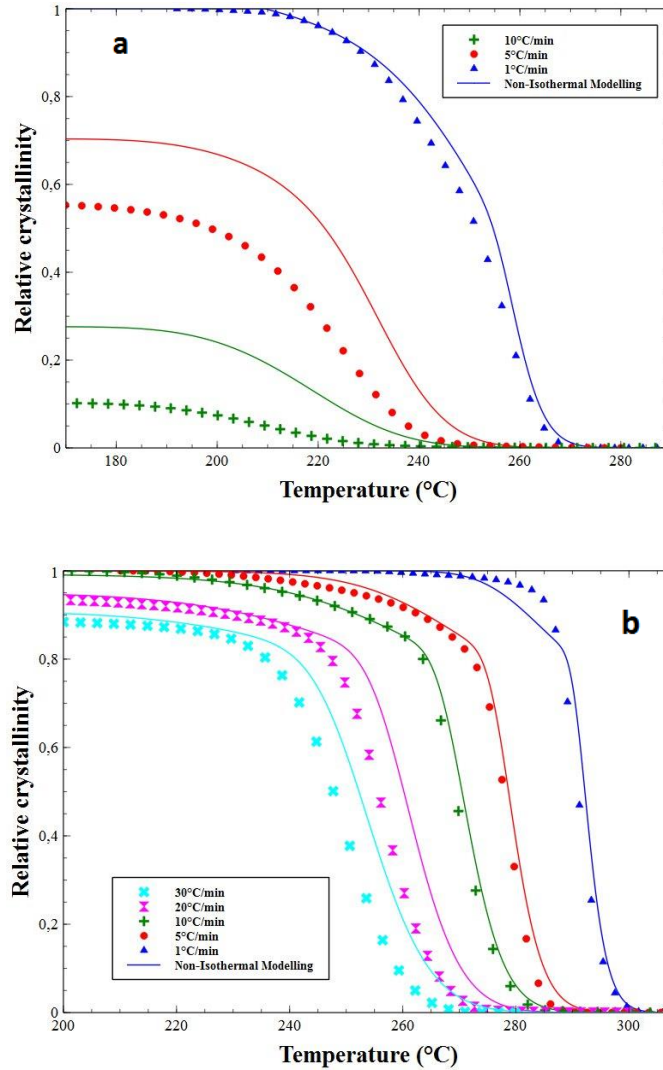


Fig. II.26 : Relative crystallinity $\alpha(t)$ vs temperature for neat PEKK 6002 (a) and 7002 (b) crystallized from the melt at different cooling rates with the modified non-isothermal crystallization kinetics modelling

It can be observed for both PEKK 6002 and PEKK 7002 that the non-isothermal crystallization kinetic modelling is overpredicting the experimental results and this phenomenon is more pronounced for high cooling rates. This observation has already been reported by different authors in the literature [41,55–57] and explained by the fact that the Patel and Spruiell model would not account for the induction (lag) time for nucleation. As for isothermal induction time reported for the first approach in paragraph II.3.2.3, the origin of this non-isothermal induction time has no real physical background and has the function to take into account a delay of the crystallization beginning to better fit data with physical models. As the induction time can only be measured for isothermal crystallization, Chan et al. [56] and Kenny et al. [41] calculated the non-isothermal induction time from the measured isothermal induction times according to the following equation:

$$t_{i,non-iso} = \int_0^t \frac{dt}{t_{i,iso}(T)} \quad \text{Equation II.36}$$

where $t_{i,iso}$ is the isothermal induction time as a function of temperature.

We rather think that this phenomenon is due to the iso-kinetic hypothesis assuming that the nucleation and the growth kinetics are proportional which could not be fully true for non-isothermal crystallization. Then, we modified the Hoffman and Lauritzen parameters for the primary crystallization process identified for isothermal crystallization in Table II.3 to have a better correspondence between the non-isothermal crystallization kinetics modelling and experiments. Results of the non-isothermal crystallization modelling with the modified kinetics parameters are presented for PEKK 6002 and 7002 in Fig. II.27.a and Fig. II.27.b respectively. The modified kinetics parameters are presented in Table II.4 and the plots of the modified Hoffman and Lauritzen curves with those new parameters for PEKK 6002 and 7002 are presented in Fig. II.28.a and Fig. II.28.b respectively.

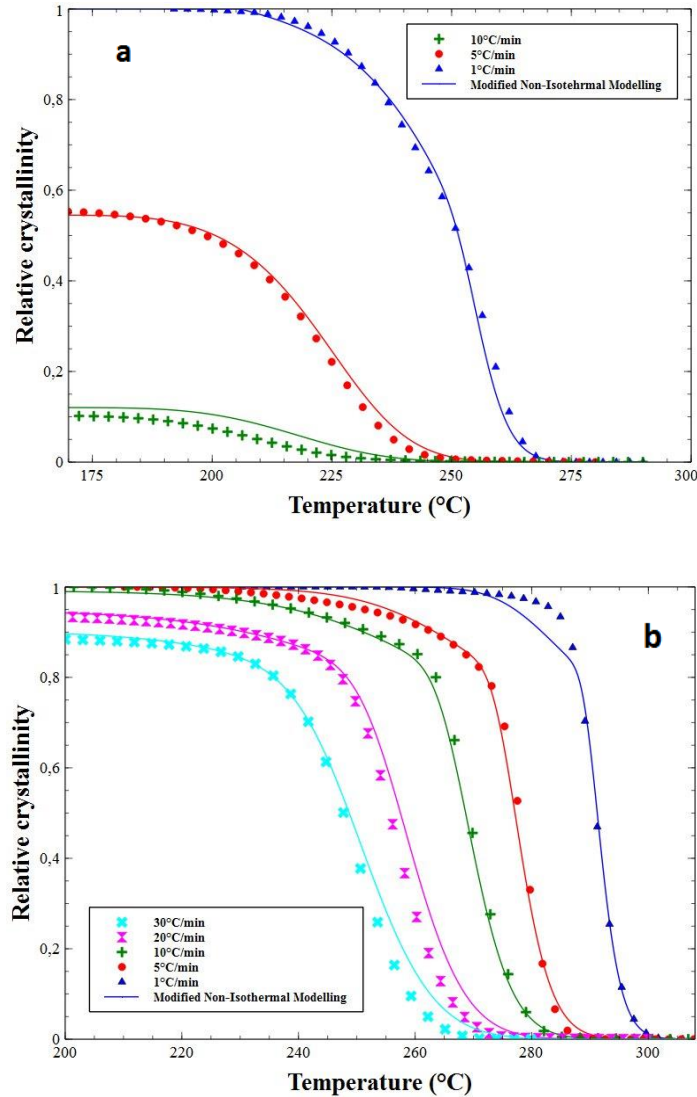


Fig. II.27 : Relative crystallinity $\alpha(t)$ vs temperature for neat PEKK 6002 (a) and 7002 (b) crystallized from the melt at different cooling rates with the modified non-isothermal crystallization kinetics modelling

It can be observed a good agreement for the different cooling rates between the non-isothermal modelling and experiments for PEKK 6002 and PEKK 7002 which validates this new method for the non-isothermal crystallization kinetics modelling. A small discrepancy between data and modelling occurs at low cooling rate (1°C/min) and high conversion rate. In fact, the crystallization kinetics modelling is lower than experiments at the end of crystallization which might be due to too low w_1 at high temperatures (above 270°C). This

means that $w_1(T)$ is probably not constant for PEKK 7002 (see Fig. II.23). To identify this phenomenon, isothermal at temperatures between 280°C and 300°C should have been done, but it is very difficult to do such experiments at so low crystallization kinetics.

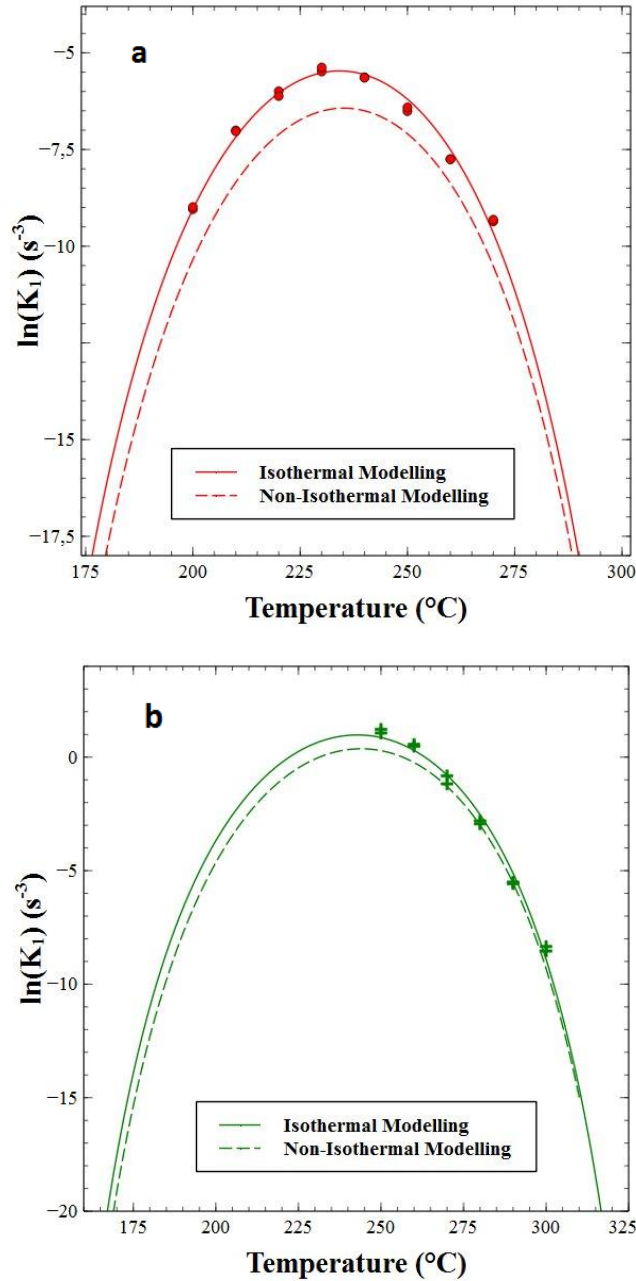


Fig. II.28 : Comparison of the Hoffman and Lauritzen plots with isothermal and non-isothermal crystallization kinetics parameters for neat PEKK 6002 (a) and PEKK 7002 (b) crystallized from the melt

By modifying the crystallization kinetics parameters, the Hoffman and Lauritzen curve is shifted to the bottom decreasing the non-isothermal crystallization kinetics modelling.

Hoffman and Lauritzen parameters	PEKK 6002		PEKK 7002	
	Isothermal	Non-Isothermal	Isothermal	Non-Isothermal
K_{01} (min^{-3})	$1.1 \cdot 10^{14}$	$1.2 \cdot 10^{14}$	$1.79 \cdot 10^{16}$	$1.79 \cdot 10^{16}$
K_{g1} (K^2)	$3.60 \cdot 10^5$	$3.65 \cdot 10^5$	$4.0 \cdot 10^5$	$4.0 \cdot 10^5$
U^* ($\text{J} \cdot \text{mol}^{-1}$)	$4.70 \cdot 10^3$	$4.95 \cdot 10^3$	$4.7 \cdot 10^3$	$4.9 \cdot 10^3$

Table II.4 : Isothermal and non-isothermal crystallization kinetics parameters for PEKK 6002 and 7002 crystallized from the melt

Crystallization peaks for an isothermal crystallization at 230°C from the melt modeled with the identified isothermal and non-isothermal crystallization kinetics parameters (Table II.4) have been plotted in Fig. II.29.

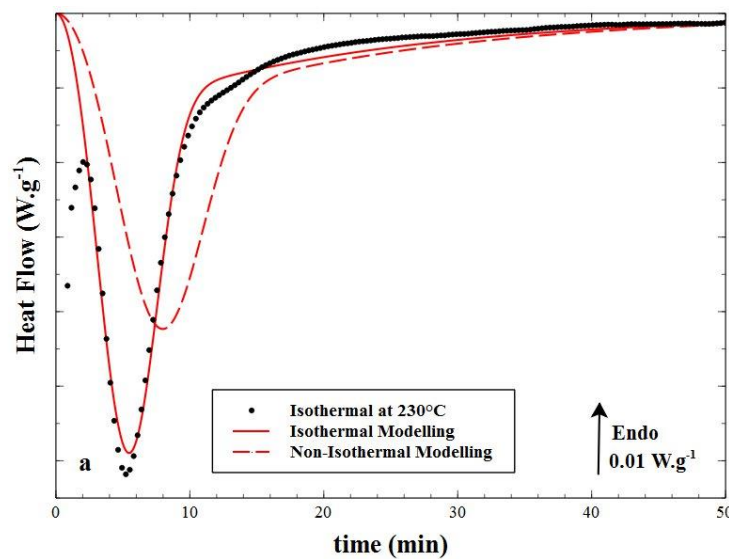


Fig. II.29 : Comparison of the isothermal crystallization peak modelling for crystallization at 230°C from the melt for isothermal and non-isothermal kinetics parameters

It can be observed that the two crystallization peaks modelling are very different whereas the Hoffman Lauritzen modelling of K_1 for non-isothermal crystallization (Fig. II.28) was just shown to be slightly shifted to lower kinetics compared to isothermal crystallization. In other words, the differences between the grow rate modeling in Fig. II.27 could not be due to experimental dispersions.

II.4 INFLUENCE OF CRYSTALLIZATION ON THE MATRIX MECHANICAL PROPERTIES

In this part, we have been carried out experiments to identify the influence of the crystallinity on the mechanical properties of PEKK.

II.4.1 Crystallinity measurement of PEKK plates

DSC measurements were carried out on PEKK plates crystallized with different thermal conditions in which tensile samples were machined to associate the mechanical properties to the crystallization conditions. For example, in Fig. II.30 is plotted the crystallinity of PEKK 6002 plates crystallized at 230°C from the glassy state as a function of the crystallization

time compared to the Hillier modelling drawn with identified parameters in II.3.2.6 corresponding to the same crystallization conditions. It can be observed a good agreement between the Hillier modelling the experimental points which validates the ability of our modelling to predict the crystallinity depending on the crystallization conditions.

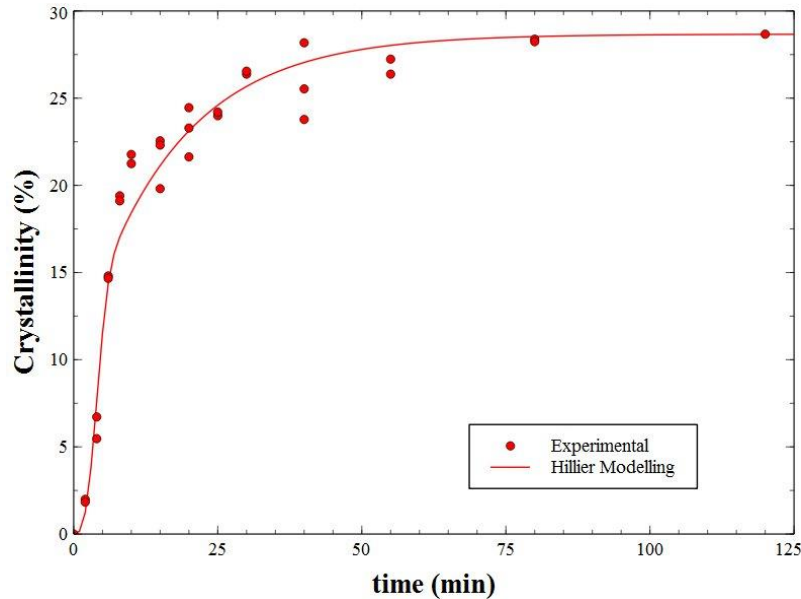


Fig. II.30 : Comparison between the crystallinity of PEKK 6002 plates crystallized at 230°C from the glassy state during different times and the Hillier modelling

II.4.2 Influence of crystallinity on PEKK matrix mechanical properties

II.4.2.1 Dynamic Mechanical Analysis

DMA experiments were first carried out on fully crystallized PEKK samples to investigate the evolution of the mechanical properties with temperature. Results of the storage modulus as a function of the temperature for fully crystallized PEKK 6002, PEKK 7002 and PEKK 8002 are presented in Fig. II.31. For all, the storage modulus is quasi constant until T_g where it collapses until another plateau. The storage modulus of the first plateau is around 3 GPa and the glass transition was measured around 155°C. Above T_g the amorphous phase of the polymer is in a rubbery state which explains very low moduli in this temperature range.

It can be observed that for temperatures below T_g , the storage modulus for the three materials are very close whereas above T_g , a strong difference between them can be noticed. PEKK 8002 has the highest storage modulus, followed by PEKK 7002 and finally PEKK 6002. This phenomenon is attributed to the fact that they have different maximum crystallinity. At 230°C, PEKK 8002 crystallized with 38%, PEKK 7002 with 33% and PEKK 6002 with 28% which explains that PEKK 8002 has a higher storage modulus than PEKK 7002 and that PEKK 7002 has a higher storage modulus than PEKK 6002. Above T_g , it is the crystalline phase which gives the mechanical strength to the matrix which explains a more important difference between the storage modulus of three PEKK matrices above T_g .

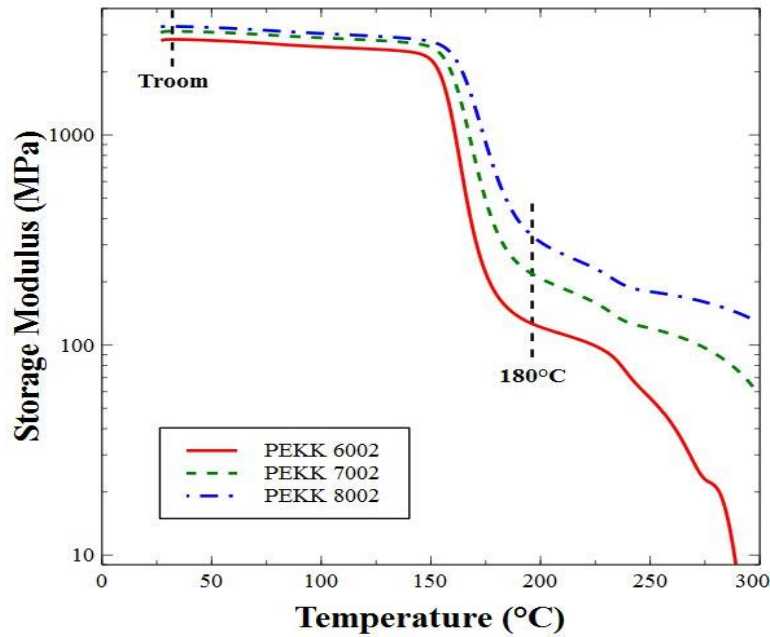


Fig. II.31 : Storage modulus vs temperature for fully crystallized at 230°C from the glassy state PEKK 6002, PEKK 7002 and PEKK 8002

In the next paragraph, tensile tests were carried out at room temperature and at 180°C (above T_g) to understand the impact of crystallinity on the mechanical properties.

II.4.2.2 Tensile tests

II.4.2.2.1 Tensile tests at room temperature

In Fig. II.32, the evolution of the stress as a function of the strain for amorphous and fully crystallized PEKK 6002 tensile specimens tested at room temperature is presented. For both, at the beginning of the test, stresses rise rapidly until the stress at yield corresponding to the elastic domain. It can be observed a higher stress at yield for the fully crystallized specimen compared to the amorphous one. A higher Young modulus were also measured for fully crystallized PEKK specimen which is consistent with the literature [3,5–8]. Then, the stress drops corresponding to the decrease of the section over all the specimen length. Finally, the fully crystallized specimen breaks around 50% whereas the amorphous specimen stress increases of about 40 MPa from 100% until 185%. This phenomenon called strain hardening is well known for thermoplastic polymers and is attributed to the alignment of the macromolecular chains in the direction of the stress (up to a “so called” strain induced crystallization) increasing the material strength in the stress direction.[4,58–60]. To conclude, regarding those two curves, it can be assumed that crystallization increases elastic mechanical properties but makes the matrix more brittle. It also means that amorphous PEKK 6002 in the glassy state is not fragile and the ductile-fragile transition is below ambient temperature for the considered strain rates.

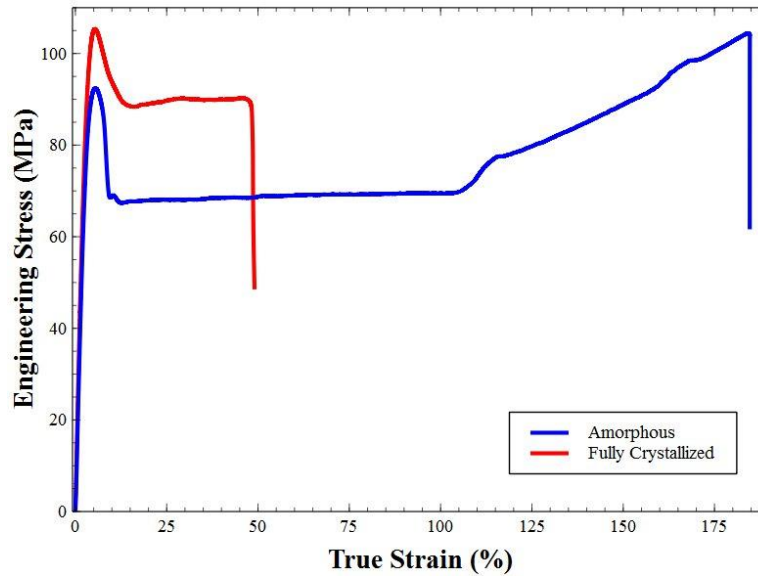


Fig. II.32 : Tensile measurements of amorphous and fully crystallized at 230°C from the glassy state neat PEKK 6002 tested at room temperature

Same tests as in Fig. II.32 were carried out on specimens with different crystallinities to investigate the evolution of PEKK mechanical properties regarding crystallinity. The change of the Young modulus, the stress at yield and the strain at break as a function of crystallinity for tensile tests carried out at room temperature are presented in Fig. II.33, Fig. II.34 and Fig. II.35 respectively. We can observe that the Young modulus and the stress at yield increases linearly with crystallinity whereas there is a drop of the strain at break at around 22% of crystallinity which collapses from 130% to 50%. As the maximum crystallinity of PEKK 8002 and 7002 is more important than for PEKK 6002, their Young moduli are higher.

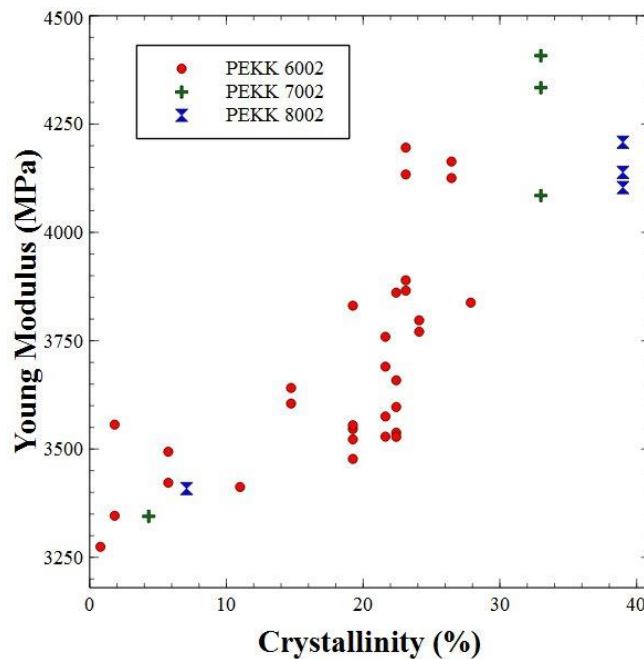


Fig. II.33 : Young modulus vs crystallinity at room temperature of neat PEKK crystallized at 230°C from the glassy state

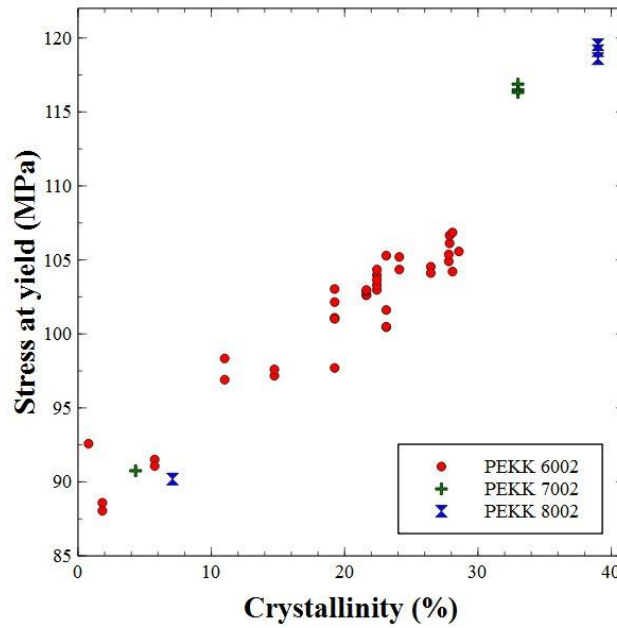


Fig. II.34 : Stress at yield vs crystallinity at room temperature of neat PEKK crystallized at 230°C from the glassy state

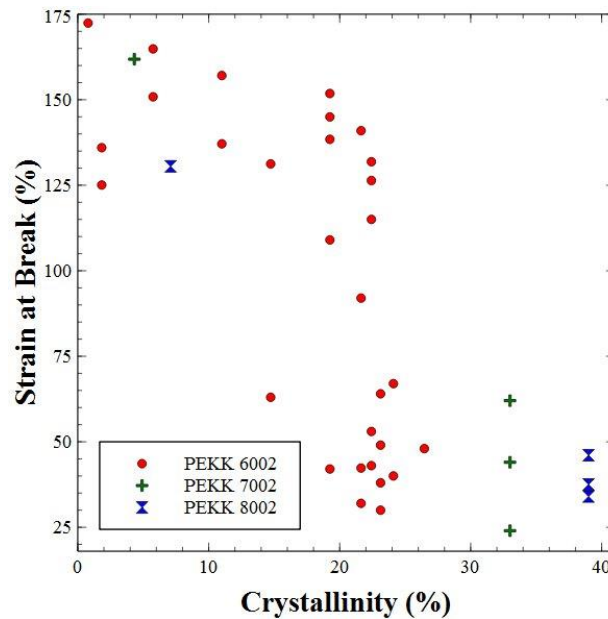


Fig. II.35 : Strain at break vs crystallinity at room temperature of neat PEKK crystallized at 230°C from the glassy state

II.4.2.2.2 Tensile tests at 180°C

In Fig. II.36, the evolution of the stress as a function of the strain for amorphous and fully crystallized PEKK 6002 tensile specimens tested at 180°C (above T_g) is presented. It can be observed much lower stress compared to test at room temperature which is due to the fact that at 180°C, the amorphous phase is in a rubbery state. It was noticed a strong difference between those two specimens which is consistent with DMA results. In fact, above T_g , the crystallinity has a strong impact on the mechanical properties. Strain hardening was observed for both specimens (not observable for the amorphous specimen in Fig. II.36).

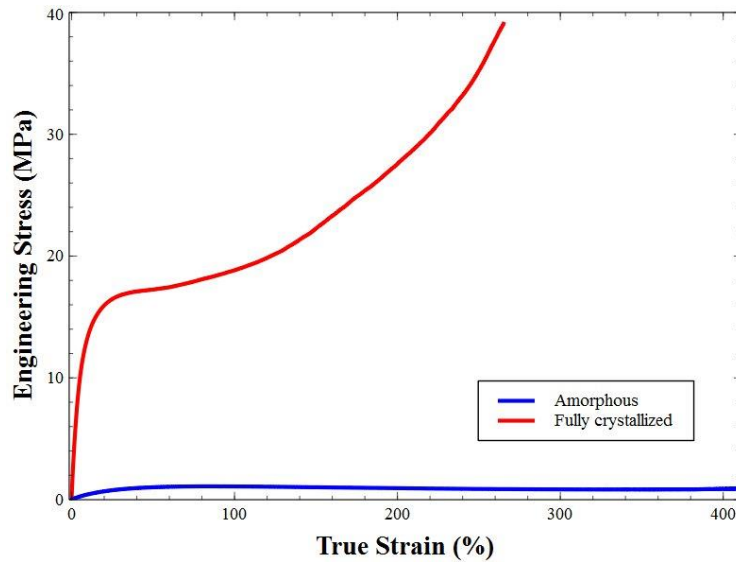


Fig. II.36 : Tensile measurements of amorphous and fully crystallized at 230°C from the glassy state neat PEKK 6002 tested at 180°C with a strain rate of 3.3 s⁻¹

In Fig. II.37, Fig. II.38 and Fig. II.39, the change of the Young modulus and the stress at yield as a function of crystallinity for tensile tests at 180°C is presented. It can be observed that PEKK are more sensitive to crystallinity at 180°C than at room. In fact, above T_g , the amorphous phase is ductile and thus the mechanical properties of the polymer only depend on the crystalline phase. The highest Young modulus has been measured for PEKK 8002 due to a higher crystallinity. For this temperature test, high strains at break were not able to be measured due to the maximum tensile test machine displacement.

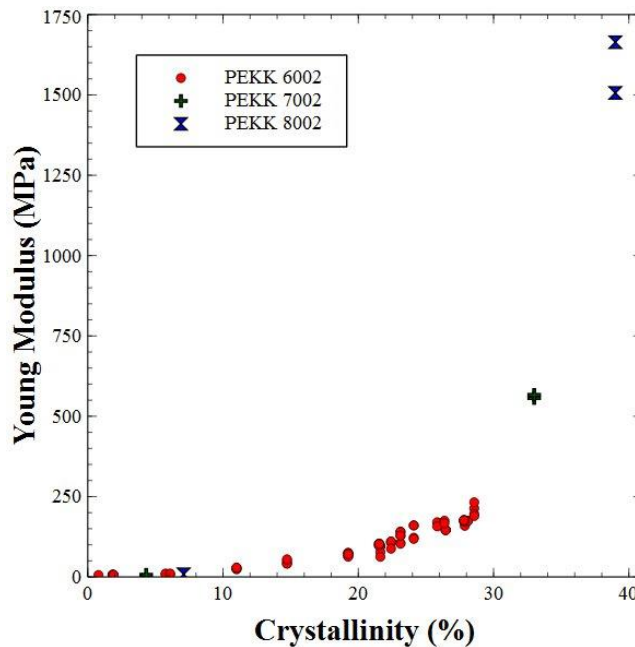


Fig. II.37 : Young modulus vs crystallinity at 180°C of neat PEKK crystallized at 230°C from the glassy state with a strain rate of 3.3 s⁻¹

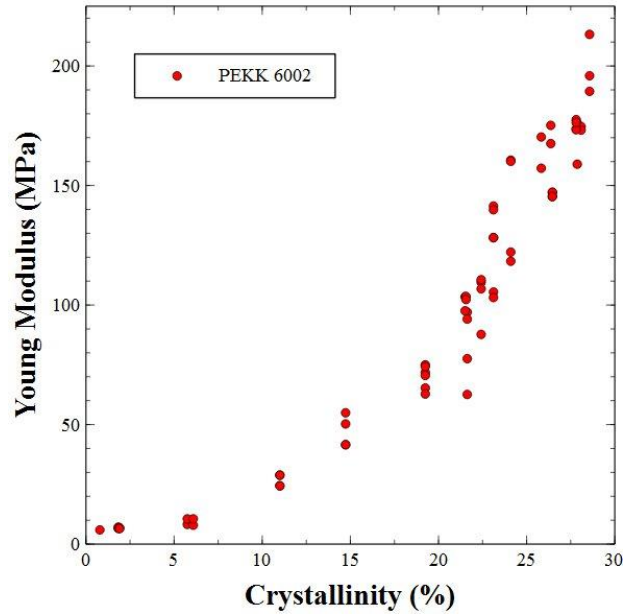


Fig. II.38 : Young modulus vs crystallinity at 180°C of neat PEKK 6002 crystallized at 230°C from the glassy state with a strain rate of 3.3 s⁻¹

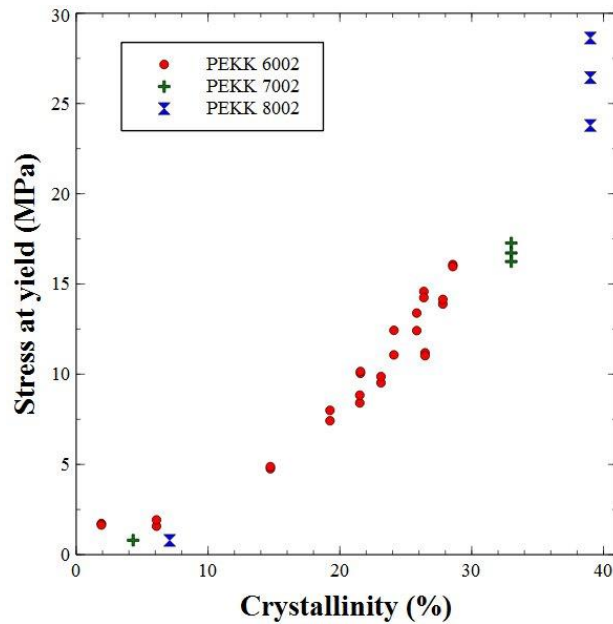


Fig. II.39 : Stress at yield vs crystallinity at 180°C of neat PEKK crystallized at 230°C from the glassy state with a strain rate of 3.3 s⁻¹

II.4.3 Influence of crystalline morphologies on PEKK 6002 mechanical properties

In this part, the effect of the crystallization temperature on the mechanical properties were carried out by testing PEKK 6002 specimens crystallized at 200°C, 230°C and 260°C from the glassy state and at 260°C from the melt. In fact, depending on the crystallization temperature the crystalline morphologies are not the same. Large spherulites were observed for crystallization at 260°C from the melt (Fig. II.7) whereas at 200°C from the glassy state, spherulites are too small to be observable by optical microscopy.

As the mechanical properties are less sensitive to crystallinity at room temperature than at 180°C, only results for tensile tests at 180°C are presented. In Fig. II.40 and Fig. II.41 is plotted the evolution of the Young modulus and the stress at yield depending on the crystallinity for specimens crystallized with different conditions. It can be observed that the influence of the crystallization conditions is more pronounced for the stress at yield than the Young modulus.

It seems that the Young modulus and the stress at yield for crystallization at 200°C are higher than for the other crystallization temperatures. Secondly, the results for crystallization at 230°C and 260°C are closed regarding the Young modulus. This could be due to the fact that for crystallization at 260°C, the polymer begins to crystallize during the heating until the crystallization temperature especially as the polymer passes through high crystallization kinetics temperatures around 240°C (Fig. II.15) and this is why we also investigate crystallization at 260°C from the melt. It can be observed that the Young modulus for crystallization at 260°C from the melt is close to crystallization at 200°C from the glassy state until 20% and then it stabilizes around 110 MPa. For the stress at yield, it is noticeable that it is less important for crystallization at 260°C from the melt. It could thus be assumed that above T_g , the presence of small spherulites (crystallization from the glassy state at temperatures close to T_g) enhances the elastic properties of PEKK matrices compared to large spherulites (crystallization from the melt at temperatures close to T_f). This is consistent with Kargin et al. [61] and Chan et al. articles [2] which showed that high nucleation density and thus small crystallites involve a more homogeneous crystalline structure and thus higher mechanical properties.

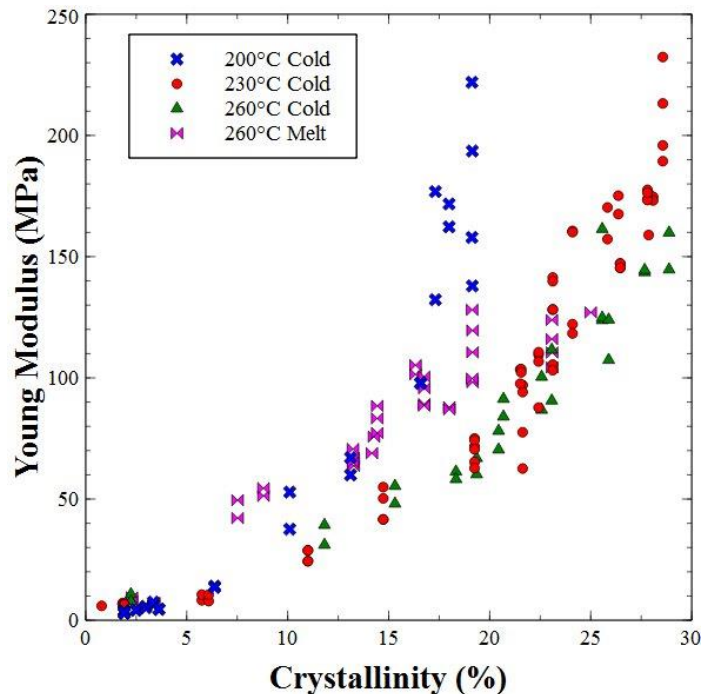


Fig. II.40 : Comparison of the evolution of the Young modulus vs crystallinity at 180°C of neat PEKK 6002 depending on the crystallization conditions with a strain rate of 3.3 s^{-1}

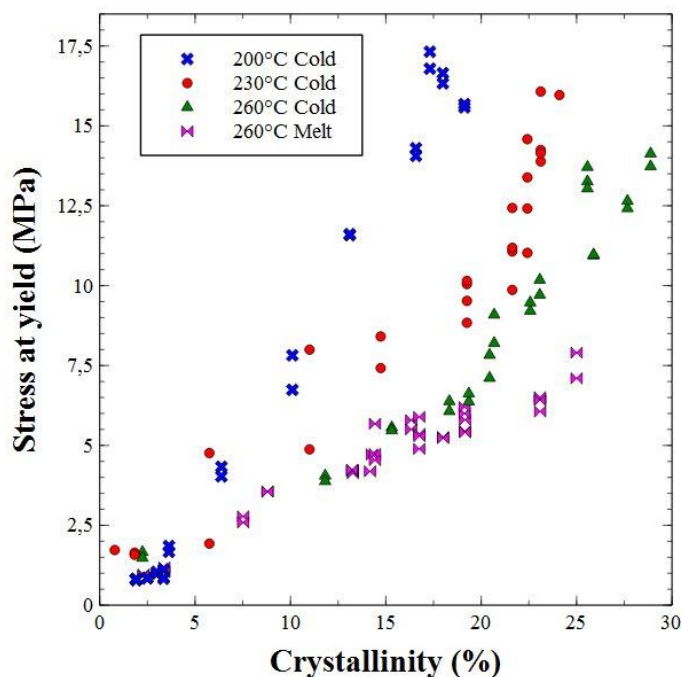


Fig. II.41 : Comparison of the evolution of the stress at yield vs crystallinity at 180°C of neat PEKK 6002 depending on the crystallization conditions with a strain rate of 3.3 s^{-1}

II.5 CONCLUSION

As reported in the literature, we have observed from optical microscopic and X-ray measurements that PEKK matrices crystallize with spherulitic growth and for low mobility crystallization conditions, they can crystallize with two different crystalline morphologies which have different unit cell dimensions. A secondary crystallization was identified with the apparition of an additional melting peak which corresponds to the melting of an interlamellar structure growing within crystalline lamellae. PEKK 6002 has the lowest melting temperature (around 305°C) and crystallizes much slowly than PEKK 7002 and 8002. It has also lower final crystallinity.

The modelling of PEKK crystallization kinetics were found to be difficult due to the secondary crystallization which has to be taken into account into the modelling and a truncation of all isothermal crystallization peaks beginning measured by DSC hindering the integration of the peaks and the fitting of crystallization models with experimental curves. To solve this problem, a new method has been established from the derivative of the Hillier isothermal crystallization kinetics model which can be fitted directly with the crystallization heat flow measured by DSC. Isothermal crystallizations kinetics of PEKK 6002 and 7002 crystallized from the glassy state and from the melt have been modelled with this method. Cold crystallization was shown to be faster than crystallization from the melt due to a lower final degree of crystallinity. PEKK 7002 was shown to crystallize much faster than PEKK 6002 with fast crystallization kinetics around 240°C. According to the linear modeling of the primary crystallization weight factor w_1 , the secondary mechanism was found to be enhanced for low degree of supercooling due to a high diffusion process. Isothermal Time Transformation Temperature (TTT) diagrams of the crystallinity have been built for PEKK 6002 and 7002 providing a useful tool for PEKK processing.

The derivative isothermal crystallization kinetics Hillier model has been established allowing the prediction of the non-isothermal crystallization kinetics of neat PEKK. This new modelling was observed to overpredict experimental results. This phenomenon was assumed to be attributed to the failure to comply isokinetics hypothesis for non-isothermal crystallization conditions. Hence, overall crystallization kinetics parameters were slightly modified to take it into account. Consequently good agreements were observed between experiments and modelling.

As expected, it has been shown that the Young modulus and the stress at yield increase with crystallinity whereas this is the opposite for the strain at break. This behavior is emphasized for testing temperatures above the glass transition as for those temperatures the amorphous phase is ductile and the mechanical properties of the polymer only depend on the crystalline phase. Finally, higher young modulus and stress at yield have been observed for low crystallization temperatures involving small spherulites which was attributed to a more homogeneous crystalline structure compared to large spherulites.

CHAPTER III. IMPACT OF TIME/TEMPERATURE PARAMETERS ON THE PROCESSING WINDOW

During thermal exposure, it is known that PEEK can be degraded by free radicals formation. These radicals, in lack of oxygen, can react with themselves and thus lead to a crosslinking by a termination process. Our first objective in this chapter is to check out if this crosslinking process occurs for PEKK and to assess the kinetic associated to this process as a function of temperature of exposure. A second objective is quantified these macromolecular modifications, model their apparition kinetics and finally their consequences on crystallization kinetics and mechanical properties. We mainly focused on anaerobic conditions, i.e. degradation under nitrogen. Indeed, from an applied point of view, the PEKK matrix can be also oxidized during consolidation phase in air. However, oxidation process is confined only at surface (~10 nm in depth) in contact with air during processing since oxidation is very fast compare to oxygen diffusion.

III.1 EXPERIMENTAL

III.1.1 Thermo-Gravimetric Analysis (TGA)

Thermogravimetric measurements were carried out on a TA Instruments Q500 equipped with a Gazmix system allowing monitoring the ratio between oxygen and nitrogen content of the atmosphere with a flow rate of 50 mL/min. Tests were made with an atmosphere containing 100% of nitrogen and a ratio of 21% of oxygen and 79% of nitrogen. For every test, PEKK 6002 amorphous granules of about 7-8 mg were introduced in a platinum nacelle. The weight loss of PEKK 6002 specimens was followed isothermally at 400°C during 15h and non-isothermally from room temperature to 900°C with a heating rate of 10°C/min.

III.1.2 Rheological measurements

Rheological properties of PEKK 6002 were measured with an Anton Paar MCR 502 rheometer under nitrogen for isothermal temperatures conditions. PEKK 6002 amorphous granules previously dried at 120°C during 48h were first introduced between 25 mm diameter aluminum parallel plates at the testing temperature and then crushed by the plates separated by a 1 mm gap. The melted polymer between plates was then deburred. After this step, the polymer is thermally stabilized at the testing temperature before the beginning of the test. This procedure was done the most rapidly has possible to neglect the possible modification of the polymer before the analysis. Sinusoidal deformation mode was used with a strain amplitude of 1% to stay in the viscoelastic linear domain and a frequency of 1 rad.s⁻¹ to carry out tests in the Newtonian domain.

III.1.3 Differential Scanning Calorimetry (DSC)

Isothermal crystallization analyses were carried out in a TA Instruments Q2000 on PEKK 6002 amorphous granules of about 7-8 mg previously heated at 400°C under nitrogen during 1h, 2h, 3h and 4h in the same TGA instrument presented in paragraph (III.1.1). Specimens were first heated at 10°C.min⁻¹ from room temperature to 360°C during 5 minutes. This temperature is above PEKK equilibrium melting temperatures [10] to erase the thermal history and obtain a fully amorphous polymer. Specimens were then cooled at 40°C.min⁻¹ to 230°C during 240 minutes and finally cooled at 40°C.min⁻¹ to room temperature. This cooling rate was high enough to make sure that the polymer does not crystallize before annealing

and the annealing time was long enough to allow the polymer to fully crystallize. Finally, a heat scan at $10^{\circ}\text{C}\cdot\text{min}^{-1}$ to 400°C was carried out to measure the glass transition, the melting temperature and the melting enthalpy induced by the crystallization cycle. The glass transition temperature was measured as the inflexion point.

III.1.4 Gel Permeation Chromatography (GPC)

GPC measurements were performed by Arkema Company on a Waters Alliance 2695 device with a Waters 2414 RID detector. Samples preparation and experimental conditions are confidential.

III.1.5 Mechanical tests

Mechanical tests were carried out with an extensometric tensile test machine Instron 5966 equipped with an oven to make tests at high temperature. Tests were done on normalized 1BA tensile samples (ISO 527) with length of 75 mm, width of 5 mm for the fitting length and a thickness of 2 mm machined from amorphous plates of $100\times 100\text{ mm}^2$ crystallized in an oven (see paragraph II.1.4.1). Plates were first dried at 120°C during 48h, heated above their melting temperature at 400°C during 1h, 2h, 3h and 4h and then cooled until 260°C during 4h to fully crystallize the polymer. A casing was used during the crystallization to keep the plate flat with the same dimensions. Plates were put in a complex environment described in paragraph II.1.4.1 due to a problem of bubbles apparition on the surface of plates. Specimens were tested at room temperature and 180°C (above T_g) with testing speed of $1\text{ mm}\cdot\text{min}^{-1}$ and $100\text{ mm}\cdot\text{min}^{-1}$ respectively. At 180°C , PEKK matrices are at the rubbery state and the testing speed must be high enough to measure entanglements network properties and not chain flow due to disentanglement. At this temperature, the crystallization kinetics is low enough to assume that the polymer do not crystallize during the test.

III.2 MACROMOLECULAR MODIFICATION MECHANISMS

During the consolidation of PEKK composite parts occurring at high temperature (around 360°C), PEKK matrices can evolve due to chemical transformation of the macromolecule chains. This modification could alter the matrices properties and consequently the final mechanical properties of the composite parts. It has been reported by different authors for PEEK [40,62–65,65–67] that it occurs at high temperature (around 400°C) in both nitrogen and air in an early stage due to crosslinking mechanisms of the macromolecular chains. This mechanism under nitrogen atmosphere is presented in Fig. III.1 [67]. It is initiated by scissions of macromolecular chains located in the carbonyl and ether bonds (Step 1), creating radicals which miss hydrogen molecules (Step 2). Day et al. suggested in a first article [63] that first scissions occurs at the carbonyl functional groups. In a second article [64] as for Tsai et al. [68], they assumed that chain scissions begin at the ether linkages. Other authors [62,66,68] made the assumption that they begin at the same time since activation energies of bond dissociations for ether and carbonyl linkages are very close. Radicals can then rearrange by removing hydrogen molecules from aromatics cycles forming phenyl radicals (P°) (Step 3), which can rearrange with an adjacent radical to produce crosslinks (Step 4). Another possibility for phenyl radical is to rearrange by internal combination, to produce dibenzofuran or fluorenone derivatives:

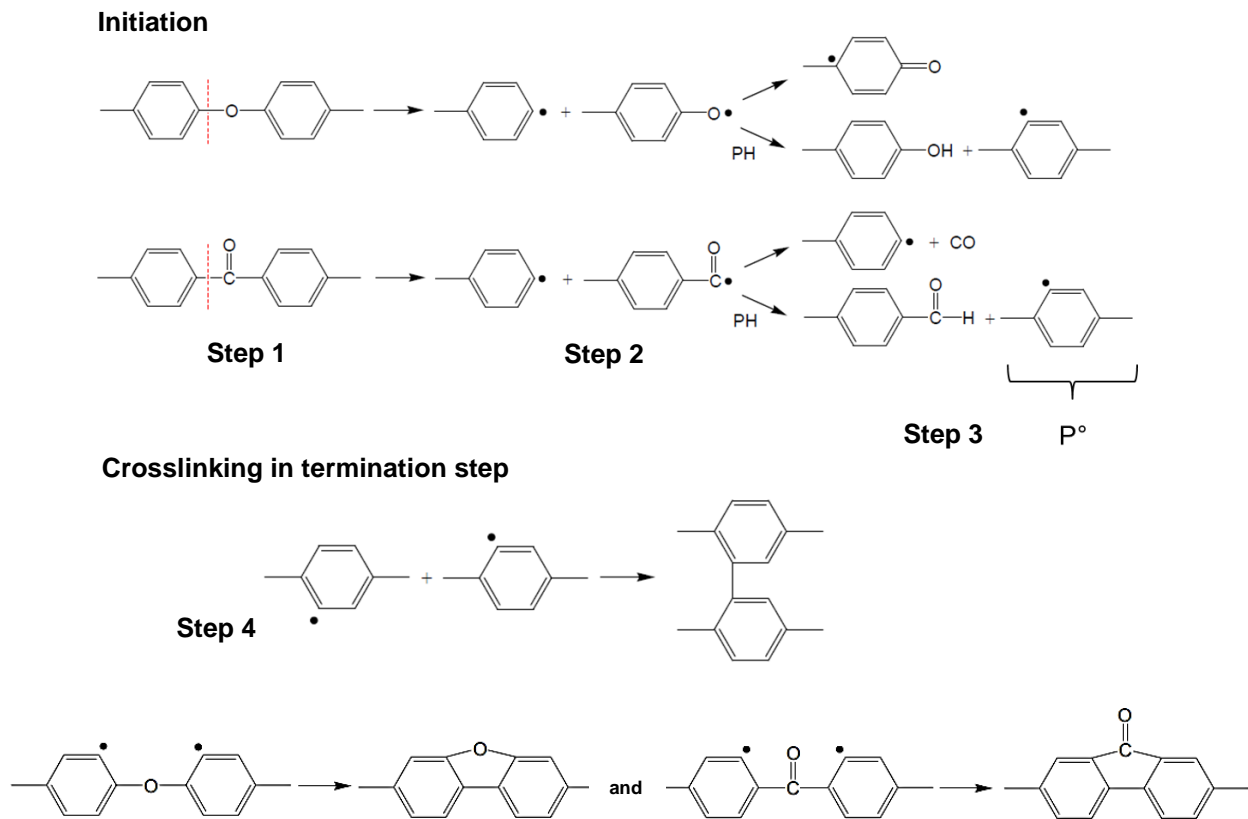


Fig. III.1 : Crosslinking mechanism steps of PEEK [67]

As a result, the crosslinking increases viscosity of the matrix which can involve bad impregnation of the carbon fibers during processing and thus impact the final health and performance of composite parts. This phenomenon also decreases the crystallization kinetics and the final crystallinity [1,2,40,69,70] and thus the final mechanical properties of the composite parts [1,2].

III.3 CROSSLINKING KINETICS

III.3.1 Weight changes

III.3.1.1 Non-isothermal analysis

Non-isothermal TGA is often used to monitor degradation of polymer: it is then assumed that the degradation mechanism leads to volatiles formation and mass loss. Non-isothermal TGA measurements on PEKK 6002 under nitrogen and air are presented in Fig. III.2. Until 550°C, weight curves of PEKK tested under nitrogen and air were observed to be confounded with an onset of the weight loss measured about 500°C which is lower than the value reported by Patel et al. [66] for PEEK at about 580°C. This temperature is much higher than PEKK consolidation temperature which is around 360°C. Even if no weight loss were measured below 500°C, it cannot be concluded that PEKK is not modified below this temperature. In fact, as we presented previously, crosslinking mechanism occurs in this range of temperature but produce few volatiles since the radicals rearrangement kinetics is high. For this range of temperature, the oxidative environment does not seem to have an impact on the weight loss which not necessary explains that it has not impact on the crosslinking mechanisms as assumed by Patel et al. [71]. Above 500°C, an important weight loss occurs reaching a

maximum kinetics around 560°C. This value is also lower than the value reported by Patel et al. for PEEK about 600°C. However, the maximum weight loss kinetics were measured to be about 9 %/min under nitrogen and 7%/min under air which is lower than for PEEK (around 17%/min). Around 700°C, as for PEEK, it can be observed a second decomposition step attributed to the cracking and dehydrogenation of the crosslinked residue produced in the first stage of decomposition and results in a thermally stable carbonaceous char [71]. This step is much more important under air than under nitrogen. Finally, the weight stabilizes around 63% under nitrogen which is higher than for PEEK (around 40%). Under air, the weight drops until the fully decomposition of the polymer showing the strong impact of the oxidative environment on PEKK decomposition. As for tests under nitrogen, the measured weight loss kinetics was higher than for PEEK. To conclude, it appears that the decomposition of PEKK 6002 is initiated before PEEK decomposition but its decomposition kinetics is lower than for PEEK.

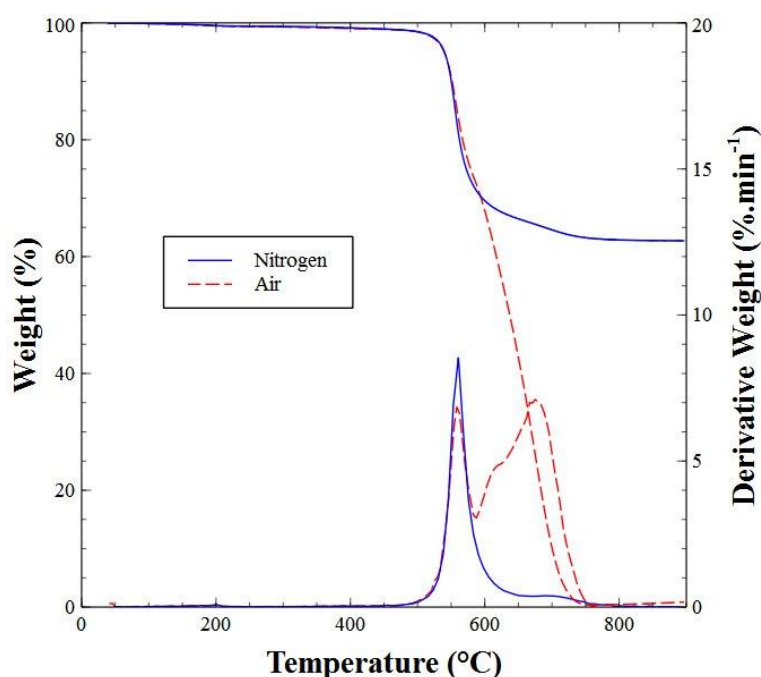


Fig. III.2 : Weight loss vs temperature for neat PEKK 6002 under nitrogen and air

III.3.1.2 Isothermal analysis

In order to investigate the mechanisms involved during degradation, isothermal analysis has been performed at 400°C. In Fig. III.3 is presented the evolution the weight as a function of time for PEKK 6002 annealed at 400°C under nitrogen and air. It can be observed a decrease of the weight with values of 94,5% and 88.5% for measurements under nitrogen and air respectively during 15h. It can consequently be assumed that a degradation of PEKK is occurring at 400°C and it is faster under air which was not observable for non-isothermal conditions. This is consistent with the literature comparing to PEEK decomposition. In fact, the isothermal activation energy of PEEK degradation is lower under air than nitrogen due to oxidation reactions [72–74] involving higher weight loss kinetics.

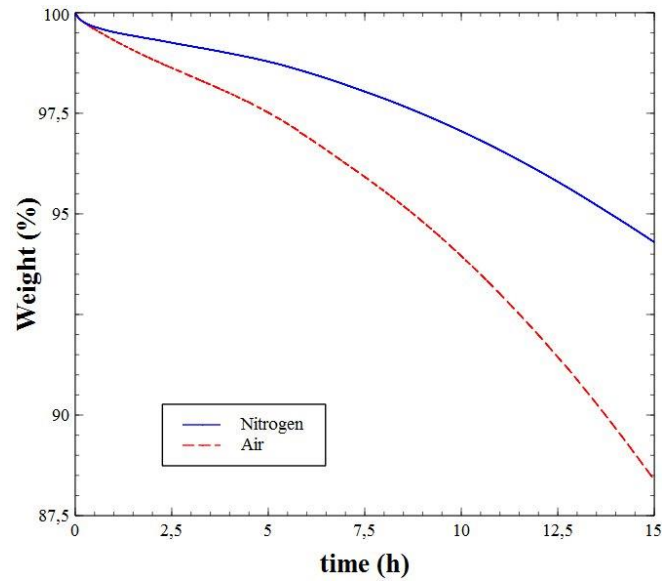


Fig. III.3 : Weight loss vs time for neat PEKK 6002 annealed at 400°C under nitrogen and air

III.3.2 Gel Permeation Chromatography (GPC) analysis

To investigate macromolecular changes mechanism, thick samples neat PEKK 6002 were exposed at 400°C under air for different times of exposure. After exposure, oxidized layers at the samples surface were removed in order to obtain degraded PEKK without oxygen. It was then checked out by FTIR measurements that no oxidation products were detected in the samples. Gel permeation chromatography measurements were carried out on the samples (see Fig. III.4). Less than 5% of insolubles were measured for all exposure times. Table III.1 and Fig. III.5 show the evolution of the weight and number average molar mass (M_w and M_n) and the polydispersity index (I_p) as a function of the exposure time. It can be observed an increase of M_w and I_p which is typical to crosslinking. This confirms that at 400°C, the predominant modification of PEKK 6002 is associated to crosslinking. However, the fact that M_n remains constant could imply a chain scission process. As a result, the macromolecular changes have to take into account not only a crosslinking process but also a chain scission mechanism.

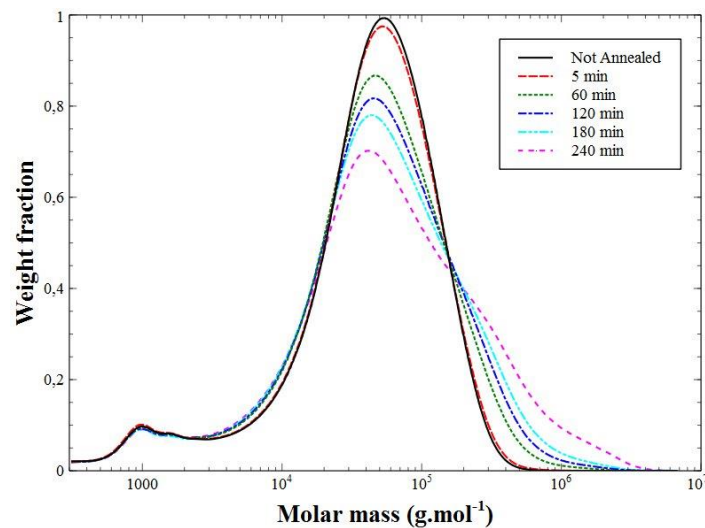


Fig. III.4 : Molar mass distributions of neat PEKK 6002 annealed at 400°C under air obtain at room temperature by GPC

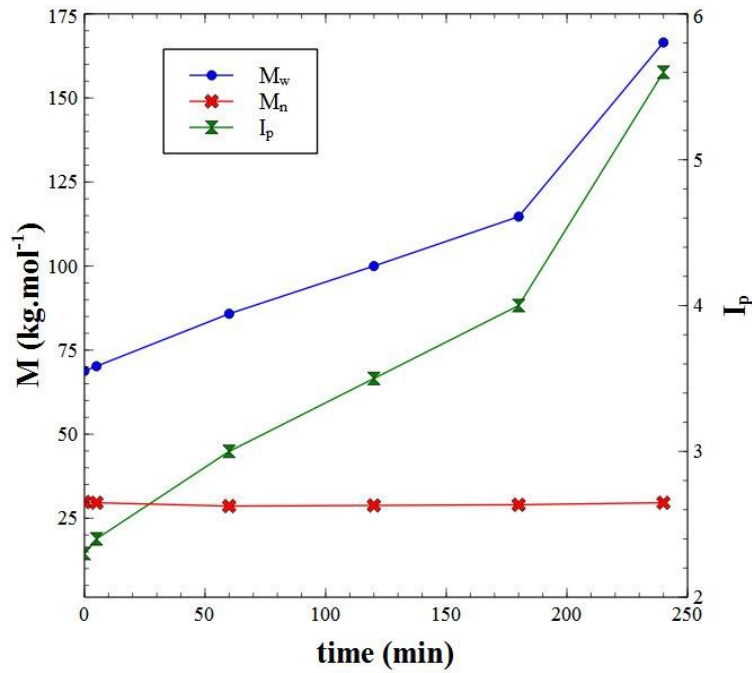


Fig. III.5 : Evolution of M_w , M_n and I_p as a function of the annealing time at 400°C under air of neat PEKK 6002

The evolution of the number of crosslinking and scission events x and s (mol.kg⁻¹) with the annealing time can be linked with the number and weight average molar mass (M_n and M_w) by using Saito's equations [75,76]:

$$s - x = \frac{1}{M_n} - \frac{1}{M_{n_0}} \quad \text{Equation III.1}$$

$$\frac{s}{2} - 2x = \frac{1}{M_w} - \frac{1}{M_{w_0}} \quad \text{Equation III.2}$$

with $M_{n_0}=29.8$ kg.mol⁻¹ and $M_{w_0}=68.8$ kg.mol⁻¹. The main hypothesis here is to consider that the macromolecules remain linear which is consistent as less than 5% of insolubles were measured for all annealing times. By solving this system, the evolution of x and s as a function of the annealing time at 400°C was calculated. Results are presented in Fig. III.6 and Table III.1. It can be observed that the values of s and x are strongly correlated. Therefore, regarding Equation III.1, as M_n is quasi constant, we can conclude that $s \approx x$. Even if the same experimental results were found (constant M_n and increasing of M_w and I_p), the Saito approach allows to assess the apparition of chain scission in parallel to crosslinking mechanism.

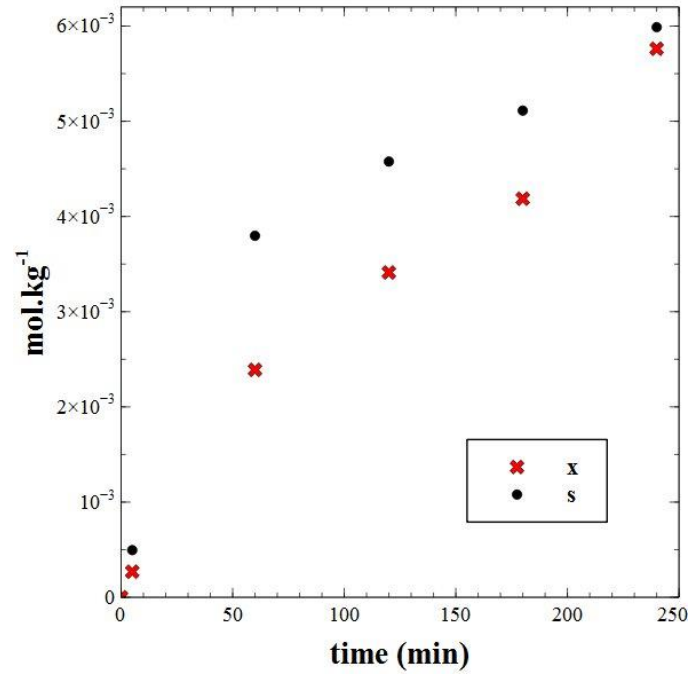


Fig. III.6 : Number of crosslinking and chain scission events x and s vs annealing time at 400°C under air of neat PEKK 6002

Time at 400°C	M _w (kg.mol ⁻¹)	M _n (kg.mol ⁻¹)	I _p =M _w /M _n	x (mol.kg ⁻¹)	s (mol.kg ⁻¹)
0	68,8	29,8	2,3	0	0
5	70,2	29,6	2,4	2.7.10 ⁻⁴	5.0.10 ⁻⁴
60	85,8	28,6	3	2.4.10 ⁻³	3.8.10 ⁻³
120	100	28,8	3,5	3.4.10 ⁻³	4.6.10 ⁻³
180	114,7	29	4	4.2.10 ⁻³	5.1.10 ⁻³
240	166,5	29,6	5,6	5.8.10 ⁻³	6.0.10 ⁻³

Table III.1 : Weight and number average molar mass (M_w and M_n), polydispersity index (I_p) and number of crosslinking x and chain scission s events of neat PEKK 6002 annealed at 400°C under air

III.3.3 Rheological analysis

To assess the thermal activation of the crosslinking kinetic, we propose here to monitor Newtonian viscosity during isothermal exposure at different temperatures.

III.3.3.1 Viscoelastic linear and Newtonian domains determination

For a sinusoidal deformation, the complex viscosity η^* of a polymer can be expressed by:

$$\eta^* = \eta' - i\eta'' \quad \text{Equation III.3}$$

where η' is the real part of the viscosity and η'' is the imaginary part of the viscosity. The real part is associated to the viscous dissipation in the polymer:

$$\eta' = \frac{G''}{\omega} \quad \text{Equation III.4}$$

where G'' is the loss modulus associated to the viscous behavior of the polymer and ω the solicitation angular frequency. The imaginary part of the complex viscosity is associated to the elastic component of the polymer:

$$\eta'' = \frac{G'}{\omega} \quad \text{Equation III.5}$$

where G' is the storage modulus associated to the elastic behavior of the polymer.

The first step of rheological measurements were to determine a strain allowing to carry out all tests in the viscoelastic linear domain that is for an angular frequency the rheological behavior only depends on the temperature. Strain sweep from 0.01% to 100% with a frequency of 100 rad.s⁻¹ at 360°C were done to identify the maximum strain to apply to stay in the viscoelastic linear domain (Fig. III.7). The isothermal temperature test 360°C corresponds to an intermediate temperature for isothermal tests presented in the next paragraph and the frequency was chosen to be high enough to make sure that the identified maximum strain was correct. It can be observed that the viscosity as a function of the strain is constant until around 20% where it drops to very low viscosities. Consequently, a value of strain of 1% was chosen to make sure to stay in viscoelastic linear domain during all tests.

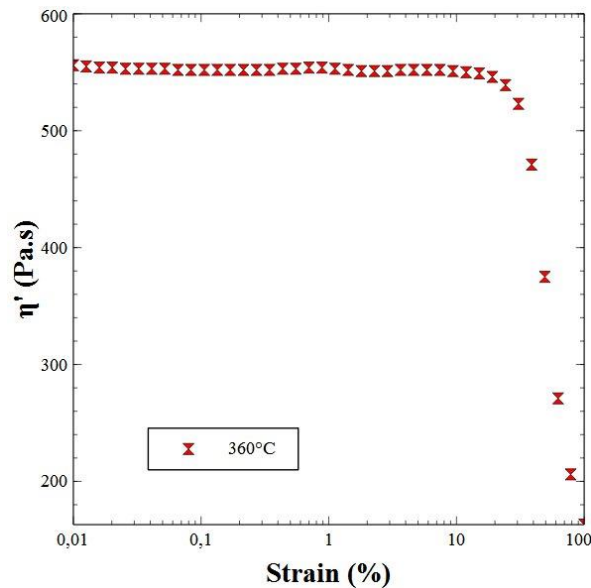


Fig. III.7 : Real viscosity vs strain of neat PEKK 6002 at 360°C for a test frequency of 100 rad.s⁻¹ under nitrogen

Secondly, following tests were carried out in the Newtonian domain of the matrix to use some properties of the viscous Newtonian liquids and investigate the crosslinking mechanism. In the Newtonian domain, the shear viscosity $\eta(\dot{\gamma})$ approaches a Newtonian plateau where it does not vary with the shear rate $\dot{\gamma}$:

$$\eta(\dot{\gamma}) = \eta_0 \quad \text{Equation III.6}$$

with η_0 the so called zero shear viscosity or the Newtonian viscosity.

According to Cox-Merz rule [77] which is an empirical relationship of great use in rheology for many polymeric systems, in the lower limits of frequency and shear rate, the relation between the shear viscosity η and the modulus of the complex viscosity $|\eta^*|$ is expressed by:

$$\lim_{\dot{\gamma} \rightarrow 0} \eta(\dot{\gamma}) = \lim_{\omega \rightarrow 0} |\eta^*(\omega)| \quad \text{Equation III.7}$$

Consequently, the modulus of the complex viscosity $|\eta^*|$ can be expressed as a function of the Newtonian viscosity by:

$$\lim_{\omega \rightarrow 0} |\eta^*(\omega)| = \eta_0 \quad \text{Equation III.8}$$

The Cox-Merz rule goes even further by assuming that $\eta(\dot{\gamma}) = |\eta^*(\omega)|$ whatever the frequency and the shear rate for most of neat polymers, which allows us assessing easily the viscosity at plateau for frequency in the rheological measurement range, typically 1s^{-1} .

Frequency sweeps from 0.1 to 100 rad.s^{-1} for isothermal tests from 300°C to 400°C with a strain of 1% are presented in Fig. III.8. Tests were made from high frequencies to low frequencies to have a maximum number of points before a potential modification of the matrix. For all tests the viscosity increases with the decrease of the angular frequency. At 300°C , it can be observed a beginning of the Newtonian plateau around 1 rad.s^{-1} and then the viscosity increases which is associated to the crystallization of the polymer. At 320°C and 340°C , the Newtonian plateau was more apparent. Above 340°C , it was noticed an increase of the viscosity after the Newtonian plateau which occurred at increasingly angular frequencies with isothermal temperatures. This phenomenon is related to a thermal degradation of the polymer due to crosslinking reactions. Consequently, a value of angular frequency of 1 rad.s^{-1} was chosen to stay in the Newtonian domain of the polymer for all tests.

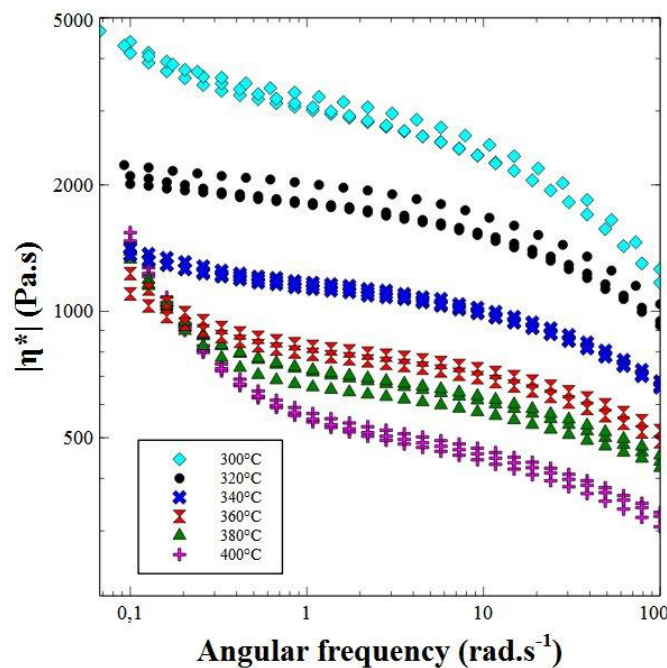


Fig. III.8 : Modulus of the complex viscosity vs frequency of neat PEKK 6002 for different isothermal tests with a strain of 1% under nitrogen

The evolution of the logarithm of the Newtonian viscosity measured with Fig. III.8 as a function of the inverse of the isothermal test temperature is plotted in Fig. III.9. It can be observed a linear evolution of the logarithm of the Newtonian viscosity in this graph showing that it is thermally activated and follows an Arrhenius law:

$$\eta_0 = \eta_{0i} \exp\left(\frac{E_{a\eta_0}}{RT}\right) \quad \text{Equation III.9}$$

where R is the perfect gas constant, η_{0i} is a pre-exponential constant and $E_{a\eta_0}$ is the Newtonian viscosity activation energy. Equation III.9 can be written as:

$$\ln(\eta_0) = \ln(\eta_{0i}) - \frac{E_{a\eta_0}}{R} \frac{1}{T} \quad \text{Equation III.10}$$

From the linear fitting of the Arrhenius law logarithm (Equation III.10), the Newtonian viscosity activation energy $E_{a\eta_0}$ and the pre-exponential constant η_{0i} have been determined to be equal to 60.8 kJ.mol⁻¹ and 9.2.10⁻³ Pa.s.

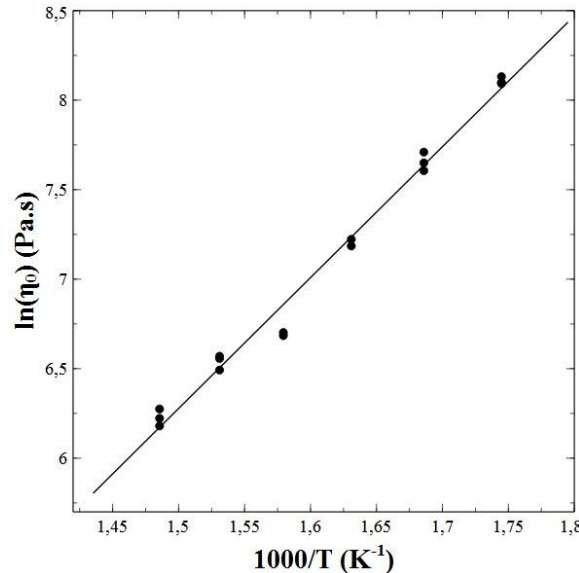


Fig. III.9 : Arrhenius plot of the Newtonian viscosity of neat PEKK 6002 under nitrogen

III.3.3.2 Evolution of the viscosity at during isothermal exposure

In this part, we investigated the evolution of PEKK 6002 matrix properties with isothermal rheological measurement for temperatures above T_m . Fig. III.10 shows the evolution of the viscosity under nitrogen atmosphere as a function of time for different temperatures measured with a strain rate of 1% and a frequency sweep of 1 rad.s⁻¹ determined in the previous paragraph. For annealing temperature between 320°C and 360°C, the viscosity seems constant with the annealing time whereas above 360°C, the viscosity increases as a function of the annealing time with a onset of 130 minutes at 380°C and 60 minutes at 400°C. At 400°C, the impact of the annealing time is very important. This phenomenon is the same as observed for PEEK by Chan et al. [1] and is consistent with the formation of crosslinking for PEKK heated at high annealing temperatures.

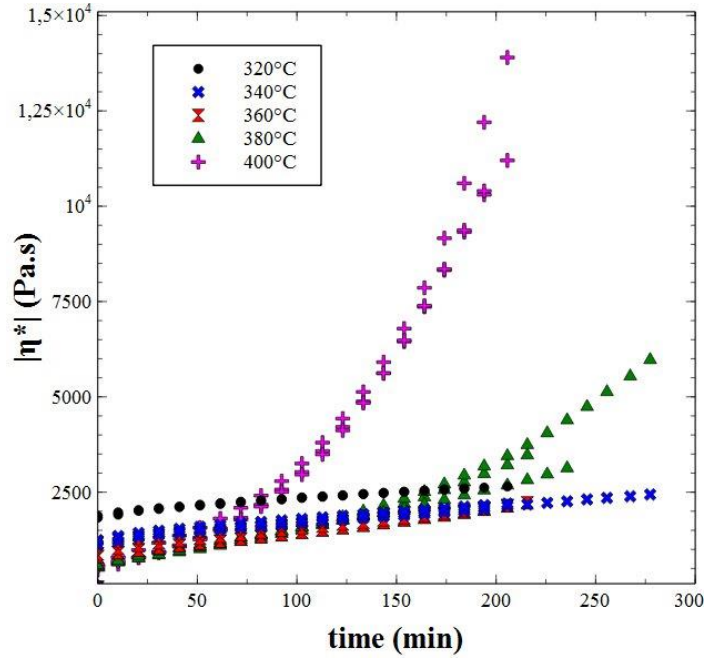


Fig. III.10 : Modulus of the complex viscosity vs annealing time of neat PEKK 6002 for different isothermal tests under nitrogen

III.3.3.3 Link between the viscosity and the weight average molar mass

From the Ostwald-de Waele and Cox-Merz laws (Equation III.7), for a Newtonian regime, the modulus of the complex viscosity at a temperature T can be expressed by:

$$|\eta^*| = K M_w^{3.4} \quad \text{Equation III.11}$$

where K is a constant depending on the temperature. For low exposure time, it can be written:

$$K(T) = \frac{\eta_0(T)}{M_{w_0}^{3.4}} \quad \text{Equation III.12}$$

with $M_{w_0}=68.8 \text{ kg.mol}^{-1}$. Thus, the evolution of the weight average molar mass for a temperature T can be calculated with:

$$M_w = M_{w_0} \left(\frac{|\eta^*|}{\eta_0} \right)^{\frac{1}{3.4}} \quad \text{Equation III.13}$$

The evolution of the weight average molar mass under nitrogen atmosphere as a function of time for different temperatures is plotted in Fig. III.11. As expected, it can be observed an increase of M_w with the annealing time due to crosslinking. We can witness that the increase of M_w doesn't exhibit a significant induction period and the increase rate is maximum at the beginning of the exposure. At last, it is noteworthy that this phenomenon is increasingly important with the annealing temperature.

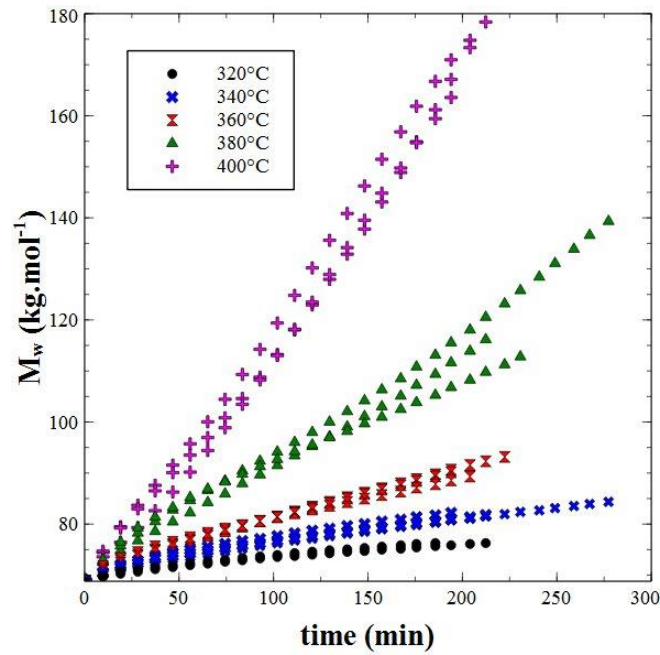


Fig. III.11 : Weight average molar mass vs annealing time of neat PEKK 6002 for different isothermal tests under nitrogen

Fig. III.12 presents the comparison of the values of the weight average molar mass of PEKK 6002 annealed at 400°C determined by rheological and GPC measurements. Although both methods assume several hypothesis (especially linear macromolecules), a good correlation between both methods is put in evidence. However, the values of M_w for PEKK 6002 assessed by GPC are slightly lower than for those assessed by the rheological measurements. As it was already mentioned, this discrepancy can be attributed to the branching of macromolecular chains making them no more linear and perhaps also to the insoluble fraction which is filtered in GPC measurements. In other words, non-linear macromolecules and insoluble fraction contribute to the viscosity increase witnessed during isothermal rheological measurements.

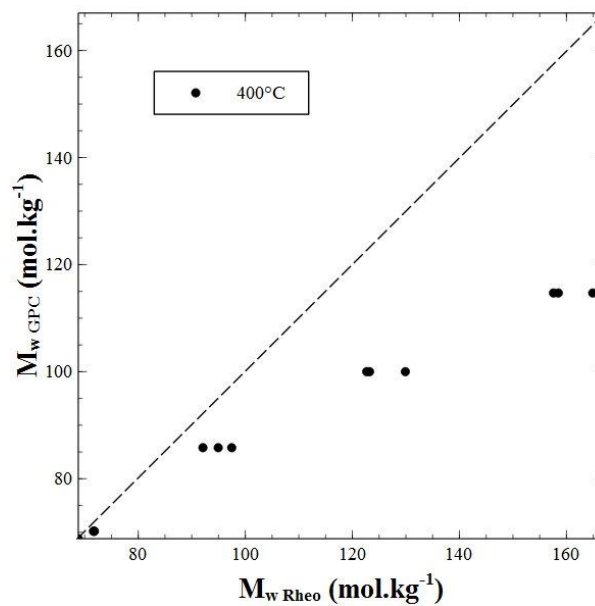


Fig. III.12 : Comparison of the weight average molar mass of PEKK 6002 annealed at 400°C determined by rheological measurements and GPC measurements

III.3.3.4 Link between the viscosity and macromolecular changes

As it was proposed in the GPC measurements part (see paragraph III.3.2) the evolution of the number and weight average molar masses (M_n and M_w) with the annealing temperature can be linked with the number of crosslinking x and chain scissions s events (mol.kg^{-1}) from Saito's equations (Equation III.1 and Equation III.2).

As it was shown from GPC measurements, the number average molar mass is quasi-constant and consequently $s \approx x$. With this assumption, from **Erreur ! Source du renvoi introuvable.**, the number of crosslinking events x can be expressed by:

$$x = -\frac{2}{3} \left(\frac{1}{M_w} - \frac{1}{M_{w_0}} \right) \tag{Equation III.14}$$

From Equation III.11 and Equation III.14, it can be written:

$$x = \frac{2}{3M_{w_0}} \left[1 - \left(\frac{\eta_0}{|\eta^*|} \right)^{\frac{1}{3.4}} \right] \tag{Equation III.15}$$

where $M_{w_0} = 68.8 \text{ kg.mol}^{-1}$. The evolution of x as a function of time calculated with Equation III.15 is plotted in Fig. III.13. As expected, it can be observed an increase of x with the annealing time. We can witness that the crosslinking process doesn't exhibit a significant induction period: the crosslinking rate is maximum at the beginning of the exposure.

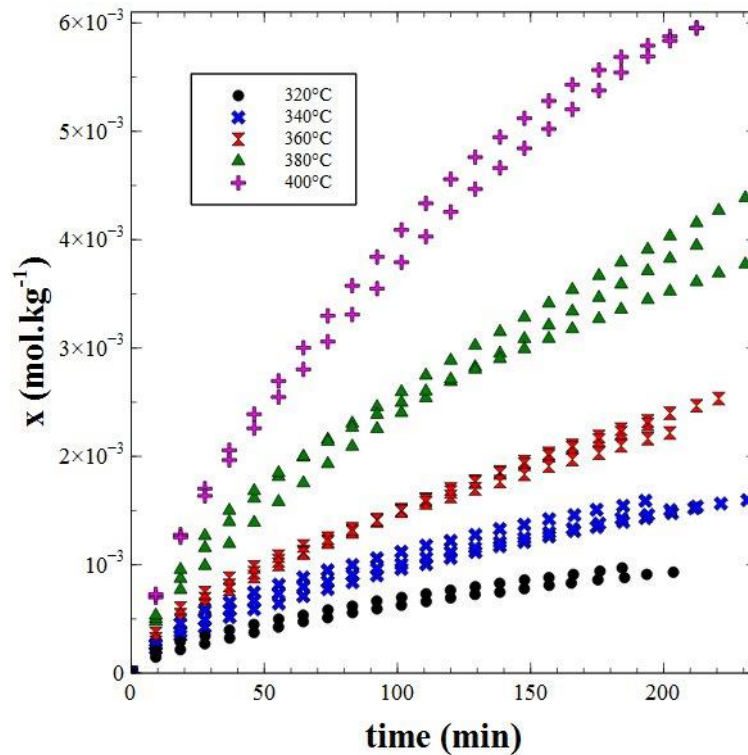


Fig. III.13 : Number of crosslinking events x vs annealing time of neat PEKK 6002 for different isothermal tests under nitrogen

Fig. III.14 presents the comparison of the values of the number of crosslinking events x of PEKK 6002 annealed at 400°C determined by rheological and GPC measurements. A good correlation between both methods is put in evidence. In the same way as the molar mass (Fig. III.12), the values of x for PEKK 6002 assessed by GPC are slightly lower than for those assessed by the rheological measurements which is probably due to the branching of macromolecular chains making them no more linear.

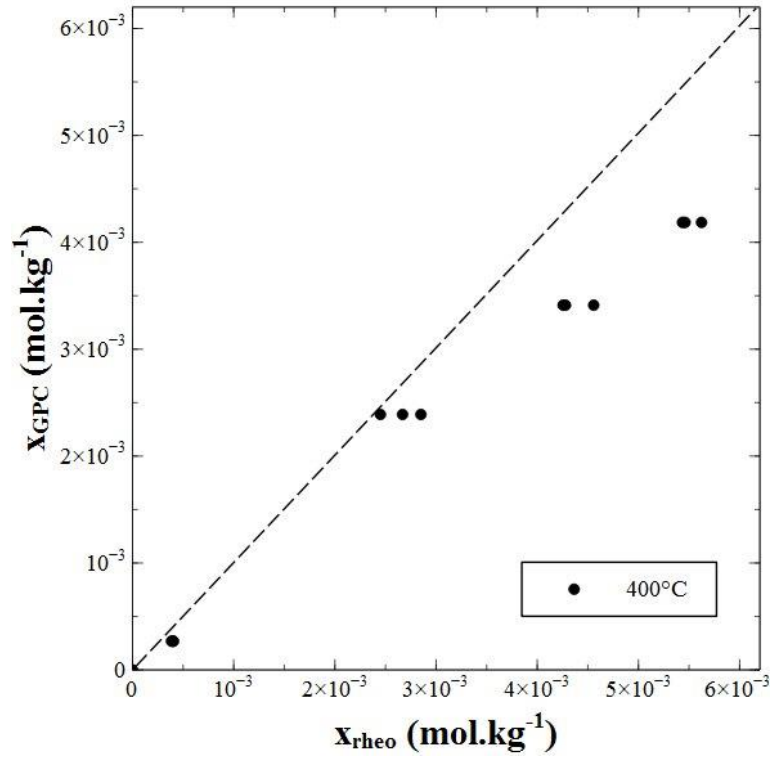


Fig. III.14 : Comparison of the number of crosslinking events x of PEKK 6002 annealed at 400°C determined by rheological measurements and GPC measurements

III.3.4 DSC measurements

DSC measurements were carried out on PEKK samples annealed at 400°C under nitrogen during different times. The evolution of T_g as a function of the annealing time at 400°C under nitrogen is plotted in Fig. III.15. It can be observed an increase of the T_g as a function of the annealing time of about 5°C. This phenomenon has already been seen for PEEK [40,69,70] and was attributed to crosslinking decreasing the macromolecular mobility.

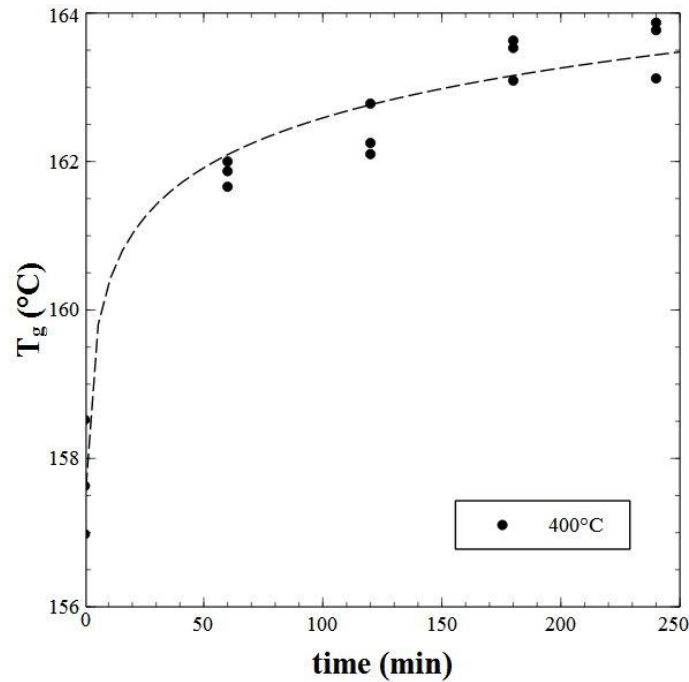


Fig. III.15 : Glass transition temperature T_g vs annealing time at 400°C under nitrogen of neat PEKK 6002

In the literature, some authors [78] attempted to follow the evolution of the number crosslinking events x with the glass transition temperature T_g thanks to the Fox Flory law [79]:

$$T_g = T_{g_\infty} - \frac{k_{FF}}{M_n} \quad \text{Equation III.16}$$

where T_{g_∞} is the theoretical glass transition of a linear polymer with an infinite molar mass and $k_{FF}=203.6 \text{ K.kg.mol}^{-1}$ is the constant of Fox Flory determined for PEEK. Thus, the difference of T_g before and after annealing is expressed by:

$$T_g - T_{g_0} = -k_{FF} \left(\frac{1}{M_n} - \frac{1}{M_{n_0}} \right) \quad \text{Equation III.17}$$

where T_{g_0} is the glass transition at the initial time. From Equation III.1, Equation III.17 can thus be written:

$$T_g - T_{g_0} = -k_{FF} (s - x) \quad \text{Equation III.18}$$

However, in our case the number of chain scission and crosslinking events was found to be equal, thus T_g should be constant with this law which is not consistent regarding our results.

Thus, in our case the Fox Flory law cannot be used to assess the evolution of the number crosslinking events. The main cause could be explained by the fact that the Fox Flory law was established for linear chains polymer. In our case, a branching mechanism should occur during the crosslinking process.

III.4 CROSSLINKING KINETICS MODELLING

A mechanistic approach can be carried out to model x depending on the temperature for any exposure time by exploiting the chemical reaction equations leading to crosslinking. As presented in paragraph III.2, the different steps of the crosslinking mechanism under nitrogen atmosphere can be expressed by:



where PH corresponds to the macromolecular chains, P° to phenyl radicals, x to the number of crosslinking events (mol.kg^{-1}) and k_0 , k_3 and k_4 to the reaction rate constants of the initiation, propagation and termination by crosslinking steps respectively.

The kinetic scheme of crosslinking mechanism can thus be written:

$$\frac{d[P^\circ]}{dt} = 2k_0[PH] - 2k_4[P^\circ]^2 \quad \text{Equation III.22}$$

$$\frac{d[PH]}{dt} = -k_0[PH] \quad \text{Equation III.23}$$

$$\frac{dx}{dt} = \gamma_4 k_4 [P^\circ]^2 \quad \text{Equation III.24}$$

where $[P^\circ]$, $[PH]$ correspond to the concentration of PEKK monomer and macromolecular chains respectively, k_0 , k_3 and k_4 to the reaction constants and γ_4 is a constant which is between 0 and 1 allowing to take into account the fact that radicals can also rearrange by internal combination.

In first approach, it can be assumed that at low degree of conversion the PH consumption is negligible. Hence, Equation III.22 becomes:

$$\frac{d[P^\circ]}{dt} = 2k_0[PH]_0 - 2k_4[P^\circ]^2 \quad \text{Equation III.25}$$

With $[PH]_0$ the initial concentration of PH which depends on the number of potentially sites which can be activated for crosslinking reactions so precisely the sites where macromolecular chains can be broken:

$$[PH]_0 = n_{sites} \frac{1}{M_{0PEKK}} d_{PEKK} \quad \text{Equation III.26}$$

Where n_{sites} is the number of sites which can be activated, $M_{0PEKK}=300.3 \text{ g.mol}^{-1}$ is the molar mass and $d_{PEKK}=1.3$ is the density. n_{sites} can take three different values, if chains scissions occurs at the carbonyl functional groups $n_{sites}=4$, if chains scissions occurs at the ether bonds $n_{sites}=2$ and finally if we consider that the chain scission occurs randomly at the carbonyl and ether bonds $n_{sites}=6$.

By solving Equation III.25, the concentration of alkyls radicals P° can be expressed by:

$$[P^\circ] = [P^\circ]_{stat} \frac{1 - \exp\left(-\frac{t}{\tau}\right)}{1 + \exp\left(-\frac{t}{\tau}\right)} \quad \text{Equation III.27}$$

With $[P^\circ]_{stat}$ the concentration of alkyl radicals at the stationary state equal to:

$$[P^\circ]_{stat} = \left(\frac{k_0 [PH]_0}{k_4} \right)^{1/2} \quad \text{Equation III.28}$$

And the characteristic time to reach the stationary state τ equal to:

$$\tau = \frac{1}{4(k_0 k_4 [PH]_0)^{1/2}} \quad \text{Equation III.29}$$

As alkyl radicals (P°) are highly reactive ($k_4 > 10^7 \text{ mol.l}^{-1}.\text{s}^{-1}$), the stationary state for P° is reached at the very beginning of exposure. Thus, at low degree of conversion, it can be written:

$$[P^\circ] = \left(\frac{k_0 [PH]_0}{k_4} \right)^{1/2} \quad \text{Equation III.30}$$

Consequently, for low exposure time, by resolving Equation III.24, the number of crosslinking events x is equal to:

$$x = \gamma_4 k_0 [PH]_0 t \quad \text{Equation III.31}$$

This equation corresponds to a linear equation which passes by 0 with a slope of $\gamma_4 k_0 [PH]_0$ which corresponds to the apparent crosslinking kinetics k_{app} . Consequently, straight lines were fitted with the beginning of the number of crosslinking events x curves plotted in Fig. III.13 ($t < 20 \text{ min}$) to determine k_{app} depending on the exposure temperature (Fig. III.16).

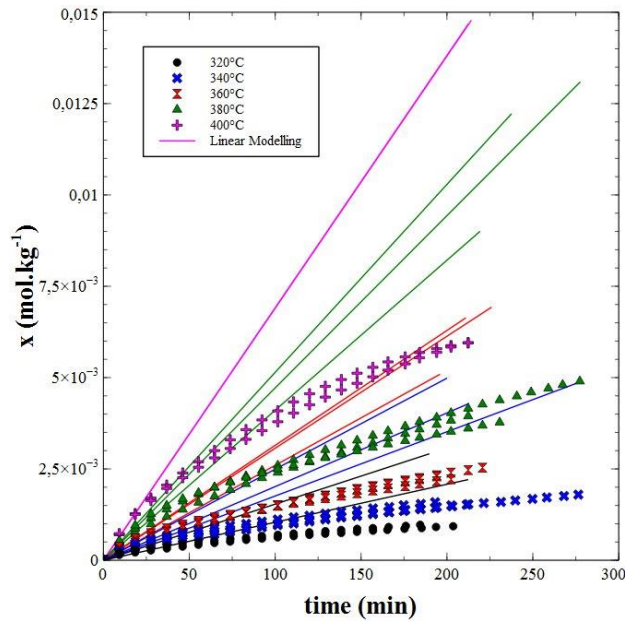


Fig. III.16 : Number of crosslinking events x vs annealing time of neat PEKK 6002 for different temperatures under nitrogen with the linear modelling

The evolution of the logarithm of the apparent crosslinking kinetics k_{app} as a function of the inverse of the isothermal test temperature is plotted in Fig. III.17. It can be observed a linear evolution of the logarithm of k_{app} in this graph showing that it is thermally activated and follows an Arrhenius law:

$$k_{app} = k_{app0} \exp\left(\frac{-E_{akapp}}{RT}\right) \quad \text{Equation III.32}$$

where k_{app0} is a pre-exponential constant and E_{akapp} is the apparent crosslinking activation energy. From the linear fitting of the logarithm Arrhenius law (Fig. III.17), the apparent crosslinking activation energy E_{akapp} and k_{app0} have been determined to be equal to 65.9 kJ.mol⁻¹ and 8.27 mol.kg⁻¹min⁻¹. The crosslinking activation energy of PEKK is lower than the value reported in the literature for PEEK equal to 168 kJ.mol⁻¹ [65].

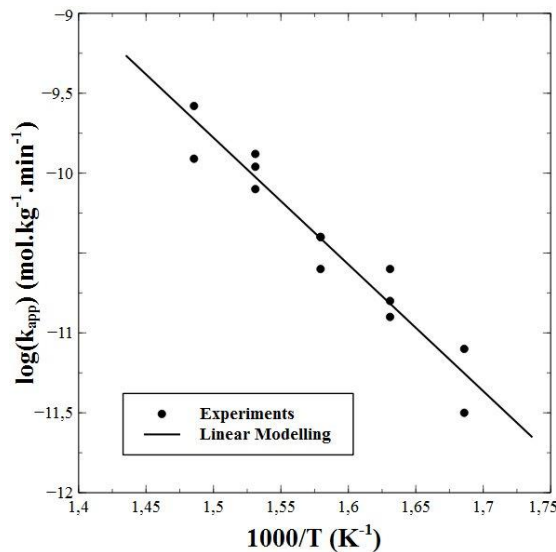


Fig. III.17 : Arrhenius plot of the apparent crosslinking kinetics of neat PEKK 6002 under nitrogen

We can thus finally determine the number of crosslinking events for any temperature as a function of the annealing time for low enough exposure times ($t < 20$ min) with:

$$x = k_{app0} \exp\left(\frac{-E_{k_{app}}}{RT}\right) t \quad \text{Equation III.33}$$

In a second approach, it would be interesting to model the number of crosslinking events x for longer exposure times. In this case, the assumption PH constant is no more valid. We expect that the substrate consumption of PH (Equation III.23) will lead to the bending of the x curve. The only way to take into account the PH consumption is to solve numerically the system of differential equations (Equation III.22, Equation III.23 and Equation III.24. Thanks to numerical solving, the evolution of P° and PH could then also be determined as a function of the exposure time for the different annealing temperatures. The initial conditions are fixed by considering that at initial time, no phenyl radicals is formed $[P^\circ]_0 = 0$ and thus no crosslinking reaction $x_0 = 0$. The initial concentration of PH is expressed in Equation III.25. Unfortunately, we did not have enough time to investigate more this part.

III.5 IMPACT OF MACROMOLECULAR CHANGES ON CRYSTALLIZATION KINETICS

III.5.1 Crystallization peak analysis

The impact of crosslinking on crystallization has been studied by different authors and was shown to decrease crystallization kinetics and final crystallinity [2,40,69,70]. In fact, crosslinking decreases the chain mobility and macromolecular chains have more difficulties to reorganize to form crystallites. Crystallization peaks of PEKK 6002 crystallized from the melt after different annealing times at 400°C measured by DSC are presented in Fig. III.18. It can be noticed that the crystallization peak decreases with the annealing time at 400°C which is consistent with the literature. Even if we have seen that chain scission mechanism occurs in the same time, it seems that crystallization is governed by crosslinking process.

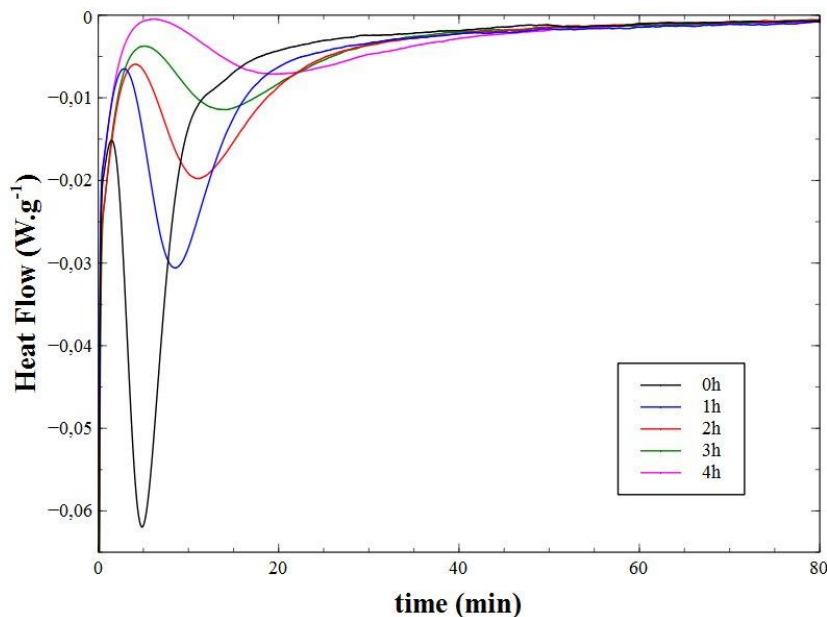


Fig. III.18 : DSC thermograms of neat PEKK 6002 crystallized at 230°C from the melt after different annealing times at 400°C under nitrogen

The evolution of the melting enthalpy of PEKK 6002 annealed at 400°C during different times under nitrogen and crystallized at 230°C is plotted in Fig. III.19. The melting enthalpy decreases with the annealing time with a value of about 25 J.g⁻¹ after 4h annealing at 400°C. This shows that the polymer crystallizes less after annealing due to crosslinking reactions.

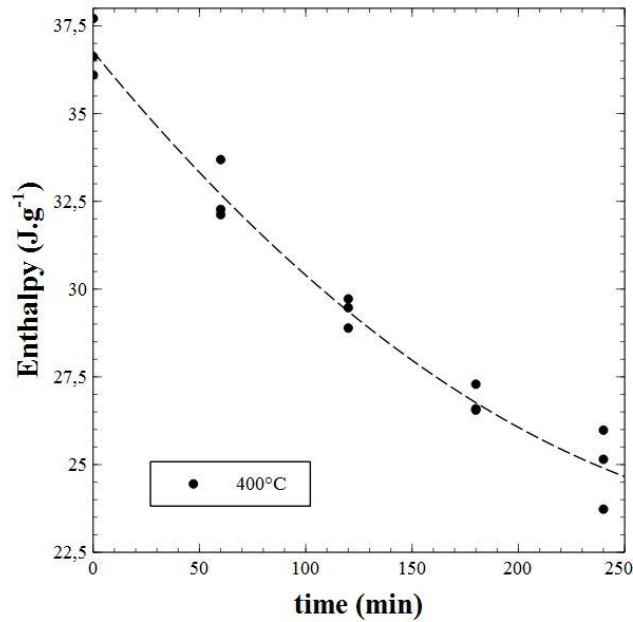


Fig. III.19 : Melting enthalpy vs time of neat PEKK 6002 annealed at 400°C under nitrogen during different times and crystallized at 230°C

As we assessed previously the evolution of the number of crosslinking events and the melting enthalpy with the annealing time at 400°C under nitrogen for neat PEKK 6002 (Equation III.13 and Fig. III.19), it was possible to plot the evolution of the crystallinity as a function of the number of crosslinking events (see Fig. III.20).

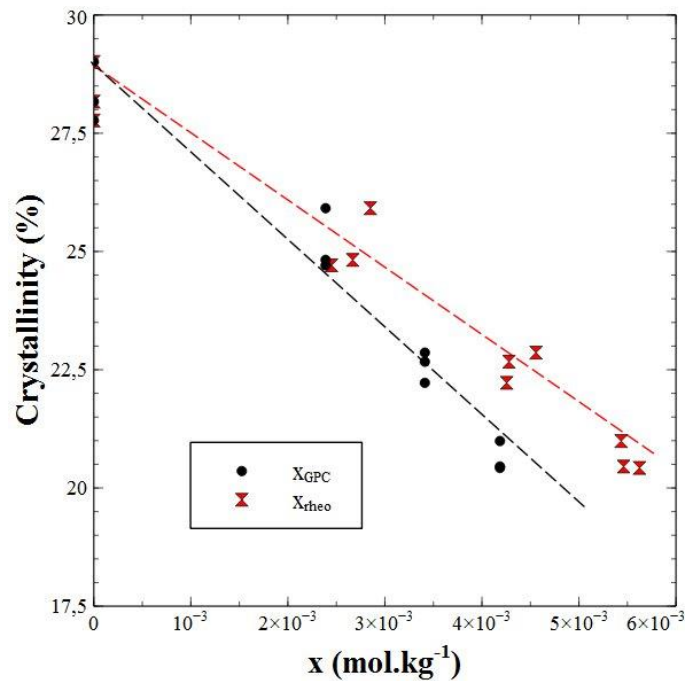


Fig. III.20 : Crystallinity vs number of crosslinking events x for neat PEKK 6002

III.5.2 Modification of the Hillier crystallization kinetic parameters

The influence of crosslinking on crystallization kinetics was investigated by Deslandes et al. [69] and Jonas et al. [40] for PEEK by measuring the crystallization half time depending on the annealing temperature. They reported an increase of the crystallization half time with the annealing time. This is a first approach to evaluate the influence of crosslinking on crystallization kinetics however it does not take into account the influence of crosslinking on the primary and the secondary crystallization mechanisms. In order to assess the influence of crosslinking on both crystallization mechanisms kinetics, the derivative Hillier model established in paragraph II.3.2.4 were fitted with the crystallization peaks measured by DSC in Fig. III.18. The identified Hillier parameters as a function of the annealing time at 400°C are plotted in Fig. III.21, Fig. III.22 and Fig. III.23. We supposed that the primary crystallization has a spherulitic growth ($n_1=3$) and the secondary crystallization a one dimensional growth ($n_2=1$). The crystallization rate constants K_1 and K_2 were observed to decrease with the annealing time at 400°C which shows that crystallization kinetics of the primary and the secondary crystallization decrease with crosslinking.

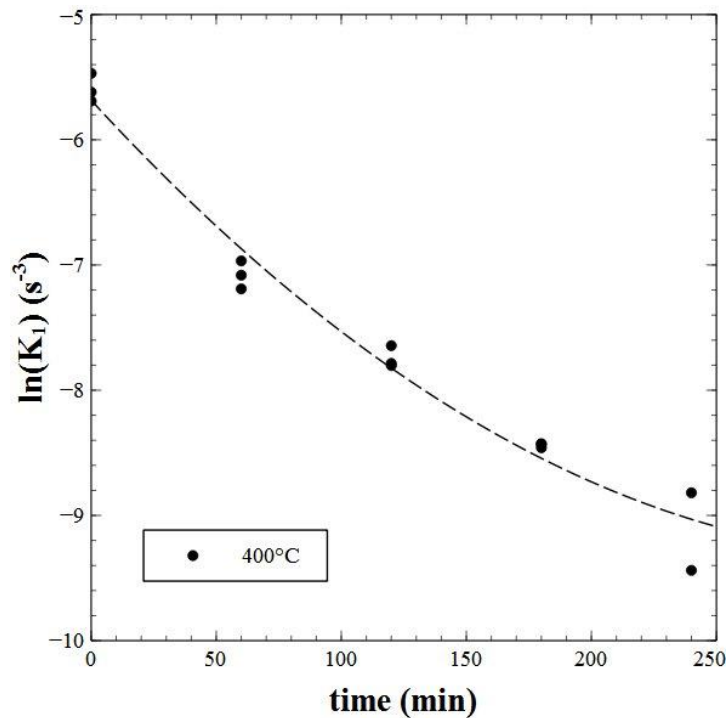


Fig. III.21 : Logarithm of the primary crystallization rate constant K_1 vs annealing time at 400°C under nitrogen of neat PEKK 6002 crystallized at 230°C

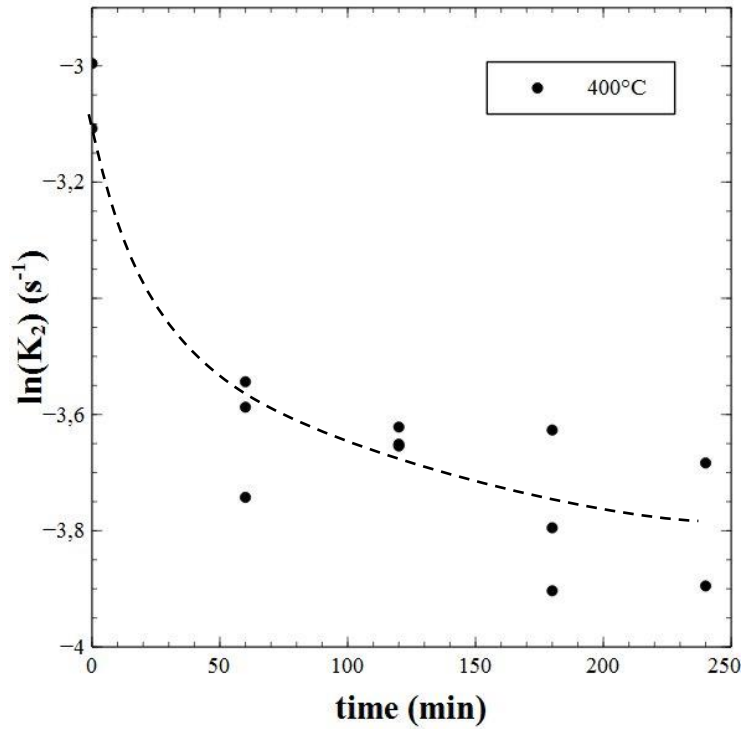


Fig. III.22 : Logarithm of the secondary crystallization rate constant K_2 vs annealing time at 400°C under nitrogen of neat PEKK 6002 crystallized at 230°C

The weight factor w_1 also drop with the annealing time which is consistent with the fact that crosslinking involves lower chain mobility and thus a less perfect crystallization which let more space to the secondary crystallization attributed to the growth of an interlamellar crystalline structure within lamellae.

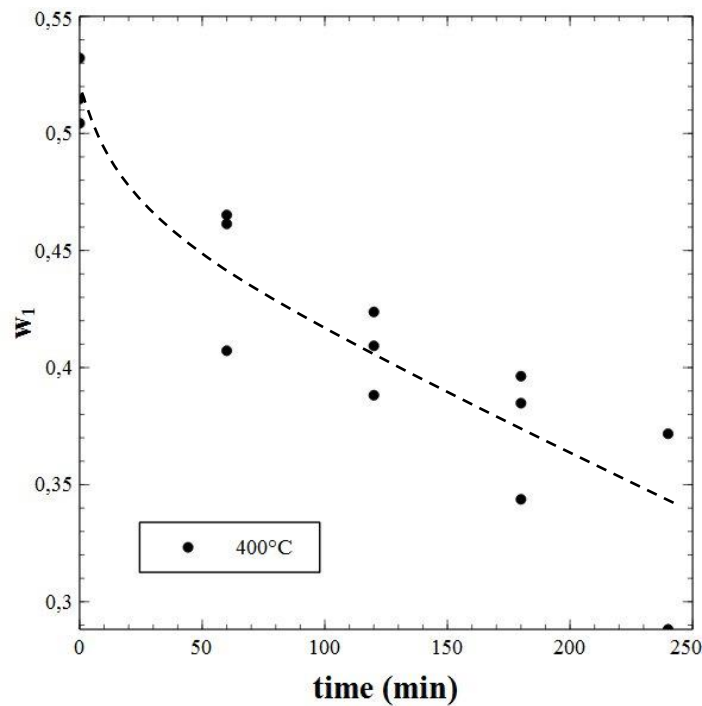


Fig. III.23 : Primary crystallization weight factor vs annealing time at 400°C under nitrogen of neat PEKK 6002 crystallized at 230°C

III.6 IMPACT OF MACROMOLECULAR CHANGES ON MECHANICAL PROPERTIES

The impact of crosslinking on the mechanical properties was studied by Chan et al. [1,2] for PEEK. They reported that the young Modulus increases with crosslinking but especially it is strongly linked to the crystallinity which decreases with crosslinking. In Fig. III.24 and Fig. III.25 are plotted the evolution of the Young modulus and the stress at yield as a function of the annealing time at 400°C of neat PEKK 6002 crystallized at 260°C from the melting state. Only tensile tests results at 180°C are presented as no significant differences were observed at room temperature due to higher dispersion of the measurements and the lower sensibility of the mechanical properties to crystallinity. It can be observed that the Young modulus and the stress at yield decrease with the annealing time which was assumed to be mainly attributed to the decrease of the crystallinity reported in Table III.2.

Annealing time at 400°C (min)	Crystallinity (%)	Young modulus (MPa)	Stress at yield (MPa)
Not annealed	25	145	7.5
60	20.1	130	6.1
120	18.5	106	4.8
180	17.4	89	4.7
240	12.2	58	3.1

Table III.2 : Mechanical properties at 180°C of neat PEKK 6002 annealed at 400°C and crystallized at 260°C from the melting state

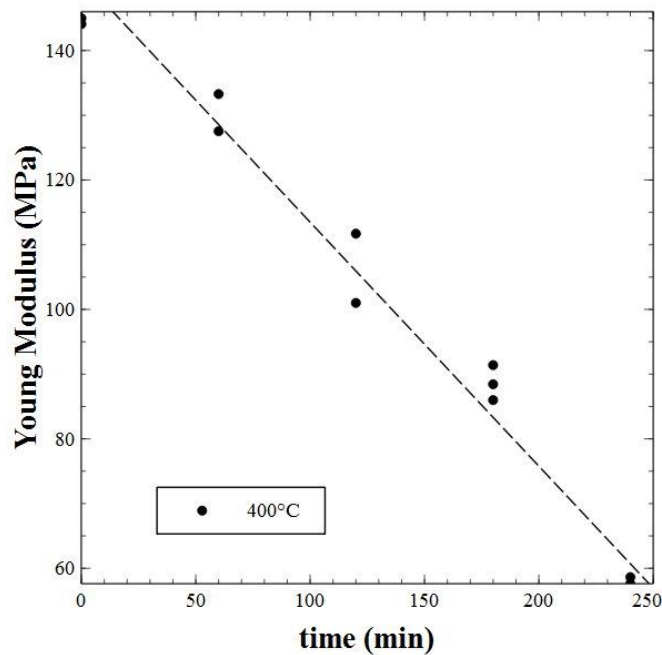


Fig. III.24 : Young modulus vs annealing time at 400°C under air of neat PEKK 6002 crystallized at 260°C from the melting state tested at 180°C

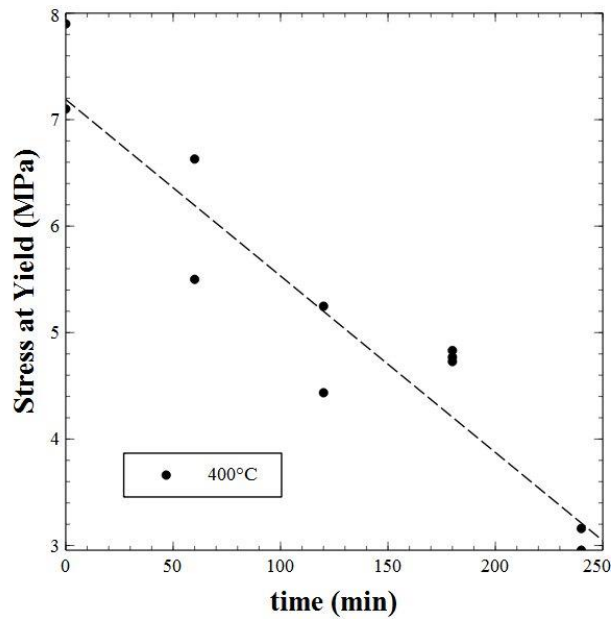


Fig. III.25 : Stress at yield vs annealing time at 400°C under air of neat PEKK 6002 crystallized at 260°C from the melting state tested at 180°C

To assess the impact of macromolecular changes on the mechanical properties independently of the crystallinity, the Young modulus and the stress at yield for annealed and not annealed specimens at 400°C as a function of the crystallinity were compared in Fig. III.26 and Fig. III.27. Regarding the results, there is little difference between the annealed and not annealed specimens which shows that macromolecular changes involve lower mechanical properties due to the significant decrease of the crystallinity. It appears thus clearly that the crosslinking process modifies the mechanical properties investigated here only by decreasing crystallinity. In other words, the fact that the amorphous phase architecture (linear chains towards branched chains) is largely modified does not contribute to the mechanical properties changes for a given crystallinity.

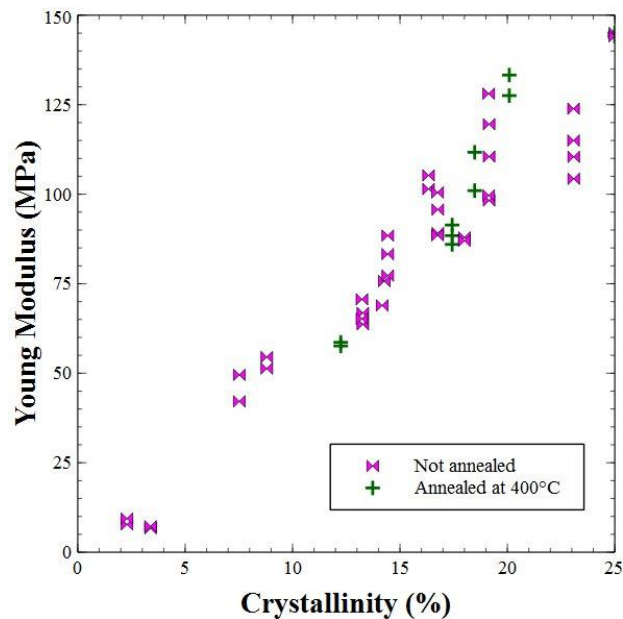


Fig. III.26 : Young modulus vs crystallinity at 180°C of annealed and not annealed PEKK 6002 at 400°C under air crystallized at 260°C from the melting state

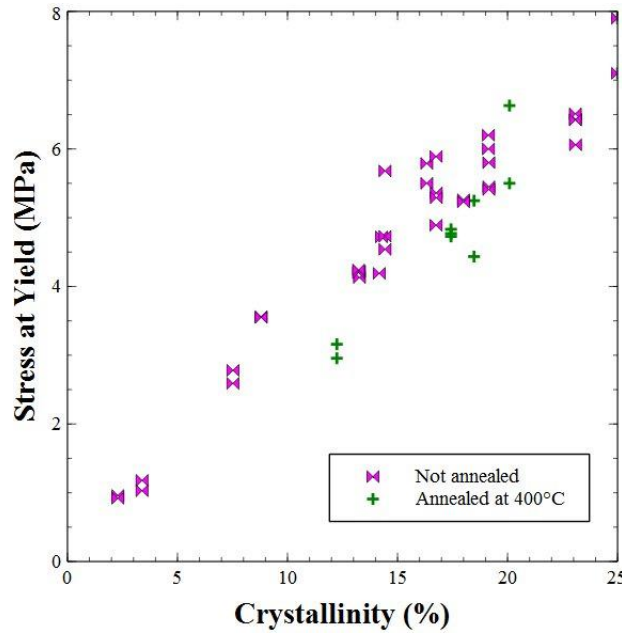


Fig. III.27 : Stress at yield vs crystallinity at 180°C of annealed and not annealed PEKK 6002 at 400°C under air crystallized at 260°C from the melting state

III.7 CONCLUSION

In this chapter, thanks to TGA, rheological, GPC and DSC measurements under air and nitrogen, it has been shown that PEKK 6002 matrix is modified above 320°C associated to the apparition of weight losses, an increase of the weight average molar mass M_w and an increase of the glass transition temperature T_g . All these phenomena are typical to the apparition of crosslinking mechanisms. In addition, according to Saito's approach and from GPC measurements, a chain scission mechanism was found to occur in parallel to crosslinking. These mechanisms have been observed to be thermally activated and following an Arrhenius law. Mainly thermal degradation occurs as the oxidation process is confined only at surface (~10 nm in depth) in contact with air during processing since oxidation is very fast compare to oxygen diffusion. From the kinetic scheme of crosslinking mechanism, crosslinking kinetics has been modelled with a linear model for low exposure times ($t < 20$ min).

Crosslinking occurring at the melt state has been found to decrease crystallinity and crystallization kinetics with the decrease of the crystallization kinetics parameters K_1 and K_2 . The primary crystallization weight factor w_1 has also been observed to decrease with crosslinking which was assumed to be attributed to less perfect crystallization due to the branching of the macromolecular chains which let more space to the growth of the secondary crystallization.

At last, it has been shown that the mechanical properties decrease with crosslinking. This decrease was assumed to be mainly associated to the decrease of the crystallinity with crosslinking. This result is consistent with the results shown in the previous chapter establishing the relationship between the mechanical properties and the crystallinity.

CHAPTER IV. APPLICATION TO PEKK STRUCTURAL COMPOSITES

In this chapter, we investigated the impact of carbon fibers on crystalline morphologies and crystallization kinetics of PEKK matrices. We particularly discussed about the change of the value of the Avrami exponent n_1 due to the potential modification of the crystalline morphologies with carbon fibers. The different manufacturing steps of $\pm 45^\circ$ and unidirectional PEKK composite plates from tape prepregs and consolidated by autoclave or press, the processing tools and the processing conditions are presented. Finally, from composite plates manufactured with different processing thermal conditions, we studied the impact of crystallinity and crystalline morphologies on PEKK composite mechanical properties.

IV.1 EXPERIMENTAL

IV.1.1 Differential Scanning Calorimetry (DSC)

Isothermal and non-isothermal crystallization analyses were carried out on a TA Instruments Q2000 on disk staking cut from tape prepregs with a total weight of about 21 mg. All specimens were first heated at $10^\circ\text{C}\cdot\text{min}^{-1}$ from room temperature to 360°C for PEKK 6002 prepregs and 380°C for PEKK 7002 prepregs and kept during 5 minutes at these temperatures. Those temperatures are above PEKK equilibrium melting temperatures [10] to erase the thermal history and obtain a fully amorphous polymer.

For isothermal crystallization from the melt, specimens were then cooled at $40^\circ\text{C}\cdot\text{min}^{-1}$ to annealing temperatures and kept at the annealing temperature during 240 minutes and finally cooled to room temperature at $40^\circ\text{C}\cdot\text{min}^{-1}$. The chosen cooling rate was high enough to make sure that the polymer does not crystallize before annealing and the annealing time was long enough to allow the polymer to fully crystallize.

For non-isothermal crystallization, specimens were then cooled at cooling rates between $1^\circ\text{C}/\text{min}$ to $10^\circ\text{C}/\text{min}$ to room temperature.

For all specimens after crystallization, a heat scan at $10^\circ\text{C}\cdot\text{min}^{-1}$ from room temperature to 400°C was carried out to measure the glass transition, the melting temperature and the melting enthalpy induced by the crystallization cycle.

IV.1.2 Optical microscopy

IV.1.2.1 Crystallization observations

The optical microscope used was a polarizing Nikon Eclipse LV100 model equipped with a Nikon DS Digital Sight DS-Fi1 camera and a hot stage Linkam LTS-420. Observations were carried out with an ocular lens on PEKK film with a thickness of $10\ \mu\text{m}$ prepared with a Leica RM-2235 microtom and with AS4 carbon fibers. Films were first heated at $10^\circ\text{C}\cdot\text{min}^{-1}$ from room temperature to 360°C during 5 minutes to erase the thermal history of the specimen. Carbon fibers were then incorporated into the bulk. Finally, specimens were cooled down at $40^\circ\text{C}\cdot\text{min}^{-1}$ to 270°C during two hours. This annealing temperature corresponds to a low supercooling i.e. to a low nucleation rate allowing the formation of large spherulites.

IV.1.2.2 Prepregs and composite optical microscopic observations

Microscopic measurements were performed on a Zeiss optical microscope. Samples were preliminary pre-grinded with 80, 180, 800 and 2500 grades SiC papers and finally grinded with 6 μm , 3 μm and 1 μm synthetic diamonded solutions.

IV.1.3 Scanning Electron Microscope (SEM)

Measurements were carried out on a Hitachi Field Emission Gun (FEG) Scanning Electron Microscope (SEM) SU70-1 with a secondary electron detector. The maximum resolution was of about 1 nm. The acceleration tension was 5 KeV and the working distance about 15mm.

IV.1.4 Composite manufacturing processes

IV.1.4.1 Press

The press used for PEKK composite manufacturing was a Pinette Emidecau Industries (PEI) 75 ton laboratory press with a maximum pressure of 285 bars. The dimensions of the plates were 700x700mm². The heat rate capacity was between 1 and 10°C.min⁻¹ with a maximum temperature of 450°C. The maximum cooling rate capacity was about 20°C.min⁻¹.

IV.1.4.2 Autoclave

The autoclave used for PEKK composite manufacturing was a Pecquet Tesson (PTC) autoclave with a volume of 11.9 m³ and a maximum pressure of 50 bars. The cooling and heating rate capacity was between 1 and 5°C.min⁻¹.

IV.1.5 Tensile tests

Mechanical tests were carried out with a tensile test machine Instron 5966 equipped with an oven to make tests at high temperature. Tests were done on normalized composites tensile samples described in Fig. IV.1. Two different samples were tested, unidirectional 8 plies stratified samples with a thickness of about 1 mm and a width of 10 mm (norm AITM1-007) and 16 \pm 45° plies stratified samples with a thickness of about 2 mm and a width of 25 mm (norm AITM1-0002). According to the norms, tabs made with \pm 45° 3 glass fibers plies were bonded at the tensile specimen ends. Tensile and shear modulus were measured with a 4 points system painted on each specimen followed with a camera during the entire test (Fig. IV.2). Acquired images were exploited with an image processing program. The shear modulus was measured with the following equation:

$$G = \frac{\Delta P}{2wt(\Delta\varepsilon_{0^\circ} - \Delta\varepsilon_{90^\circ})} \quad \text{Equation IV.1}$$

where w and t are the width and the thickness respectively, $\Delta\varepsilon_{0^\circ} = (\varepsilon_{0^\circ})_2 - (\varepsilon_{0^\circ})_1$ with the longitudinal strains $(\varepsilon_{0^\circ})_2 = 2500 \cdot 10^{-6}$ and $(\varepsilon_{0^\circ})_1 = 500 \cdot 10^{-6}$, $\Delta\varepsilon_{90^\circ} = (\varepsilon_{90^\circ})_2 - (\varepsilon_{90^\circ})_1$ with $(\varepsilon_{90^\circ})_2$ and $(\varepsilon_{90^\circ})_1$ the corresponding transverse strains to longitudinal strains and ΔP is the difference in corresponding tensile loads to longitudinal strains. Specimens were tested at room temperature and 180°C (above T_g) with testing speed of 1 mm.min⁻¹ according to the norms. At 180°C, the crystallization kinetics is low enough to assume that the polymer do not crystallize during the mechanical test.

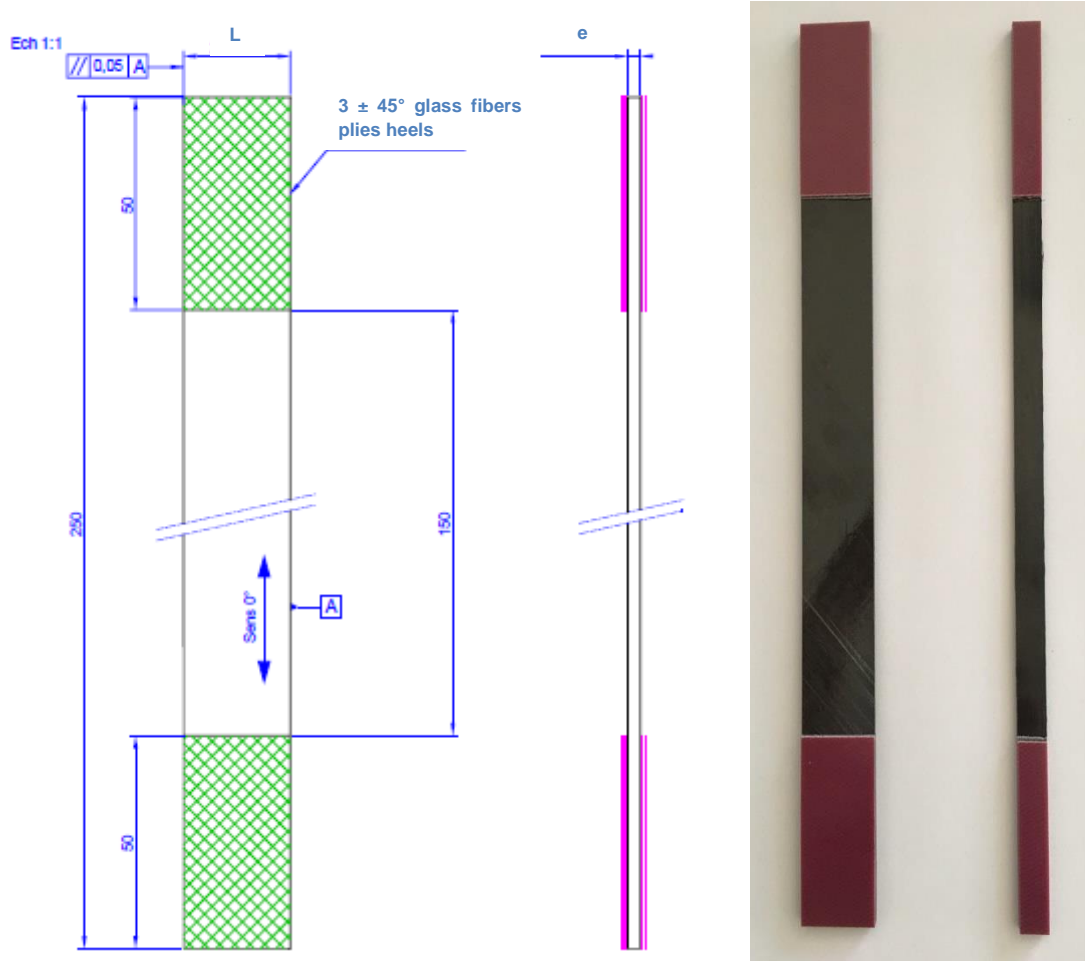


Fig. IV.1: Dimensions of the normalized composites specimens



Fig. IV.2: Measurement system of composite tensile tests

IV.2 PEKK PREPREGS

Received PEKK prepregs tapes were first analyzed by optical microscopic and SEM observations to control the impregnation quality (Table IV.1). It can be observed for both PEKK 6002 and 7002 prepregs a quite good repartition of the fibers into the matrix and all fibers seemed to be well impregnated with the matrix. However, prepregs tapes were observed to be split at different lengths of the roll due to dry areas of matrix (Fig. IV.3).

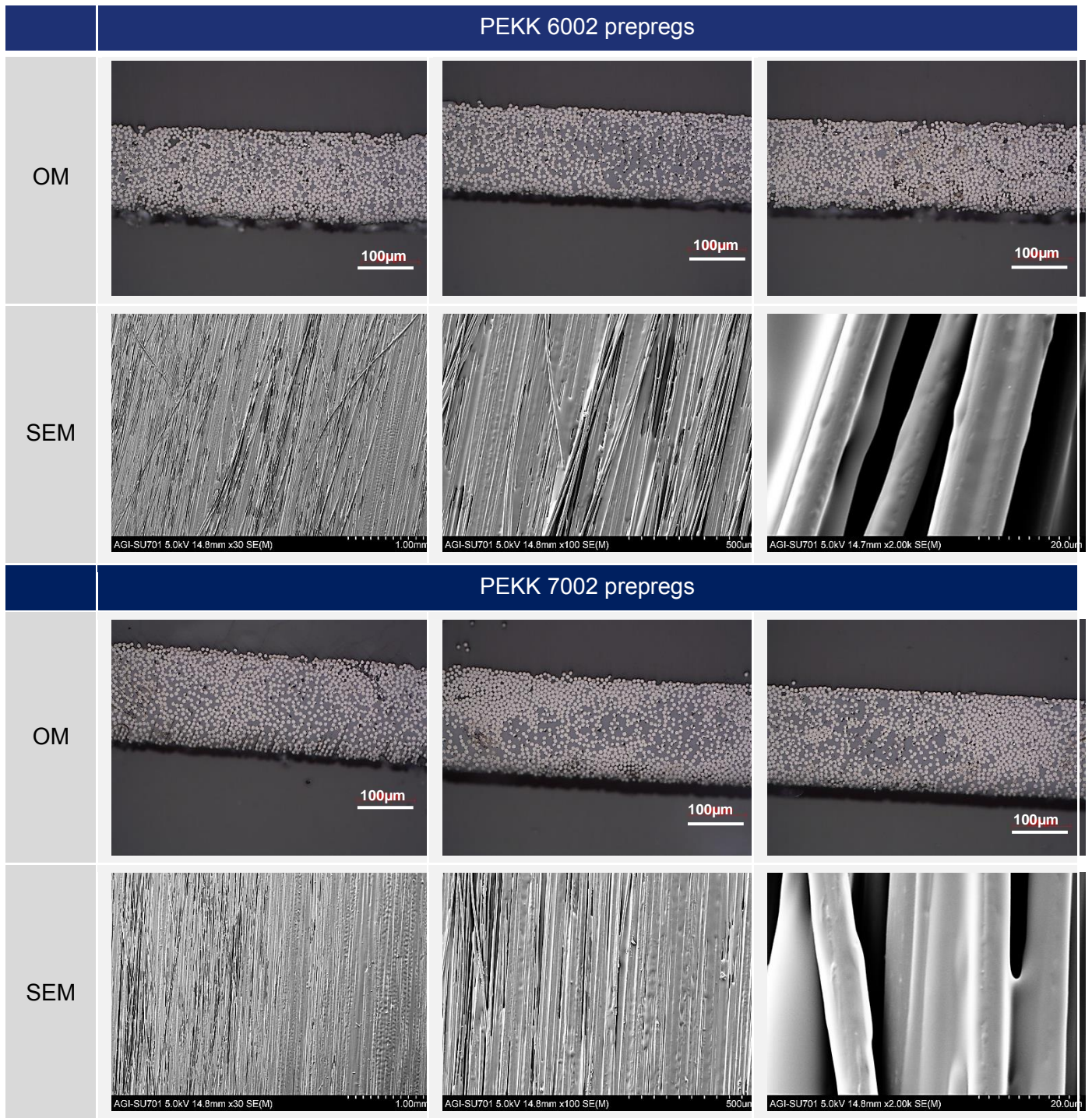


Table IV.1: Optical microscopic and SEM observations of PEKK 6002 and 7002 prepregs

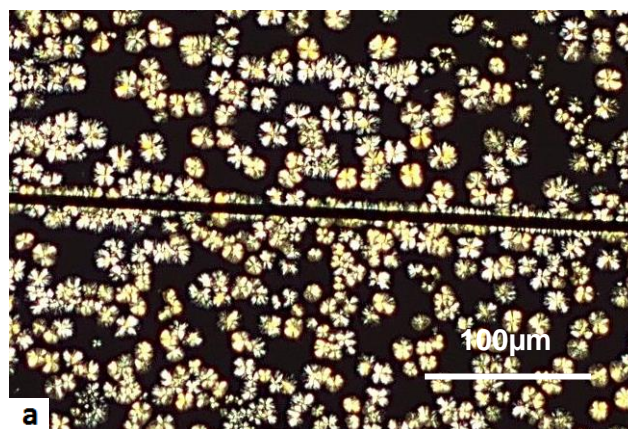


Fig. IV.3: Picture of PEKK prepregs tape split in the middle

IV.3 IMPACT OF CARBON FIBERS ON CRYSTALLIZATION

IV.3.1 Impact of carbon fibers on crystalline morphologies

The influence of carbon fibers on crystalline morphologies was investigated by optical microscopy. Fig. IV.4 shows the crystal growth of a PEKK 6002 resin crystallized from the melt at 270°C during 2 hours in the presence of a carbon fiber. Two distinct crystalline phases were observed. A first one corresponding to the matrix bulk crystallization with spherulitic crystalline entities and a second one to a so-called transcrystalline phase [80,81,6] occurring at the surface of the fibers and growing perpendicularly to them. In fact, carbon fibers act as nucleating agents from which crystalline entities grow. As nuclei are closed to each other at the surface of the fibers, the impingement between neighboring nuclei forces the crystallization to grow normally to the fibers.



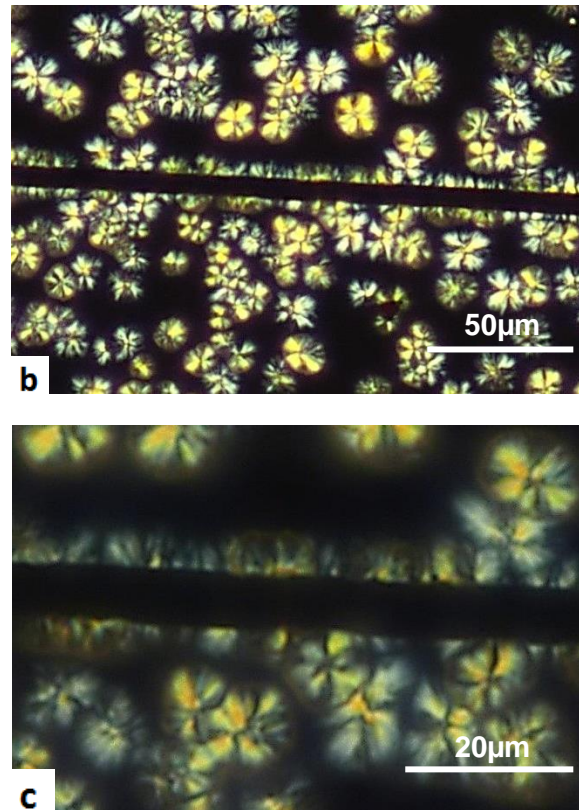


Fig. IV.4: Micrographs of PEKK 6002 with carbon fibers crystallized from the melt at 270°C during 2h

IV.3.2 Impact of carbon fibers on crystallization kinetics

IV.3.2.1 Isothermal crystallization kinetics

As we showed in paragraph IV.3.1, carbon fibers are effective nucleating sites for the resin matrix which could potentially modify the crystallization kinetics of the neat resin. It can be added that as carbon fibers are closed to each other in the prepregs (a few micrometers), the crystallization of the matrix could be hindered in the same time. The effect of carbon fibers on crystallization kinetics was studied by DSC measurements and the same methodology as presented in CHAPTER II was carried out to model the crystallization kinetics of PEKK prepregs. The fitting of the derivative Hillier model established in CHAPTER II with the heat flow measured by DSC for isothermal crystallization at 210°C and 270°C are presented in Fig. IV.5. As microscopic observations exhibited two distinct crystallization mechanisms, two different modelling were investigated. A first one with an Avrami exponent $n_1=3$ corresponding to the 3D spherulitic growth related to the resin bulk crystallization (Fig. IV.5.a) and a second one with an Avrami exponent $n_1=2$ related to the 2D transcrystalline growth normally to the carbon fiber surfaces (Fig. IV.5.b).

For $n_1=2$, it can be observed that the model fits better with experiment for crystallization at 270°C than at 210°C and an important induction time t_i about 15 minutes at 270°C was found to obtain the best with experiments which physically does not seem consistent. For $n_1=3$, this is the opposite, the model fits better with experiments for crystallization at 210°C compared to 270°C. This phenomenon could be attributed to the fact that at low crystallization temperatures, the nucleation kinetic in the bulk is very fast promoting the growth of spherulites ($n_1=3$) whereas at high crystallization temperatures, the nucleation kinetic in the bulk is very low and thus the main crystallization mechanism would occur from nuclei at the

surface of the carbon fibers promoting involving 2D transcrystalline growth ($n_1=2$). This is consistent with Lee and Porter [80] who showed that the surface of carbon fibers and nuclei in the matrix compete for crystallization growth and the number of spherulites decrease as a more pronounced transcrystalline region is developed. It can be assumed that for intermediary temperatures, the Avrami exponent n_1 evolves between 2 and 3 which has no physical sense: a double domain crystallization model should be developed.

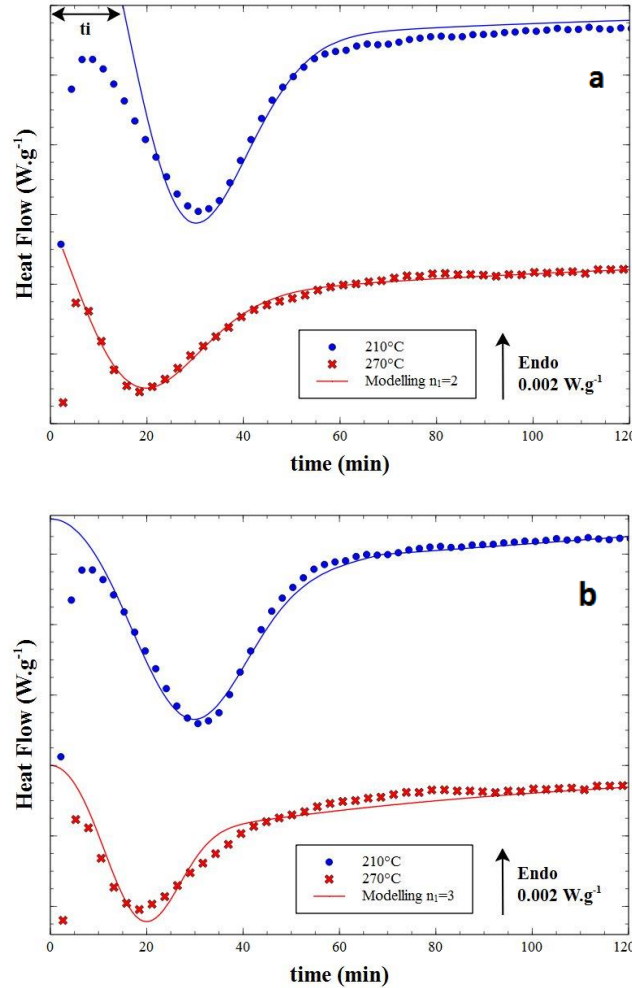


Fig. IV.5: DSC thermograms of PEKK 6002 prepregs crystallized from the melt at 210°C and 270°C with the fitting of the derivative Hillier model (solid line) with $n_1=2$ (a) and $n_1=3$ (b)

The logarithm of K_1 and K_2 determined from the derivative Hillier model fitting for PEKK 6002 prepregs with $n_1=3$ and $n_1=2$ compared to the neat PEKK 6002 resin crystallized from the melt have been plotted in Fig. IV.6 and fitted with the Hoffman and Lauritzen model. Results for K_{0i} , K_{gi} and U^* are presented in Table IV.2. It can be noticed that for $n_1=2$, the unity of the primary crystallization rate constant K_1 is in min^{-2} regarding the Avrami equation and the Hoffman and Lauritzen equation for K_1 becomes:

$$K_1(T) = K_{01} \exp\left(-\frac{2U^*}{R(T-T_\infty)}\right) \exp\left(-\frac{2K_{g1}}{T\Delta T f}\right) \quad \text{Equation IV.2}$$

It can be observed that the maximum value of K_1 is shifted to a higher temperature for PEKK prepregs than for the neat resin with a value of about 250°C. By comparing K_1 for PEKK prepregs with $n_1=3$ and for the neat resin, the crystallization kinetics seems to be lower for

the preregs for temperatures below 265°C whereas above this temperature this is the opposite. This phenomenon could be explained by the fact that carbon fibers induce the formation of new nuclei at their surface which initiate crystallization earlier and thus increase crystallization kinetics. However, at lower temperatures the nucleation kinetics in the bulk is more important and thus the nuclei induced by carbon fibers have less effect on the crystallization kinetics. For the lower crystallization kinetics for the preregs compared to the neat resin for temperatures below 265°C, we could also suppose that carbon fibers hinder the macromolecular chain mobility and thus decrease crystallization kinetics, but it is not realistic knowing that confined crystallization occurs for domains in which thicknesses are less than 50 - 100 nm

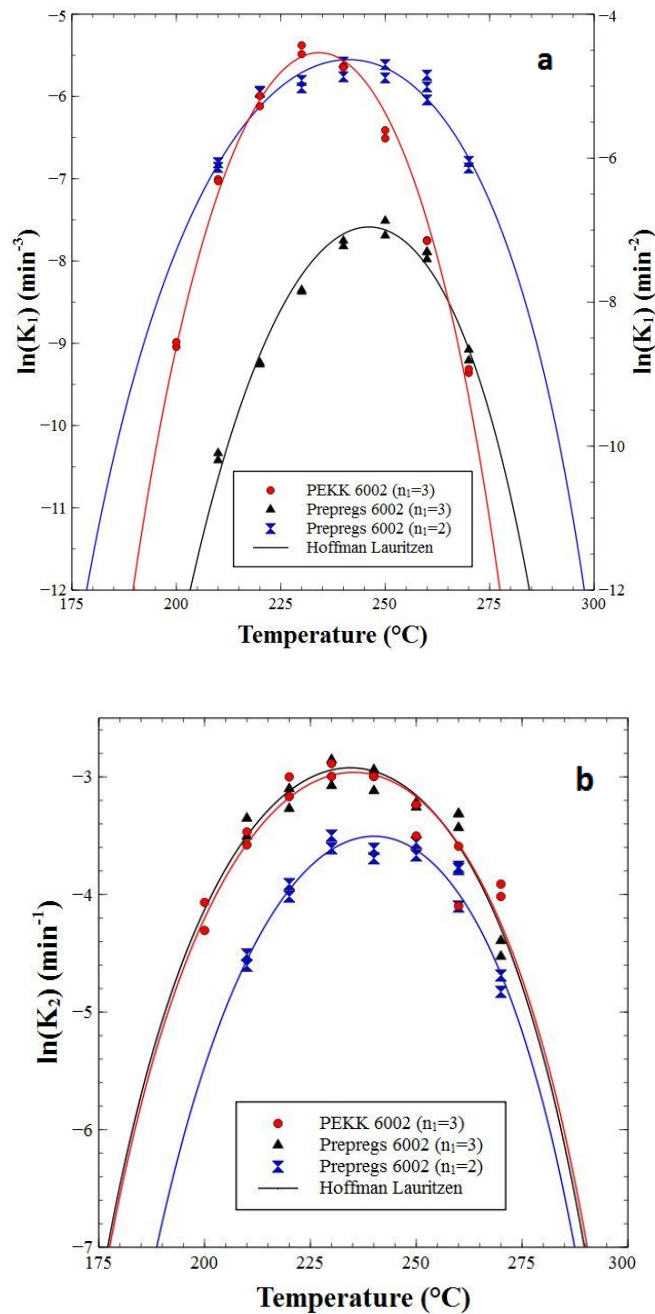


Fig. IV.6: Logarithmic plot of the primary (a) and the secondary crystallization (b) rate constants vs temperature for neat PEKK 6002 and preregs isothermal crystallization from the melt with the Hoffman and Lauritzen model fitting

The primary crystallization weight factor (w_1) for PEKK 6002 prepregs with $n_1=3$ and $n_1=2$ compared to the neat PEKK 6002 resin has been plotted as a function of temperature in Fig. IV.7 with the linear model fitting. Results for a_1 and b_1 are presented in Table IV.2. It can be observed that for a given crystallization temperature w_1 is lower for the prepregs than for the neat resin which could be explained by the fact that as carbon fibers modify crystallization, crystalline entities are less perfect than for the neat resin increasing the amount of secondary crystallization. However, another hypothesis could be that transcrystalline phase involves more secondary crystallization than the spherulitic phase.

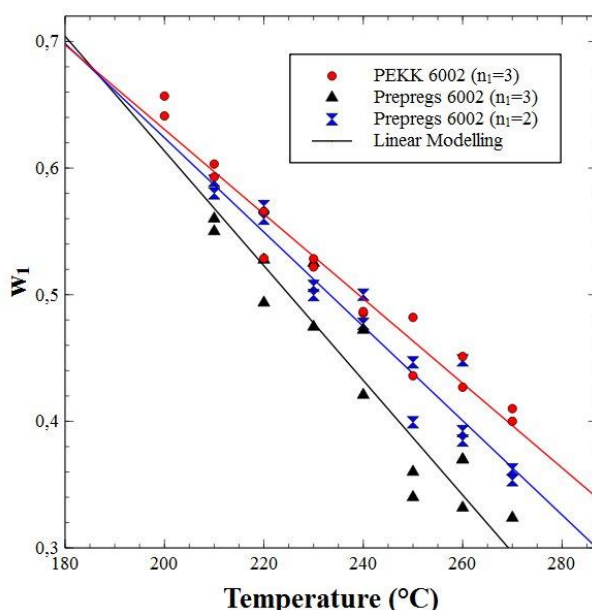


Fig. IV.7: Weight factor of the primary crystallization vs temperature for neat PEKK 6002 and prepregs isothermal crystallization from the melt with the linear model fitting

Kinetics paramaters	PEKK 6002 prepregs ($n_1=2$)	PEKK 6002 prepregs ($n_1=3$)
T_{m0} (°C)	340	340
K_{01} (min^{-2})	$1.4 \cdot 10^6$	
K_{01} (min^{-3})		$2.1 \cdot 10^9$
K_{02} (min^{-1})	$7.8 \cdot 10^4$	$1.5 \cdot 10^4$
K_{g1} (K^2)	$2.4 \cdot 10^5$	$2.2 \cdot 10^5$
K_{g2} (K^2)	$3.8 \cdot 10^5$	$3.6 \cdot 10^5$
U_1^* ($\text{J} \cdot \text{mol}^{-1}$)	$4.1 \cdot 10^3$	$4.7 \cdot 10^3$
U_2^* ($\text{J} \cdot \text{mol}^{-1}$)	$6.3 \cdot 10^3$	$4.7 \cdot 10^3$
a_1 (K^{-1})	$-3.7 \cdot 10^{-3}$	$-4.5 \cdot 10^{-3}$
b_1	2.4	2.8

Table IV.2: Parameters of the kinetic models for the crystallization rate constants (K_1 and K_2) and the weight factor (w_1) for PEKK 6002 prepregs crystallized from the melt with $n_1=2$ and $n_1=3$

Finally, TTT diagrams of PEKK 6002 prepregs with $n_1=2$ and $n_1=3$ have been built from Hillier modelling and plotted in Fig. IV.8.a. and Fig. IV.8.b. respectively. For high crystallization temperature above around 270°C, it can be assumed from the derivative Hillier model fitting (Fig. IV.5) that the main crystallization mechanism is a 2D transcrySTALLINE growth corresponding to an Avrami exponent $n_1=2$ (Fig. IV.8.a) whereas for low crystallization temperatures below around 210°C, the main mechanism is assumed to be a 3D spherulitic growth associated to an Avrami exponent $n_1=3$. For intermediary temperatures, both crystalline phases coexist with an Avrami exponent n_1 between 2 and 3 depending on the crystallization temperature. If we compare TTT diagram of the neat resin and the prepreg, it can be observed that crystallization kinetics are not much modified with the presence of carbon fibers even if the TTT diagram for the prepregs is slightly shifted to higher temperatures due to the nucleation occurring at the surface of carbon fibers.

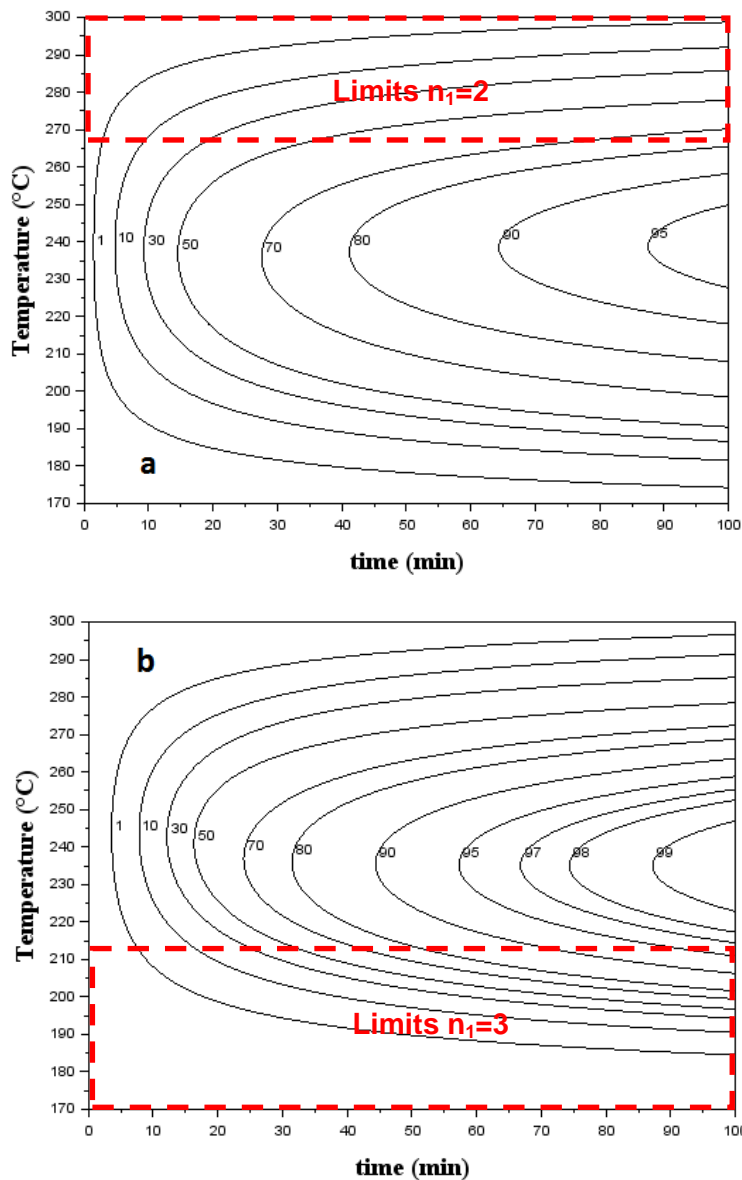
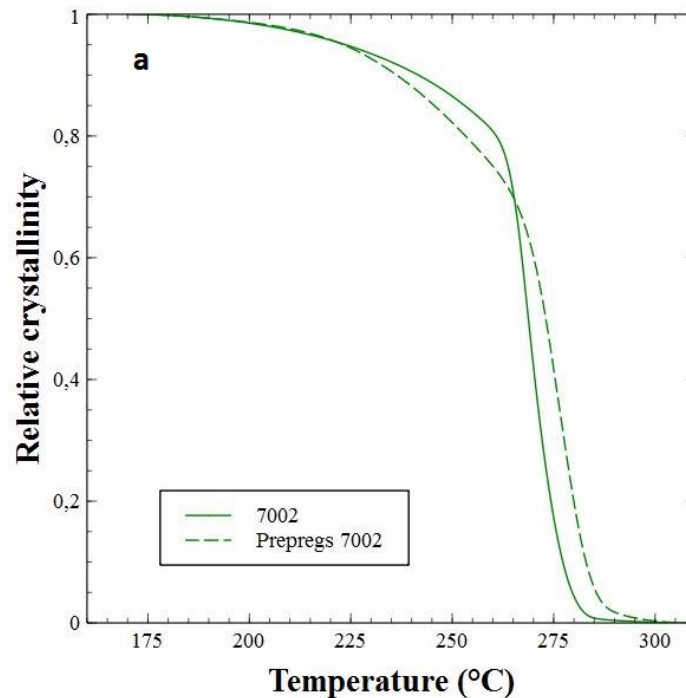


Fig. IV.8: TTT diagram of the relative crystallinity for the overall crystallization for PEKK 6002 prepregs crystallized from the melt with Avrami exponent $n_1=2$ (a) and $n_1=3$ (b)

IV.3.2.2 Non-isothermal crystallization kinetics

A non-isothermal crystallization kinetics study was also performed to investigate the impact of carbon fibers on crystallization kinetics. As it was only possible to put around 21 mg of preregs in the DSC capsules which corresponds to 6.7 mg of matrix according to the matrix mass content (32%) of the preregs and due to low crystallinity, DSC crystallization peaks of PEKK 6002 preregs were very small, thus only non-isothermal crystallization for PEKK 7002 preregs could be studied. Results for neat PEKK 7002 and PEKK 7002 preregs crystallized from the melt at $5^{\circ}\text{C}\cdot\text{min}^{-1}$ and $10^{\circ}\text{C}\cdot\text{min}^{-1}$ are presented in Fig. IV.9. It can be observed that crystallization initiates earlier for the preregs than for the neat resin attributed to the nucleation from carbon fibers. At $10^{\circ}\text{C}\cdot\text{min}^{-1}$ (Fig. IV.9.a), the crystallization kinetics of the neat resin becomes higher than the preregs around 265°C . This phenomenon is consistent with the comparison of the evolution of K_1 as a function of the temperature for the preregs and the neat resin which was higher for the preregs than for the neat resin for temperatures below 265°C . At $5^{\circ}\text{C}\cdot\text{min}^{-1}$ (Fig. IV.9.b), the crystallization kinetics for the preregs is higher than for the neat resin during all the cooling which is due to the fact that as the cooling rate is slow, crystallization mainly occurs at temperatures above 265°C (around 90%) where K_1 is higher for the preregs than for the neat resin.



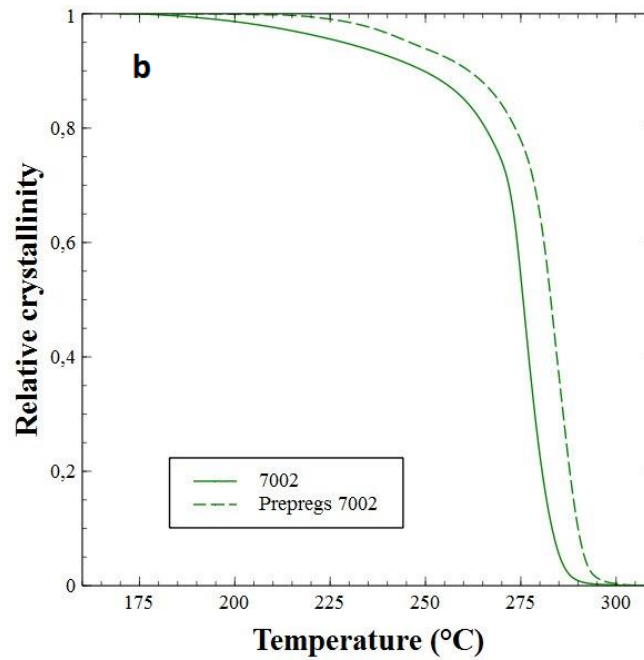


Fig. IV.9: Relative fraction crystallinity $\alpha(t)$ vs temperature for neat PEKK 7002 and PEKK 7002 prepregs crystallized from the melt at $10^{\circ}\text{C}\cdot\text{min}^{-1}$ (a) and $5^{\circ}\text{C}\cdot\text{min}^{-1}$ (b)

IV.4 PEKK COMPOSITE MANUFACTURING

IV.4.1 Protocol

The impact of carbon fibers on mechanical properties were investigated by manufacturing composite plates from PEKK 6002 and 7002 prepregs with different orientations of the carbon fibers and different thermal conditions. As it was carried out for the neat resin in CHAPTER II, the aim was to study the impact of crystallinity and crystalline morphologies on PEKK composites. Two different types of plates were manufactured, unidirectional 8 plies stratified plates with a thickness of about 1 mm and $16 \pm 45^{\circ}$ plies stratified plates with a thickness of about 2 mm. In fact, tensile test on UD composites will provide mainly the fiber mechanical properties whereas $\pm 45^{\circ}$ composites will give more information on the matrix. Prepregs tapes were first cut straight or 45 degrees, welded edge to edge and cut again to the dimensions of the plate of $200 \times 300 \text{mm}^2$. The different plies were finally stacked.

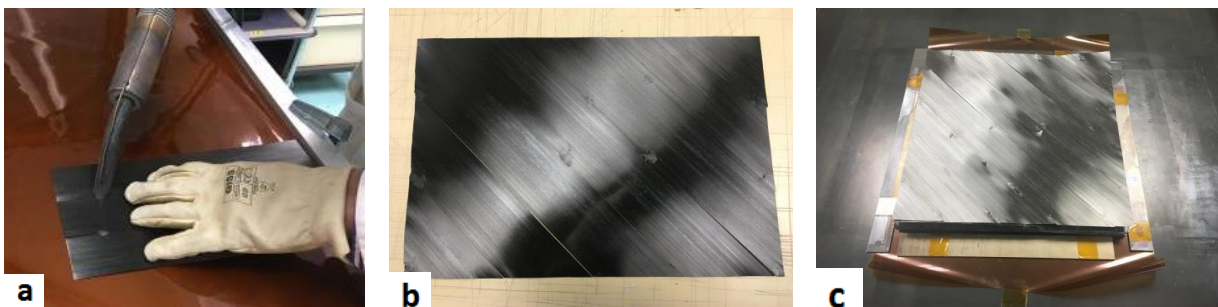


Fig. IV.10: Pictures of the edge to edge welding of PEKK tapes (a), a 45° ply (b) and a $\pm 45^{\circ}$ stack (c)

Five different processing thermal conditions were tested in order to manufacture composite plates with fully crystallized matrix, amorphous matrix, high and low temperature crystallized matrix corresponding to potentially high and low amount of transcrystalline phase respectively (Table IV.3). As PEKK 7002 matrix crystallizes very fast, only PEKK 7002

composites with fully crystallized matrix were manufactured. All heating and cooling rates not listed in Table IV.3 are equal to 10°C/min.

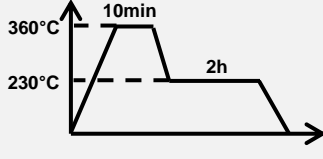
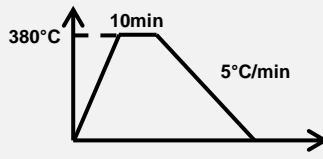
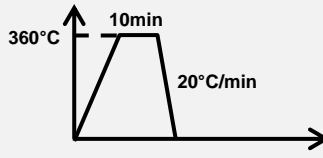
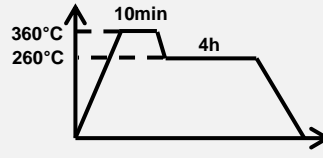
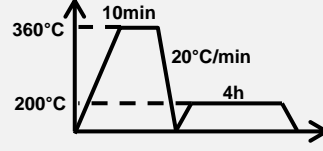
PEKK 6002 composites		PEKK 7002 composites	
Fully crystallized matrix		Fully crystallized matrix	
Amorphous matrix (press)			
High crystallization temperature (autoclave)			
Low crystallization temperature (press)			

Table IV.3: Processing thermal cycles for PEKK composite manufacturing

The composite plates were manufactured with two different processes, autoclave and press. The press was used because it can cool down the composite quickly after consolidation up to 20°C.min⁻¹ allowing to obtain PEKK 6002 composites with amorphous matrix. The autoclave was used to crystallize the matrix at high temperature due to an important overshoot of the temperature of the press at high temperature which is not the case for the autoclave. In fact, for crystallization from the melt at 260°C, during the cooling, the temperature of the press went down until 230°C and then went up to 260°C to reach the set temperature. As we showed in CHAPTER II, the crystallization kinetics of PEKK 6002 is the most important at 230°C, hence it was sure that the polymer would begin to crystallize before stabilizing at 260°C. All composite plates manufactured with the autoclave and the press were consolidated at 7 bars.

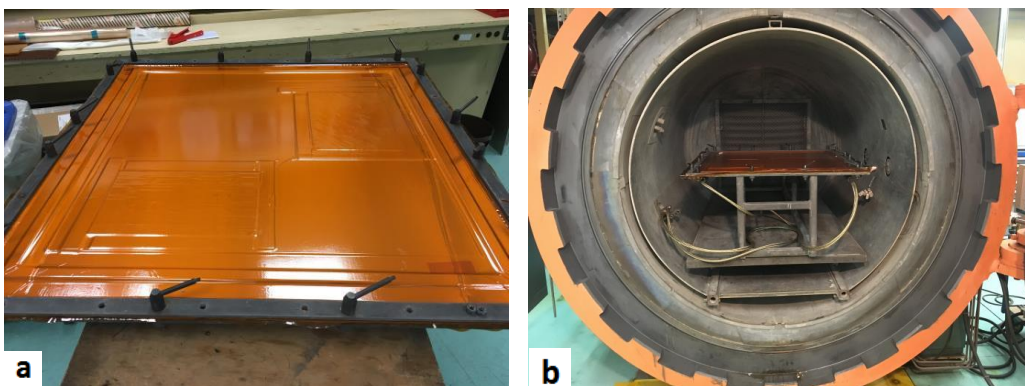


Fig. IV.11: Picture of the processing environment under autoclave (a) and the autoclave used (b)

Different processing environments are necessary with these two processes (see Fig. IV.12). Only thermal-imide shits on which release agent called Frekote were before coated to unmold the composite plate after its processing under press whereas a more complex environment were used under autoclave composed by thermal-imide, shims to avoid side effects, a 300 g.m⁻² woven fiber glass called breather to drain the air and a vacuum bag to applicate uniformly pressure and evacuate the air trapped in the composite.

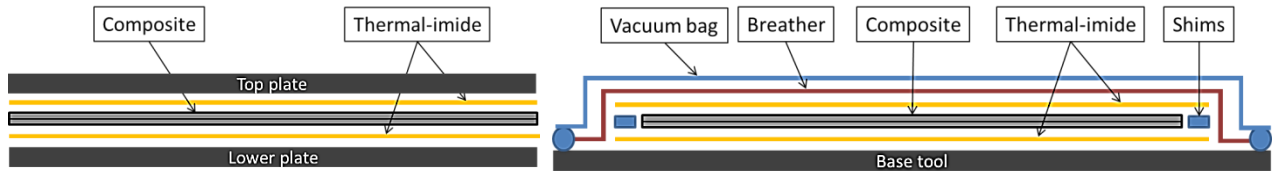


Fig. IV.12: Descriptive diagram of the processing environment of PEKK composites consolidated under press (left diagram) and autoclave (right diagram)

IV.4.2 Composite plates quality control

The quality of the composite plates manufacturing, more precisely the repartition of the fibers and the presence of porosities in the composite plates were investigated by optical microscopy (Fig. IV.13). For the PEKK 6002 composite plate crystallized at 230°C during 2h from the melt, a quite good repartition of the fibers in the matrix was observed without detectable porosities. For the plate cooled at 20°C.min⁻¹ to obtain amorphous matrix, some defects were observed at different places into the composite in particular between two plies which could be attributed to the fact that prepregs were split at different lengths of the roll. Another possibility could be that porosities are due to the very high cooling rate. However, for other processing conditions same defects were observed. A last hypothesis could be that the press plates are not perfectly paralleled inducing a non-uniform pressure on the composite during the consolidation.

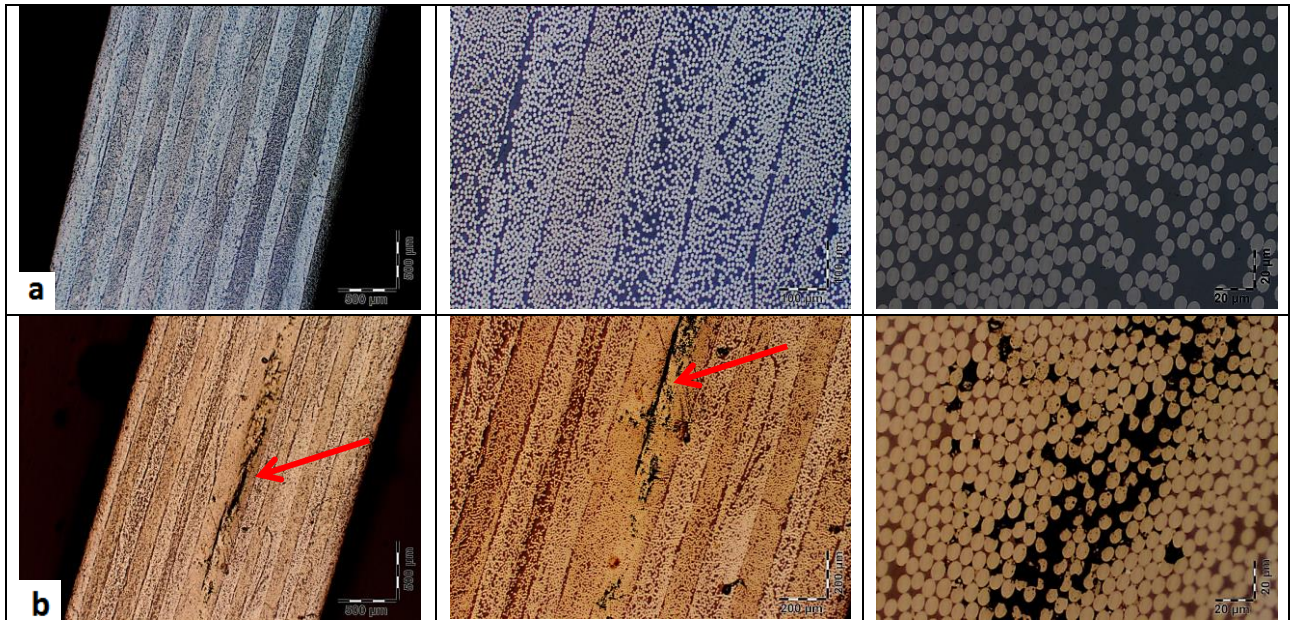


Fig. IV.13: Optical microscopic observations of ± 45° PEKK 6002 composites plates fully crystallized at 230°C during 2h (a) and cooled at 20°C.min⁻¹ (b) from the melt under press

IV.4.3 DSC analysis

DSC scan from room temperature to 400°C at 10°C/min were carried out on composites samples cut from the manufactured composite plates to measure the crystallinity. Results are presented in (Table IV.4). The crystallinity were calculated with:

$$X_c = \frac{\Delta H_m - \Delta H_{cc}}{\Delta H_{100\%} \alpha_M} \quad \text{Equation IV.3}$$

With ΔH_m the melting enthalpy (J.g⁻¹), ΔH_{cc} the cold crystallization enthalpy (J.g⁻¹), $\Delta H_{100\%}=130$ J.g⁻¹ the fully crystallized polymer enthalpy [20] and $\alpha_M=32\%$ the mass fraction of matrix in the composite calculated in CHAPTER I.

	PEKK 6002 composite		PEKK 7002 composite	
X_c (%)	Autoclave	Press	Autoclave	Press
Fully crystallized	30	30	33	28
Amorphous		5		
High crystallization temperature	28			
Low crystallization temperature		30		

Table IV.4: Crystallinity X_c (%) vs crystallization conditions for PEKK composites consolidated under autoclave and press

Differently to the neat resin, PEKK 6002 and 7002 composites seem to have the same crystallinity equal to the crystallinity measured for the neat PEKK 7002 resin. Those crystallinity values may be overpredicted since they strongly depend on the mass fraction of matrix calculated with averaged data given by the company providing the prepregs. Crystallinity were not observed to much change as a function on the crystallization conditions with a crystallinity around 30% except for PEKK 6002 composite cooled quickly at 20°C.min⁻¹ from the melt which has a quasi-amorphous matrix with a crystallinity of 5%.

IV.5 MECHANICAL PROPERTIES OF PEKK COMPOSITES

IV.5.1 Unidirectional composites

In this study, only fully crystallized UD composites manufactured under autoclave were manufactured. No UD composites consolidated under press were studied due to a lack of time. Results of the Young modulus of fully crystallized PEKK 6002 and 7002 composites tested at room temperature and at 180°C (above the glass transition temperature of both matrices) are presented in Fig. IV.14 and Table IV.5. It can be observed a drop of the Young modulus for tensile tests above the glass transition temperature about 27% for PEKK 6002 composites and 16% for PEKK 7002 composites whereas the tensile test direction is the same as carbon fibers. This shows that even for UD composite, the mechanical properties of the composite depend on the matrix properties. The Young modulus of PEKK 7002 composites seems to be higher than for PEKK 6002 composites particularly above T_g with a

difference of about 14%. This phenomenon could be associated to a slightly more important crystallinity of the matrix of PEKK 7002 composite compared to PEKK 6002 composite consolidated under autoclave (see Table IV.4).

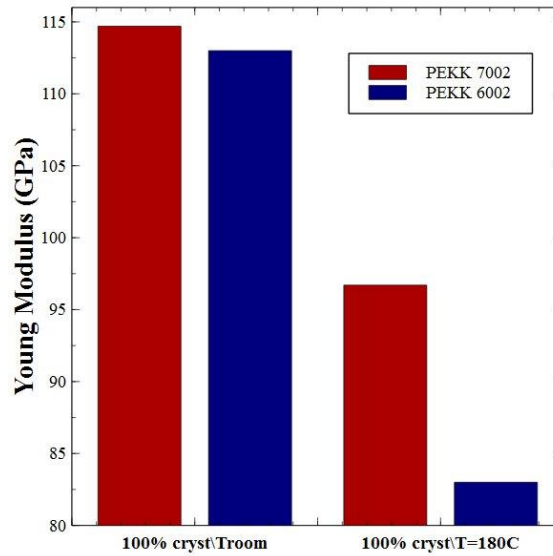


Fig. IV.14: Evolution of the Young modulus of UD fully crystallized PEKK composites manufactured under autoclave tested at room temperature and at 180°C

T _{test}	PEKK 7002 composite		PEKK 6002 composite	
	T _{room}	180°C	T _{room}	180°C
Young modulus (GPa)	115	97	113	83

Table IV.5: Young modulus of UD fully crystallized PEKK 6002 and 7002 composites manufactured under autoclave tested at room temperature and at 180°C

IV.5.2 ± 45° composites

IV.5.2.1 Influence of crystallinity on PEKK composite mechanical properties

Tensile tests were carried out at room temperature and at 180°C on PEKK composite samples with fully crystallized and quasi-amorphous matrix consolidated under press to assess the influence of crystallinity on PEKK composite mechanical properties. Results are presented in Fig. IV.15 and Table IV.6. As expected, it can be observed a drop of the mechanical properties of PEKK composites at 180°C with a decrease of about 90% of the Young modulus and the shear modulus. In addition, it can be noticed that this decrease is higher than for UD composites which confirms that ± 45° composite mechanical properties are more sensitive to the matrix properties than for UD composites which more depend on fiber properties. At room temperature, the Young modulus and the shear modulus decrease about 11% and 28% respectively for quasi-amorphous PEKK 6002 composite compared to fully crystallized PEKK 6002 composite. At 180°C, this phenomenon is much more important with a decrease of 80% and 90% for the Young modulus and the shear modulus respectively. Hence, it can be concluded that even for PEKK composites reinforced with carbon fibers, the matrix crystallinity plays a very important role for the mechanical properties

particularly above T_g , it is the crystalline phase which gives the mechanical strength to the matrix. Mechanical properties of PEKK 6002 and 7002 composites were observed to be closed even if it seems that they are lower for PEKK 7002 than for PEKK 6002 composites. This could be associated to the lower crystallinity of PEKK 7002 matrix compared to PEKK 6002 matrix for composites consolidated under press (see Table IV.4).

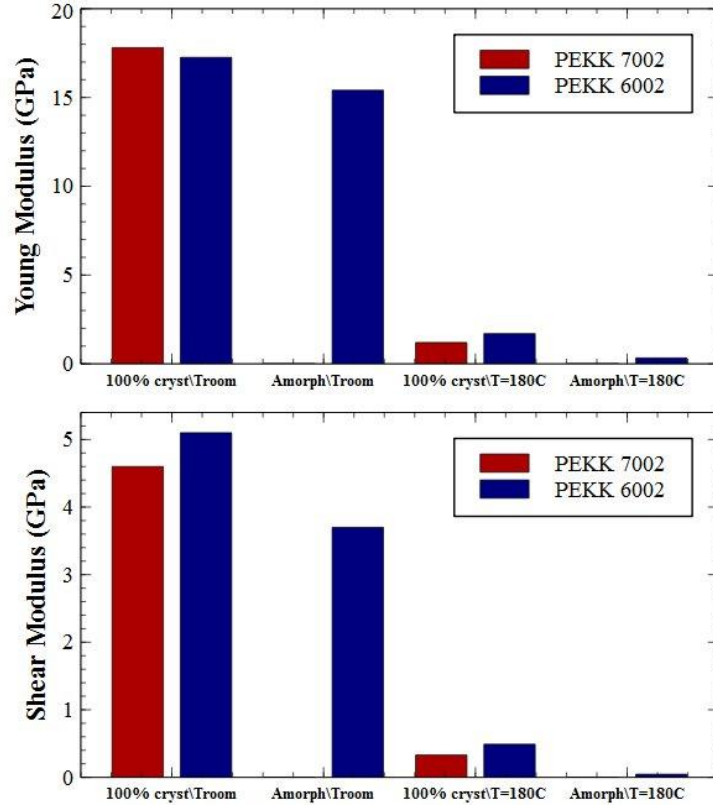


Fig. IV.15: Evolution of the Young modulus and the shear modulus of $\pm 45^\circ$ fully crystallized at 230°C from the melting state and amorphous PEKK composites manufactured under press tested at room temperature and at 180°C

T_{test}	PEKK 7002 composite				PEKK 6002 composite			
	Fully crystallized		Amorphous		Fully crystallized		Amorphous	
	T_{room}	180°C	T_{room}	180°C	T_{room}	180°C	T_{room}	180°C
Young modulus (GPa)	17.8	1.2	X		17.3	1.7	15.41	0.33
Shear modulus (GPa)	4.6	0.33			5.1	0.49	3.7	0.046

Table IV.6: Young modulus and shear modulus of $\pm 45^\circ$ fully crystallized at 230°C from the melting state and amorphous PEKK composites manufactured under press tested at room temperature and 180°C

Pictures of the tested composite tensile samples are presented in Fig. IV.16. It can be observed that all samples tested at room temperature are broken whereas at 180°C , the strain was too high to be measured with the tensile test machine. At last, an important necking process was observed for samples tested at 180°C .

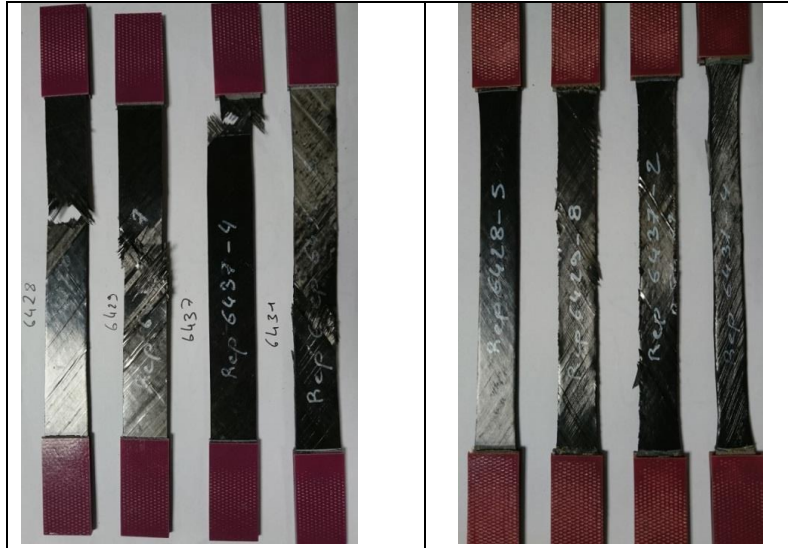


Fig. IV.16: Picture of PEKK composite samples after tensile tests at room temperature (left picture) and at 180°C (right picture)

Fully crystallized PEKK composite plates were also manufactured under autoclave with same processing parameters than under press presented in Fig. IV.15 to investigate the impact of the manufacturing process. Tensile test results are presented in Fig. IV.17 and Table IV.7. At room temperature it was difficult to identify a trend whereas at 180°C, mechanical properties of PEKK composite consolidated under autoclave were observed to be higher than under press. At 180°C, a difference of 27% and 11% for the Young Modulus and 15% and 8% for the shear modulus for PEKK 7002 and 6002 composite respectively. This could be associated to the fact that press plates are not perfectly parallel inducing a non-uniform pressure on the composite during the consolidation whereas under autoclave the pressure is uniform on the entire composite surface.

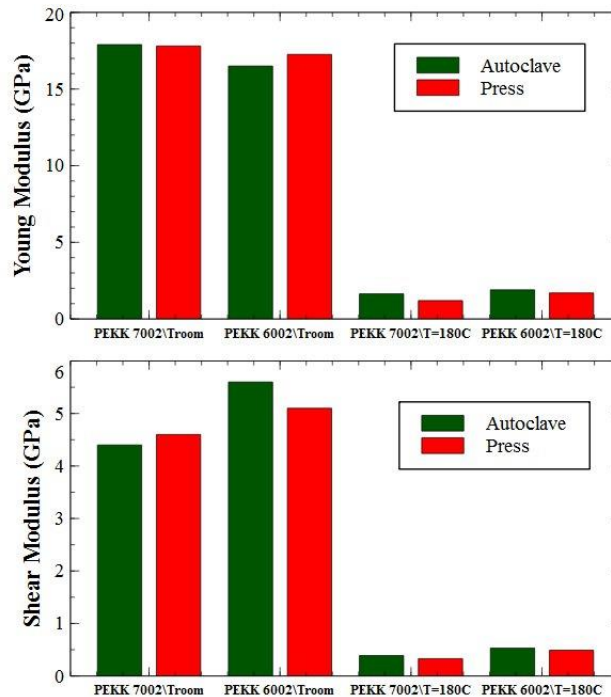


Fig. IV.17: Comparison of the Young modulus and the shear modulus of $\pm 45^\circ$ fully crystallized PEKK composites manufactured under autoclave and press tested at room temperature and at 180°C

T _{test}	PEKK 7002 composite				PEKK 6002 composite			
	Autoclave		Press		Autoclave		Press	
	T _{room}	180°C	T _{room}	180°C	T _{room}	180°C	T _{room}	180°C
Young modulus (GPa)	17.9	1.64	17.8	1.2	16.5	1.9	17.3	1.7
Shear modulus (GPa)	4.4	0.39	4.6	0.33	5.6	0.53	5.1	0.49

Table IV.7: Young modulus and shear modulus of ± 45° fully crystallized PEKK composites manufactured under autoclave and press tested at room temperature and at 180°C

IV.5.2.2 Influence of crystalline morphologies on PEKK composite mechanical properties

As for the study of the neat resin in CHAPTER II, the impact of the crystallization temperature on the mechanical properties was studied. In fact, we showed previously that depending on the crystallization temperature different crystalline morphologies can be made. Two different thermal conditions were tested; crystallization from the melt at 260°C and crystallization at 200°C from the glassy state: the first to promote transcrystalline phase growth due to low nucleation kinetics in the bulk at high crystallization temperature and the second to favor the growth of the spherulites due to high nucleation kinetics in the bulk at low crystallization temperature. Results of mechanical tests on PEKK 6002 composite samples are presented in Fig. IV.18 and Table IV.8. Higher mechanical properties were observed for PEKK composites crystallized at high temperature. The Young modulus and the shear modulus for PEKK crystallized at high temperature is higher of about 2% and 22% at room temperature and 38% and 12% respectively at 180°C. This phenomenon could be attributed to the high amount of transcrystalline phase at high crystallization temperature enhancing the adhesion between the matrix and the fibers and consequently increasing mechanical properties. This mechanism has already been observed for PEEK composites by Chen and Hsiao [81] and Gao and Kim [6] who showed that the transcrystalline interphase enhances the stress transfer efficiency between the reinforcing fiber and the matrix and thus increases the composite mechanical performances.

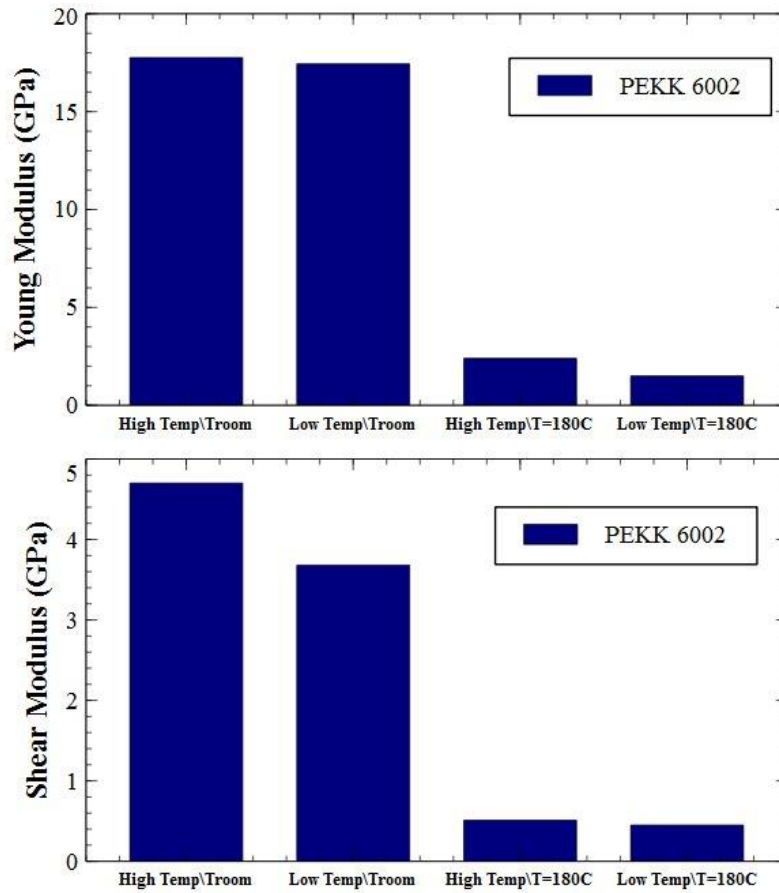


Fig. IV.18: Evolution of the Young modulus and the shear modulus of $\pm 45^\circ$ PEKK 6002 composite fully crystallized at 260°C from the melt under autoclave and at 200°C from the glassy state under press tested at room temperature and at 180°C

T_{test}	High crystallization temperature		Low crystallization temperature	
	T_{room}	180°C	T_{room}	180°C
Young modulus (GPa)	17.76	2.4	17.44	1.5
Shear modulus (GPa)	4.7	0.51	3.68	0.45

Table IV.8: Young modulus and shear modulus of $\pm 45^\circ$ PEKK 6002 composite fully crystallized at 260°C from the melt under autoclave and at 200°C from the glassy state under press tested at room temperature and at 180°C

IV.6 CONCLUSION

Carbon fibers have been shown to change crystalline morphologies and crystallization kinetics of PEKK matrices. In fact, at high crystallization temperature from the melt, it has been observed by optical microscopy an additional crystalline phase to the spherulitic phase occurring in the bulk. This phase is called transcrystalline phase and grows normally to the surface of carbon fibers. In fact, carbon fibers have been found to act as nucleating agents from which crystalline entities grow. As nuclei are closed to each other at the surface of the

fibers, the impingement between neighboring nuclei forces the crystallization to grow normally to the fibers. The derivative Hillier isothermal crystallization model established in the CHAPTER II has been shown to fit better with experiments for an Avrami exponent $n_1=3$ (3D growth) at low crystallization temperature and $n_1=2$ (2D growth) at high crystallization temperature. In fact, as surface of carbon fibers and nuclei in the matrix compete for crystallization growth, the growth of large spherulites is promoted at low crystallization temperatures since the nucleation kinetics in the bulk is high. In the opposite, at high temperature the nucleation kinetics is low decreasing the number of matrix spherulites formed and consequently favoring the growth of transcrystalline areas. Reinforced PEKK matrices crystallization kinetics have been shown to be higher at high temperature than for the neat PEKK which is probably due to the formation of the new nuclei at the surface of carbon fibers initiating crystallization earlier. However, at low temperature, it was observed the opposite which could be associated to carbon fibers hindering the matrix macromolecular chain mobility knowing that matrix domain could not be considered as confined domain by carbon fibers. It has also been shown that the weight factor w_1 is lower for the prepregs than for the neat resins which was explained by the fact that as carbon fibers hinder crystallization, crystalline entities are less perfect than for the neat resin increasing the amount of secondary crystallization.

Unidirectional and $\pm 45^\circ$ PEKK composite plates have been manufactured under press and autoclave with different thermal conditions to obtain samples with different crystallinities and crystalline morphologies. As expected, it has been shown that $\pm 45^\circ$ PEKK composite mechanical properties are more sensitive to the matrix properties than for unidirectional. Composites consolidated under autoclave have been observed to have quite higher Young modulus and shear modulus than under press which was associated to the fact that press plates are probably not perfectly paralleled not allowing a uniform pressure on the composite during the consolidation. Finally, it has been shown that PEKK composites crystallized at high temperatures from the melt promoting the formation of the transcrystalline phase seemed to have higher Young modulus and shear modulus than composite crystallized from the glassy state at low temperature. This has been explained by an enhancement of the stress transfer efficiency between the reinforcing fiber and the matrix with transcrystalline interphase.

CONCLUSION AND PROSPECTS

Poly(ether-ketone-ketone) (PEKK) high performance thermoplastics are currently studied with a great interest by the aeronautic industry as matrix for carbon fiber reinforced structural parts. In fact, PEKK composites can be consolidated out of autoclave and they have lower processing temperatures than PEEK composites. The aim of the study was to investigate and predict the evolution of PEKK composite mechanical properties depending on the processing thermal cycle to determine the best processing parameters for PEKK composite part manufacturing regarding processing times and final mechanical performances.

In the first part of the study, PEKK crystalline morphologies and crystallization kinetics have been investigated. They crystallize with spherulitic growth and for low mobility crystallization conditions, they can crystallize with two different crystalline morphologies. A secondary crystallization was identified with the apparition of an additional melting peak which corresponds to the melting of an interlamellar structure growing within crystalline lamellae. PEKK 6002 has the lowest melting temperature (around 305°C) and crystallizes much slowly than PEKK 7002 and 8002. It has also lower final crystallinity.

The modelling of PEKK crystallization kinetics were found to be difficult due to the secondary crystallization which has to be taken into account into the modelling and a truncation of all isothermal crystallization peaks beginning measured by DSC hindering the integration of the peaks and the fitting of crystallization models with experimental curves. To solve this problem, a new method has been established from the derivative of the Hillier isothermal crystallization kinetics model which can be fitted directly with the crystallization heat flow measured by DSC. Isothermal crystallizations kinetics of PEKK 6002 and 7002 crystallized from the glassy state and from the melt have been modelled with this method. Cold crystallization was shown to be faster than crystallization from the melt associated to a lower final degree of crystallinity. PEKK 7002 was shown to crystallize much faster than PEKK 6002 with fast crystallization kinetics around 240°C. According to the linear modeling of the primary crystallization weight factor w_1 , the secondary mechanism was found to be enhanced for low degree of supercooling due to a high diffusion process. Isothermal Time Transformation Temperature (TTT) diagrams of the crystallinity have been built for PEKK 6002 and 7002 providing a useful tool for PEKK processing.

The derivative isothermal crystallization kinetics Hillier model has been established allowing the prediction of the non-isothermal crystallization kinetics of neat PEKK. This new modelling slightly overestimates crystallization kinetics regarding experimental results. This phenomenon was attributed to the failure to comply isokinetics hypothesis for non-isothermal crystallization conditions. Hence, overall crystallization kinetics parameters were modified to take it into account. Consequently good agreements were observed between experiments and modelling.

The impact of crystalline morphology and crystallinity on mechanical properties has been studied. As expected, it has been shown that the Young modulus and the stress at yield increase with crystallinity whereas this is the opposite for the strain at break. This behavior is emphasized for testing temperatures above the glass transition of the amorphous phase: it was found that the mechanical properties of the polymer depend essentially on the crystalline phase content. Finally, higher young modulus and stress at yield have been observed for low

crystallization temperatures involving small spherulites which was attributed to a more homogeneous crystalline structure compared to large spherulites.

In the second part, a study of the potential degradation of PEKK matrices at high processing temperatures and its impact on crystallization kinetics and resulting mechanical properties was performed.

Thanks to TGA, rheological, GPC and DSC measurements under nitrogen, it has been shown that PEKK 6002 matrix is modified above 320°C associated to the apparition of weight losses, an increase of the weight average molar mass M_w and an increase of the glass transition temperature T_g . For thick specimens exposed in air, this thermal degradation is predominant since the oxidation process is confined only at surface (~10 nm in depth) in contact with air during processing since oxidation is very fast compared to oxygen diffusion. According to our results, thermal degradation leads to a crosslinking mechanism. In addition, according to Saito's approach and from GPC measurements, a chain scission mechanism was found to occur in parallel to crosslinking. These mechanisms have been observed to be thermally activated and following an Arrhenius law. From the kinetic scheme of crosslinking mechanism, crosslinking kinetics has been modelled with a linear model for low exposure times ($t < 20$ min).

Crosslinking occurring at the melt state has been found to decrease crystallinity and crystallization kinetics with the decrease of the crystallization kinetics parameters K_1 and K_2 . The primary crystallization weight factor w_1 has also been observed to decrease with crosslinking which was assumed to be attributed to less perfect crystallization due to the branching of the macromolecular chains which let more space to the growth of the secondary crystallization.

At last, it has been shown that the mechanical properties decrease with crosslinking. This decrease was assumed to be mainly associated to the decrease of the crystallinity with crosslinking. This result is consistent with the results shown in the previous chapter establishing the relationship between the mechanical properties and the crystallinity.

In the last part, the influence of carbon fibers on crystalline morphologies and crystalline kinetics of PEKK matrices were studied. Unidirectional and $\pm 45^\circ$ PEKK composites were manufactured under press and autoclave with different thermal processing conditions to investigate the impact of crystallization on reinforced PEKK composites.

Carbon fibers have been shown to change crystalline morphologies and crystallization kinetics of PEKK matrices. In fact, at high crystallization temperature from the melt, it has been observed by optical microscopy an additional crystalline phase to the spherulitic phase occurring in the bulk. This phase is called transcrystalline phase and grows normally to the surface of carbon fibers. In fact, carbon fibers have been found to act as nucleating agents from which crystalline entities grow. As nuclei are closed to each other at the surface of the fibers, the impingement between neighboring nuclei forces the crystallization to grow normally to the fibers. The derivative Hillier isothermal crystallization model established in the CHAPTER II has been shown to fit better with experiments for an Avrami exponent $n_1=3$ (3D growth) at low crystallization temperature and $n_1=2$ (2D growth) at high crystallization temperature. In fact, as surface of carbon fibers and nuclei in the matrix compete for crystallization growth, the growth of large spherulites is promoted at low crystallization since the nucleation kinetics in the bulk is high. In the opposite, at high temperature the nucleation kinetics is low decreasing the number of matrix spherulites formed and consequently favoring

the growth of transcrystalline areas. Reinforced PEKK matrices crystallization kinetics have been shown to be higher at high temperature than for the neat PEKK which is probably due to the formation of the new nuclei at the surface of carbon fibers initiating crystallization earlier. However, at low temperature, it was observed the opposite which could be associated to carbon fibers hindering the matrix macromolecular chain mobility knowing that matrix domain could not be considered as confined domain by carbon fibers. It has also been shown that the weight factor w_1 is lower for the prepregs than for the neat resins which was explained by the fact that as carbon fibers hinder crystallization, crystalline entities are less perfect than for the neat resin increasing the amount of secondary crystallization.

Unidirectional and $\pm 45^\circ$ PEKK composite plates have been manufactured under press and autoclave with different thermal conditions to obtain samples with different crystallinities and crystalline morphologies. As expected, it has been shown that $\pm 45^\circ$ PEKK composite mechanical properties are more sensitive to the matrix properties than for unidirectional. Composites consolidated under autoclave have been observed to have quite higher Young modulus and shear modulus than under press which was associated to the fact that press plates are probably not perfectly paralleled not allowing a uniform pressure on the composite during the consolidation. Finally, it has been shown that PEKK composites crystallized at high temperatures from the melt promoting the formation of the transcrystalline phase seemed to have higher Young modulus and shear modulus than composite crystallized from the glassy state at low temperature. This has been explained by an enhancement of the stress transfer efficiency between the reinforcing fiber and the matrix with transcrystalline interphase.

Thanks to this study, it is now possible to predict the crystallinity and the associated mechanical properties of PEKK composites depending on any thermal processing conditions taking into account the effect of potential macromolecular changes at high temperatures.

In the future, it would be interesting to model macromolecular changes for higher exposure times by solving the kinetic scheme of crosslinking mechanism. We showed that chain scissions which are at the origin of crosslinking mechanisms can occur at ether or carbonyl links. To identify where chain scissions are favored, the same study could be carried out on PEEK which has a different number of ether and ketone links than PEKK. Secondly, the impact of isophthaloyl and terephthaloyl entities on macromolecular changes which occur at high temperatures could be studied.

From the DSC measurements, it was assumed the apparition of a secondary crystallization within crystalline lamellae during isothermal crystallization. It would be interesting to confirm the presence of this subsidiary crystallization and its nature. Besides, from crystallization modelling, it has been shown that the proportion of the secondary crystallization increases with the crystallization temperature. In-situ SAXS measurements could be carried out to identify secondary crystallization and assess its kinetics. In the same time, WAXS measurements showed for PEKK an additional crystalline morphology favored for PEKK copolymers with high ratio of isophthaloyl entities and for cold crystallization. In-situ WAXS could be also performed to assess its kinetics. Finally as for crystallinity, it would be interesting to investigate the impact of the secondary crystallization and the second crystalline morphology on mechanical properties.

With the presence of carbon fibers, it was assumed that at high crystallization temperatures only transcrystalline phase grows with an Avrami exponent $n_1=2$ whereas at low crystallization temperature only spherulitic phase would occur with $n_1=3$. To confirm those

hypotheses, supplementary microscopic observations could be required. For intermediary temperatures, both mechanisms occur in parallel with different crystallization kinetics. The established Hillier model cannot take into account both mechanisms in the same time. It would be thus interesting to establish a new model able to deal with the growth of two mechanisms in parallel. Another way would be to be able to study samples with only transcrystalline phase for different crystallization temperatures in order to identify its crystallization kinetics as it was done for neat PEKK.

As regards composites, only fully crystallized or amorphous composite plates were manufactured. Composite plates with different crystallinity could be manufactured to assess the evolution of the mechanical properties with crystallinity. In the same way, it would be interesting to confirm the impact of the transcrystalline phase on mechanical properties.

Finally, the crystallization kinetics models established in this study could be coupled with the heat equation and be implemented in a finite element code to simulate the evolution of the crystallinity in the thickness of a PEKK composite part during its processing cycle.

REFERENCES

- [1] C.-M. Chan, S. Venkatraman, Crosslinking of poly(arylene ether ketone)s 1. Rheological behavior of the melt and mechanical properties of cured resin, *J. Appl. Polym. Sci.* 32 (1986) 5933–5943. doi:10.1002/app.1986.070320722.
- [2] C.-M. Chan, S. Venkatraman, Crosslinking of poly(arylene ether ketones). II. Crystallization kinetics, *J. Polym. Sci. Part B Polym. Phys.* 25 (1987) 1655–1665. doi:10.1002/polb.1987.090250808.
- [3] M.F. Talbott, G.S. Springer, L.A. Berglund, The Effects of Crystallinity on the Mechanical Properties of PEEK Polymer and Graphite Fiber Reinforced PEEK, *J. Compos. Mater.* 21 (1987) 1056–1081. doi:10.1177/002199838702101104.
- [4] P. Cebe, S.Y. Chung, S.-D. Hong, Effect of thermal history on mechanical properties of polyetheretherketone below the glass transition temperature, *J. Appl. Polym. Sci.* 33 (1987) 487–503. doi:10.1002/app.1987.070330217.
- [5] A.J. Peacock, L. Mandelkern, The mechanical properties of random copolymers of ethylene: Force-elongation relations, *J. Polym. Sci. Part B Polym. Phys.* 28 (1990) 1917–1941. doi:10.1002/polb.1990.090281104.
- [6] S.-L. Gao, J.-K. Kim, Cooling rate influences in carbon fibre/PEEK composites. Part 1. Crystallinity and interface adhesion, *Compos. Part Appl. Sci. Manuf.* 31 (2000) 517–530. doi:10.1016/S1359-835X(00)00009-9.
- [7] J. Diani, F. Bédoui, G. Régnier, On the relevance of the micromechanics approach for predicting the linear viscoelastic behavior of semi-crystalline poly(ethylene)terephthalates (PET), *Mater. Sci. Eng. A.* 475 (2008) 229–234. doi:10.1016/j.msea.2007.05.002.
- [8] A. Pawlak, A. Galeski, Plastic Deformation of Crystalline Polymers: The Role of Cavitation and Crystal Plasticity, *Macromolecules.* 38 (2005) 9688–9697. doi:10.1021/ma050842o.
- [9] J. Pascal, PEKK Un thermoplastique haute performance ultra polyvalent de la famille PAEK, (2012).
- [10] K.H. Gardner, B.S. Hsiao, R.R. Matheson, B.A. Wood, Structure, crystallization and morphology of poly (aryl ether ketone ketone), *Polymer.* 33 (1992) 2483–2495. doi:10.1016/0032-3861(92)91128-O.
- [11] J.N. Hay, D.J. Kemmish, J.I. Langford, A.I.M. Rae, The structure of crystalline PEEK, *Polym. Commun.* 25 (1984) 175–178.
- [12] S. Radhakrishnan, D.R. Saini, Polymer-induced crystallization of inorganic salts II. PEO-CaCl₂, PEO-K₂CO₃ and PEO-CaCO₃, *J. Cryst. Growth.* 129 (1993) 191–201. doi:10.1016/0022-0248(93)90448-6.
- [13] R.J. Abraham, I.S. Haworth, Molecular modelling of poly(aryl ether ketones): 2. Chain packing in crystalline PEK and PEEK, *Polymer.* 32 (1991) 121–126. doi:10.1016/0032-3861(91)90571-Y.

- [14] J.P. Jog, V.M. Nadkarni, Crystallization kinetics of polyaryl ether ketones, *J. Appl. Polym. Sci.* 32 (1986) 3317–3322. doi:10.1002/app.1986.070320133.
- [15] Arkema, Technical Data Sheet - KEPSTAN 8000 series, (2013).
- [16] Arkema, Technical Data Sheet - KEPSTAN 7000 series, (2013).
- [17] Arkema, Technical Data Sheet - KEPSTAN 6000 series, (2013).
- [18] Victrex, Technical Data Sheet - PEEK 450G, (2013).
- [19] P.C. Dawson, D.J. Blundell, X-ray data for poly(aryl ether ketones), *Polymer*. 21 (1980) 577–578. doi:10.1016/0032-3861(80)90228-1.
- [20] D.J. Blundell, B.N. Osborn, The morphology of poly(aryl-ether-ether-ketone), *Polymer*. 24 (1983) 953–958. doi:10.1016/0032-3861(83)90144-1.
- [21] D.J. Blundell, V. Bayon, The crystal structure of poly(ether ketone) copolymers, *Polymer*. 34 (1993) 1354–1360. doi:10.1016/0032-3861(93)90845-2.
- [22] S.Z.D. Cheng, R.-M. Ho, B.S. Hsiao, K.H. Gardner, Polymorphism and crystal structure identification in poly(aryl ether ketone)s, *Macromol. Chem. Phys.* 197 (1996) 185–213. doi:10.1002/macp.1996.021970115.
- [23] M. Reitman, D. Jaekel, R. Siskey, S.M. Kurtz, Chapter 4 - Morphology and Crystalline Architecture of Polyaryletherketones, in: S.M. Kurtz (Ed.), *PEEK Biomater. Handb.*, William Andrew Publishing, Oxford, 2012: pp. 49–60. <http://www.sciencedirect.com/science/article/pii/B9781437744637100041> (accessed January 29, 2015).
- [24] B.S. Hsiao, K.H. Gardner, S.Z.D. Cheng, Crystallization of poly(aryl ether ketone) copolymers containing terephthalate/isophthalate moieties, *J. Polym. Sci. Part B Polym. Phys.* 32 (1994) 2585–2594. doi:10.1002/polb.1994.090321604.
- [25] K.H. Gardner, B.S. Hsiao, K.L. Faron, Polymorphism in poly(aryl ether ketone)s, *Polymer*. 35 (1994) 2290–2295. doi:10.1016/0032-3861(94)90763-3.
- [26] R.-M. Ho, S.Z.D. Cheng, B.S. Hsiao, K.H. Gardner, Crystal Morphology and Phase Identification in Poly(aryl ether ketone)s and Their Copolymers. 3. Polymorphism in a Polymer Containing Alternated Terephthalic Acid and Isophthalic Acid Isomers, *Macromolecules*. 28 (1995) 1938–1945. doi:10.1021/ma00110a030.
- [27] B.S. Hsiao, R.-M. Ho, S.Z.D. Cheng, Time-resolved synchrotron X-ray study of crystalline phase transition in poly(aryl ether ketone) containing alternated terephthalic/isophthalic moieties, *J. Polym. Sci. Part B Polym. Phys.* 33 (1995) 2439–2447. doi:10.1002/polb.1995.090331715.
- [28] D.J. Blundell, A.B. Newton, Variations in the crystal lattice of PEEK and related para-substituted aromatic polymers: 2. Effect of sequence and proportion of ether and ketone links, *Polymer*. 32 (1991) 308–313. doi:10.1016/0032-3861(91)90019-F.

- [29] L. Quiroga Cortés, N. Caussé, E. Dantras, A. Lonjon, C. Lacabanne, Morphology and dynamical mechanical properties of poly ether ketone ketone (PEKK) with meta phenyl links, *J. Appl. Polym. Sci.* (2016) n/a-n/a. doi:10.1002/app.43396.
- [30] P. Cebe, S.-D. Hong, Crystallization behaviour of poly(ether-ether-ketone), *Polymer*. 27 (1986) 1183–1192. doi:10.1016/0032-3861(86)90006-6.
- [31] S.Z.D. Cheng, M.Y. Cao, B. Wunderlich, Glass transition and melting behavior of poly(oxy-1,4-phenyleneoxy-1,4-phenylenecarbonyl-1,4-phenylene) (PEEK), *Macromolecules*. 19 (1986) 1868–1876. doi:10.1021/ma00161a015.
- [32] P.J. Holdsworth, A. Turner-Jones, The melting behaviour of heat crystallized poly(ethylene terephthalate), *Polymer*. 12 (1971) 195–208. doi:10.1016/0032-3861(71)90045-0.
- [33] O. Verhoyen, F. Dupret, R. Legras, Isothermal and non-isothermal crystallization kinetics of polyethylene terephthalate: Mathematical modeling and experimental measurement, *Polym. Eng. Sci.* 38 (1998) 1594–1610. doi:10.1002/pen.10330.
- [34] X.F. Lu, J.N. Hay, Isothermal crystallization kinetics and melting behaviour of poly(ethylene terephthalate), *Polymer*. 42 (2001) 9423–9431. doi:10.1016/S0032-3861(01)00502-X.
- [35] I.H. Hillier, Modified avrami equation for the bulk crystallization kinetics of spherulitic polymers, *J. Polym. Sci. A*. 3 (1965) 3067–3078. doi:10.1002/pol.1965.100030902.
- [36] L. Jin, J. Ball, T. Bremner, H.-J. Sue, Crystallization behavior and morphological characterization of poly(ether ether ketone), *Polymer*. 55 (2014) 5255–5265. doi:10.1016/j.polymer.2014.08.045.
- [37] C.N. Velisaris, J.C. Seferis, Crystallization kinetics of polyetheretherketone (peek) matrices, *Polym. Eng. Sci.* 26 (1986) 1574–1581. doi:10.1002/pen.760262208.
- [38] M. Avrami, Kinetics of Phase Change. I General Theory, *J. Chem. Phys.* 7 (1939) 1103–1112. doi:10.1063/1.1750380.
- [39] B.S. Hsiao, I.Y. Chang, B.B. Sauer, Isothermal crystallization kinetics of poly(ether ketone ketone) and its carbon-fibre-reinforced composites, *Polymer*. 32 (1991) 2799–2805. doi:10.1016/0032-3861(91)90111-U.
- [40] A. Jonas, R. Legras, Thermal stability and crystallization of poly(aryl ether ether ketone), *Polymer*. 32 (1991) 2691–2706. doi:10.1016/0032-3861(91)90095-Z.
- [41] J.M. Kenny, A. Maffezzoli, L. Nicolais, A new kinetic model for polymer crystallization derived by calorimetric analysis, *Thermochim. Acta*. 227 (1993) 83–95. doi:10.1016/0040-6031(93)80252-6.
- [42] B. Wunderlich, *Macromolecular Physics*, Elsevier, 2012.
- [43] T. Choupin, B. Fayolle, G. Régnier, C. Paris, J. Cinquin, B. Brulé, Isothermal crystallization kinetic modeling of poly(etherketoneketone) (PEKK) copolymer, *Polymer*. 111 (2017) 73–82. doi:10.1016/j.polymer.2017.01.033.

- [44] D. Turnbull, J.C. Fisher, Rate of Nucleation in Condensed Systems, *J. Chem. Phys.* 17 (1949) 71–73. doi:10.1063/1.1747055.
- [45] J.D. Hoffman, J.I. Lauritzen, Crystallization of bulk polymers with chain folding: theory of growth of lamellar spherulites, *J. Res. Natl. Bur. Stand. Sect. Phys. Chem.* 65A (1961) 297. doi:10.6028/jres.065A.035.
- [46] J.D. Hoffman, R.L. Miller, Kinetic of crystallization from the melt and chain folding in polyethylene fractions revisited: theory and experiment, *Polymer*. 38 (1997) 3151–3212. doi:10.1016/S0032-3861(97)00071-2.
- [47] T. Liu, Z. Mo, S. Wang, H. Zhang, Isothermal melt and cold crystallization kinetics of poly(aryl ether ether ketone) (PEEK), *Eur. Polym. J.* 33 (1997) 1405–1414. doi:10.1016/S0014-3057(97)00016-5.
- [48] M.J. Jenkins, J.N. Hay, N.J. Terrill, Structure evolution in melt crystallised PEEK, *Polymer*. 44 (2003) 6781–6787. doi:10.1016/S0032-3861(03)00749-3.
- [49] M. Dasriaux, S. Castagnet, L. Thilly, L. Chocinski-Arnault, S.A.E. Boyer, Evolution of the amorphous fraction of PEEK during annealing at atmospheric and high pressure above the glass transition temperature, *J. Appl. Polym. Sci.* 130 (2013) 1148–1157. doi:10.1002/app.39297.
- [50] X. Tardif, B. Pignon, N. Boyard, J.W.P. Schmelzer, V. Sobotka, D. Delaunay, C. Schick, Experimental study of crystallization of PolyEtherEtherKetone (PEEK) over a large temperature range using a nano-calorimeter, *Polym. Test.* 36 (2014) 10–19. doi:10.1016/j.polymertesting.2014.03.013.
- [51] T. Ozawa, Kinetics of non-isothermal crystallization, *Polymer*. 12 (1971) 150–158. doi:10.1016/0032-3861(71)90041-3.
- [52] K. Nakamura, K. Katayama, T. Amano, Some aspects of nonisothermal crystallization of polymers. II. Consideration of the isokinetic condition, *J. Appl. Polym. Sci.* 17 (1973) 1031–1041. doi:10.1002/app.1973.070170404.
- [53] P. Cebe, Non-isothermal crystallization of poly(etheretherketone) aromatic polymer composite, *Polym. Compos.* 9 (1988) 271–279. doi:10.1002/pc.750090405.
- [54] P. Cebe, Application of the parallel Avrami model to crystallization of poly(etheretherketone), *Polym. Eng. Sci.* 28 (1988) 1192–1197. doi:10.1002/pen.760281809.
- [55] R.M. Patel, J.E. Spruiell, Crystallization kinetics during polymer processing—Analysis of available approaches for process modeling, *Polym. Eng. Sci.* 31 (1991) 730–738. doi:10.1002/pen.760311008.
- [56] T.W. Chan, A.I. Isayev, Quiescent polymer crystallization: Modelling and measurements, *Polym. Eng. Sci.* 34 (1994) 461–471. doi:10.1002/pen.760340602.
- [57] E. Bessard, O.D. Almeida, G. Bernhart, Unified isothermal and non-isothermal modelling of neat PEEK crystallization, *J. Therm. Anal. Calorim.* 115 (2013) 1669–1678. doi:10.1007/s10973-013-3308-8.

- [58] H.G.H. van Melick, L.E. Govaert, H.E.H. Meijer, On the origin of strain hardening in glassy polymers, *Polymer*. 44 (2003) 2493–2502. doi:10.1016/S0032-3861(03)00112-5.
- [59] M. Wendlandt, T.A. Tervoort, U.W. Suter, Non-linear, rate-dependent strain-hardening behavior of polymer glasses, *Polymer*. 46 (2005) 11786–11797. doi:10.1016/j.polymer.2005.08.079.
- [60] K.-H. Nitta, H. Nomura, Stress strain behavior of cold drawn isotactic polypropylene subjected to various drawn histories, *Polymer*. 55 (2014) 6614–6622.
- [61] V.A. Kargin, T.I. Sogolova, N.Y. Rapoport, I.I. Kurbanova, Effect of artificial nucleating agents on polymers structure and properties, *J. Polym. Sci. Part C Polym. Symp.* 16 (1967) 1609–1617. doi:10.1002/polc.5070160337.
- [62] J.N. Hay, D.J. Kimmish, Thermal decomposition of poly(aryl ether ketones), *Polymer*. 28 (1987) 2047–2051. doi:10.1016/0032-3861(87)90039-5.
- [63] M. Day, D. Sally, D.M. Wiles, Thermal degradation of poly(aryl-ether-ether-ketone): Experimental evaluation of crosslinking reactions, *J. Appl. Polym. Sci.* 40 (1990) 1615–1625. doi:10.1002/app.1990.070400917.
- [64] M. Day, J.D. Cooney, D.M. Wiles, The thermal degradation of poly(aryl—ether—ether—ketone) (PEEK) as monitored by pyrolysis—GC/MS and TG/MS, *J. Anal. Appl. Pyrolysis*. 18 (1990) 163–173. doi:10.1016/0165-2370(90)80005-9.
- [65] C. Nicodeau, Continuous welding modeling of thermoplastic matrix composites, phdthesis, Arts et Métiers ParisTech, 2005. <https://pastel.archives-ouvertes.fr/pastel-00001506/document> (accessed January 26, 2015).
- [66] P. Patel, T.R. Hull, R.W. McCabe, D. Flath, J. Grasmeyer, M. Percy, Mechanism of thermal decomposition of poly(ether ether ketone) (PEEK) from a review of decomposition studies, *Polym. Degrad. Stab.* 95 (2010) 709–718. doi:10.1016/j.polymdegradstab.2010.01.024.
- [67] E. Courvoisier, Y. Bicaba, X. Colin, Proposition d'un modèle cinétique pour la dégradation thermique de la matrice PEEK, *Matér. Tech.* 104 (2016) 204. doi:10.1051/mattech/2016011.
- [68] C.J. Tsai, L.H. Perng, Y.C. Ling, A study of thermal degradation of poly(aryl-ether-ether-ketone) using stepwise pyrolysis/gas chromatography/mass spectrometry, *Rapid Commun. Mass Spectrom.* 11 (1997) 1987–1995. doi:10.1002/(SICI)1097-0231(199712)11:18<1987::AID-RCM100>3.0.CO;2-Q.
- [69] Y. Deslandes, M. Day, N.-F. Sabir, T. Suprunchuk, Crystallization of poly(aryl-ether-ether-ketone): Effect of thermal history of the melt on crystallization kinetics, *Polym. Compos.* 10 (1989) 360–366. doi:10.1002/pc.750100513.
- [70] M. Day, T. Suprunchuk, J.D. Cooney, D.M. Wiles, Thermal degradation of poly(aryl-ether—ether-ketone) (PEEK): A differential scanning calorimetry study, *J. Appl. Polym. Sci.* 36 (1988) 1097–1106. doi:10.1002/app.1988.070360510.

- [71] P. Patel, T.R. Hull, R.E. Lyon, S.I. Stoliarov, R.N. Walters, S. Crowley, N. Safronava, Investigation of the thermal decomposition and flammability of PEEK and its carbon and glass-fibre composites, *Polym. Degrad. Stab.* 96 (2011) 12–22. doi:10.1016/j.polymdegradstab.2010.11.009.
- [72] M. Day, J.D. Cooney, D.M. Wiles, The kinetics of the oxidative degradation of poly(aryl-ether-ether-ketone) (PEEK), *Thermochim. Acta.* 147 (1989) 189–197. doi:10.1016/0040-6031(89)85174-3.
- [73] J.-D. Nam, J.C. Seferis, Generalized composite degradation kinetics for polymeric systems under isothermal and nonisothermal conditions, *J. Polym. Sci. Part B Polym. Phys.* 30 (1992) 455–463. doi:10.1002/polb.1992.090300505.
- [74] W.E. Moddeman, W.C. Bowling, E.E. Tibbitts, R.B. Whitaker, Thermal stability and compatibility of polyetheretherketone (PEEK) with an oxidizer and pyrotechnic blend, *Polym. Eng. Sci.* 26 (1986) 1469–1477. doi:10.1002/pen.760262102.
- [75] O. Saito, Effects of High Energy Radiation on Polymers II. End-linking and Gel Fraction, *J. Phys. Soc. Jpn.* 13 (1958) 1451–1464. doi:10.1143/JPSJ.13.1451.
- [76] B. Fayolle, X. Colin, L. Audouin, J. Verdu, Mechanism of degradation induced embrittlement in polyethylene, *Polym. Degrad. Stab.* 92 (2007) 231–238. doi:10.1016/j.polymdegradstab.2006.11.012.
- [77] W. Cox, E. Merz, Rheology of Polymer Melts—A Correlation of Dynamic and Steady Flow Measurements, (1959). doi:10.1520/STP44206S.
- [78] E. Richaud, P. Ferreira, L. Audouin, X. Colin, J. Verdu, C. Monchy-Leroy, Radiochemical ageing of poly(ether ether ketone), *Eur. Polym. J.* 46 (2010) 731–743. doi:10.1016/j.eurpolymj.2009.12.026.
- [79] T.G. Fox, P.J. Flory, Second-Order Transition Temperatures and Related Properties of Polystyrene. I. Influence of Molecular Weight, *J. Appl. Phys.* 21 (1950) 581–591. doi:10.1063/1.1699711.
- [80] Y. Lee, R.S. Porter, Crystallization of poly(etheretherketone) (PEEK) in carbon fiber composites, *Polym. Eng. Sci.* 26 (1986) 633–639. doi:10.1002/pen.760260909.
- [81] E.J.H. Chen, B.S. Hsiao, The effects of transcrystalline interphase in advanced polymer composites, *Polym. Eng. Sci.* 32 (1992) 280–286. doi:10.1002/pen.760320408.

RÉSUMÉ ÉTENDU

Performances mécaniques de composites thermoplastiques PEKK en relation avec leurs paramètres de mise en œuvre

I. INTRODUCTION

Contexte industriel

L'industrie aéronautique utilise de plus en plus de matériaux composites pour alléger ses structures et améliorer leurs performances. Ce gain en masse permet également à l'industrie aéronautique de limiter leur impact environnemental en diminuant de façon significative la consommation en kérosène des avions et les émissions de gaz à effet de serre tels que le CO₂ et le NO_x. Actuellement, les structures des avions civiles de dernière génération sont composées de plus de 50% en masse par des matériaux composites (l'Airbus A350 et le Boeing B787 en sont des exemples).

Même si la majorité de ces composites sont des composites à matrice thermodurcissable, l'utilisation des composites à matrice thermoplastique gagne du terrain dû aux nombreux bénéfices qu'ils présentent. En effet, ils ont des de bonnes tolérances aux dommages, ils sont soudables, recyclables, ils sont bien appropriés pour le placement de fibres et enfin ils sont consolidables hors autoclave. Ces deux dernières caractéristiques pourrait permettre d'augmenter les cadences de production des avions ce qui est une problématique centrale pour les fabricants aéronautiques.

Parmi ces matrices thermoplastiques, la famille des polymères Poly Aryl Ether Ketone (PAEK) pourrait être la meilleure candidate comme matrice pour des pièces de structure composites. En effet, les thermoplastiques PAEK ont des hautes performances à hautes température et des hautes résistances chimiques et à l'oxydation. Le thermoplastique le plus connu qui appartient à la famille des PAEK est le PEEK qui est déjà utilisé comme matrice pour des pièces de structure composites comme le plancher de cockpit de l'avion militaire A400M consolidé hors autoclave fabriqué par l'entreprise Daher. Cependant ce matériau est plus cher que les résines époxy et sa mise en œuvre est rendue difficile due à une température de fusion élevée (environ 400°C) impliquant des temps et des coûts de mie en œuvre élevés et une potentielle dégradation de la matrice durant la fabrication des pièces composites.

Dans ce contexte industriel, de nouvelles générations de matrices thermoplastiques hautes performances PAEK ont récemment été développées comme la gamme PEKK KEPSTAN™ d'Arkema. Les PEKK sont actuellement beaucoup étudiés dans l'industrie aéronautique pour concurrencer le PEEK comme matrice pour des pièces de structure composites. En effet, pour des performances mécaniques comparables, les matrices PEKK ont des températures de fusion plus faibles que le PEEK (environ 360°C) ce qui simplifie la fabrication des pièces composites.

Objectifs

Les performances mécaniques finales des pièces composites sont étroitement liées à leur mise en œuvre. En effet, suivant le cycle thermique de mise en œuvre choisi, les propriétés

de la matrice ainsi que les interactions entre la matrice et les fibres de carbone vont être très différentes. La première étape de fabrication des pièces composites est la consolidation qui correspond à la chauffe du composite au-dessus de la température de fusion de la matrice pour diminuer sa viscosité et ainsi évacuer les porosités grâce à la pression. Comme la température de fusion du PEKK est tout de même supérieure à 300°C, la matrice est susceptible d'être modifiée voir dégradée pendant cette étape et donc les performances mécaniques finales de la pièce composite pourraient être altérées. Dans une deuxième étape, après la consolidation, la pièce composite est refroidie jusqu'à la température ambiante. Pendant cette étape, la matrice peut cristalliser avec différents taux de cristallinité et différentes morphologies cristallines suivant les conditions de refroidissement ce qui pourraient également impacter les performances mécaniques finales des pièces composites. C'est pourquoi, ces phénomènes doivent être compris et contrôlés pour pouvoir prédire et ensuite optimiser les paramètres de mise en œuvre concernant les performances mécaniques et les temps de fabrication des pièces composites.

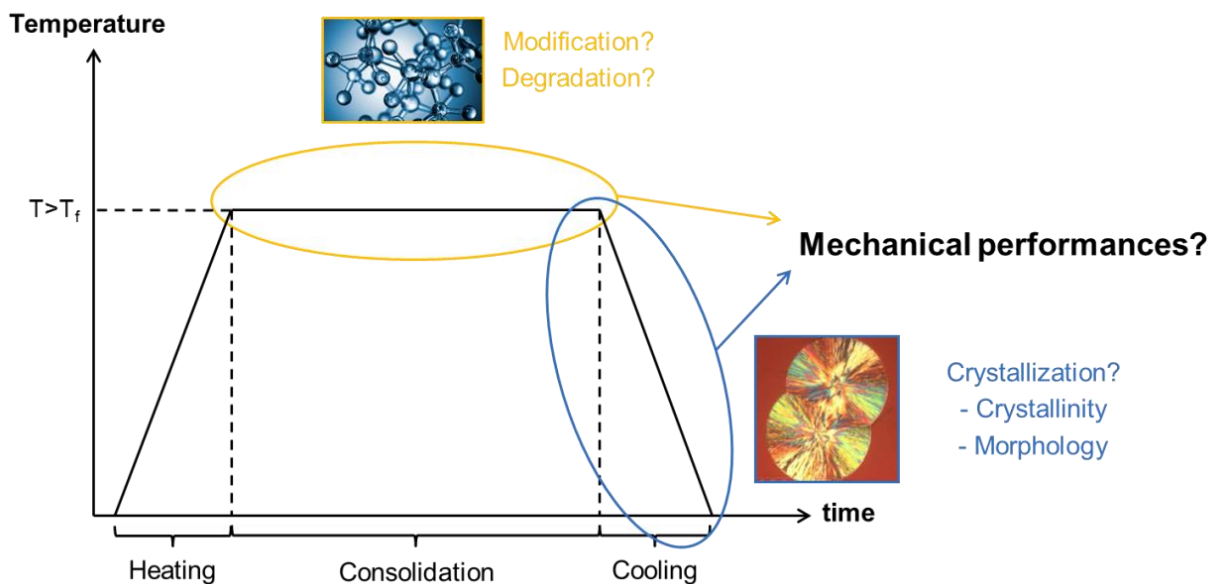


Fig. 0.1: Cycle thermique de mise en œuvre d'une pièce composite thermoplastique

En collaboration avec le laboratoire PIMM des Arts et Métiers ParisTech et du fournisseur de matériau Arkema, le leader du projet Airbus Group Innovations (AGI) a pour objectif d'explorer la capacité de ces nouveaux composites thermoplastiques hautes performances PEKK pour la fabrication de pièces de structure aéronautique. Pour répondre à cette problématique, le manuscrit est divisé en quatre chapitres distincts :

Le premier chapitre est une étude bibliographique sur les matériaux utilisés pour la thèse. Il présente les principales propriétés des prepregs tapes utilisés pour la fabrication des composites ainsi que les fibres de carbone et les matrices PEKK utilisées dans le prepregs.

Le deuxième chapitre traite de la modélisation des cinétiques de cristallisation des matrices PEKK ainsi que l'influence de la cristallinité et des morphologies cristallines sur les propriétés mécaniques des matrices PEKK.

Le troisième chapitre se concentre sur les modifications macromoléculaires des matrices PEKK pour des hautes températures de mise en œuvre sous atmosphère inerte (absence

d'oxygène) et leurs impacts sur la cristallisation et les performances mécaniques des matrices PEKK.

Le dernier chapitre présente l'influence des fibres de carbone sur les morphologies cristallines et les cinétiques de cristallisation, la fabrication de composites PEKK unidirectionnels et orientés à $\pm 45^\circ$ sous presse et sous autoclave et enfin l'impact de la cristallinité et des morphologies cristallines sur les performances mécaniques finales des composites PEKK.

II. MATÉRIAUX

Les prepregs tapes utilisés pour la fabrication des composites sont composés de 40% en volume de matrice PEKK et 60% en volume de fibres de carbone non ensimées. Les fibres de carbone sont des fibres AS4 12K fabriquées par Hexcel. Les matrices utilisées PEKK sont des copolymères composés de deux isomères différentes, les isomères isophthaloydes (I) et terephthaloydes (T) avec différents ratios suivant le copolymère.

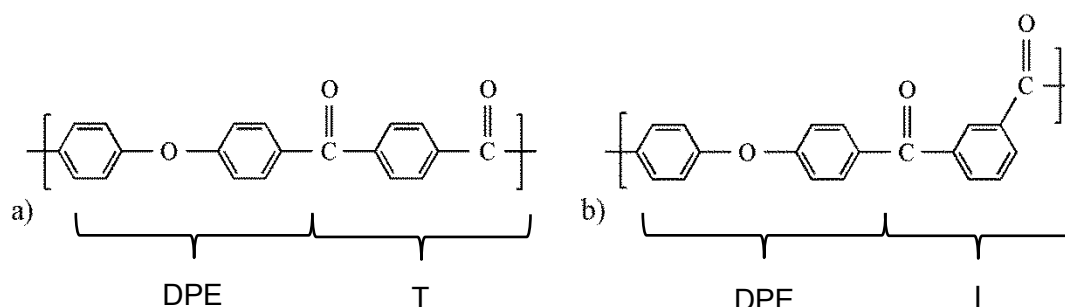


Fig. 0.2 : Isomères téréphthaloyle (T) a) et isophthaloyle (I) b)

Trois PEKK différents sont étudiés, les PEKK 8002, 7002 et 6002 qui ont des ratios T/I respectifs égales à 80/20, 70/30 et 60/40. Ils possèdent la même température de transition vitreuse ($T_g=155^\circ\text{C}$) mais présentent des températures de fusion décroissantes avec le nombre d'entités isophthaloydes (Table 0.1). On peut voir que le PEKK 6002 a une température de fusion beaucoup plus faible (305°C) que le PEEK (343°C) ce qui le rend très intéressant du point de vue de la mise en œuvre.

Grade	Ratio T/I	T_g ($^\circ\text{C}$)	T_f ($^\circ\text{C}$)
PEKK 8002	80/20	165	358
PEKK 7002	70/30	162	332
PEKK 6002	60/40	160	305
PEEK 450G		143	343

Table 0.1 : Propriétés thermiques des copolymères PEKK produits par Arkema et du PEEK produit par Victrex

Concernant les propriétés mécaniques, les propriétés des PEKK sont proches de celles du PEEK (Table 0.2).

Grade	Module d'Young (GPa)	Contrainte au seuil (MPa)	Déformation au seuil (%)	Déformation à la rupture (%)
PEKK 8002	3.8	105-125	5.2	20-30
PEKK 7002	3.8	70-110	5.2	2-20
PEKK 6002*	2.9	88	5.4	>80
PEEK 450G	3.7	100	5.5.	45

Table 0.2 : Comparaison des propriétés mécaniques des matrices PEKK produites par Arkema et PEEK produites par Victrex testées à température ambiante (le PEKK 6002 est ici à l'état amorphe comparé aux autres matrices qui sont totalement cristallisées)

Les matrices PEKK cristallisent avec une croissance sphérolitique et, en fonction du ratio T/l et des conditions de cristallisation, peuvent cristalliser avec deux morphologies cristallines différentes par leurs paramètres de mailles. De plus, une cristallisation dite secondaire qui correspond à la croissance d'une structure cristalline de nature interlamellaire peut avoir lieu après une cristallisation isotherme ou un refroidissement lent. Chaque copolymère PEKK se caractérise par leurs cinétiques de cristallisation et leur taux de cristallinité final. Le PEKK 6002 par exemple cristallise plus lentement que les PEKK 7002 et 8002 pour atteindre un taux de cristallinité plus faible.

III. IMPACT DU CYCLE THERMIQUE SUR LES PROPRIETES MECANIQUES DES MATRICES PEKK

D'une façon identique à la littérature, nous avons observé à partir d'observations microscopiques et rayons-X que les matrices PEKK cristallisent avec une croissance sphérolitique (Fig. 0.3) et pour des conditions de cristallisation impliquant de faibles mobilités macromoléculaires, elles peuvent cristalliser avec deux morphologies cristallines différentes qui ont des paramètres de mailles différents.

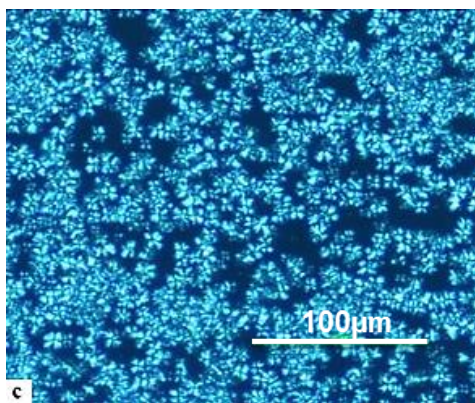


Fig. 0.3 : Observation microscopique à lumière polarisée pour un PEKK 6002 cristallisé à 270°C à partir de l'état fondu pendant 40 min

Une cristallisation secondaire a été identifiée avec l'apparition d'un pic de fusion supplémentaire qui correspond à la fusion d'une structure interlamellaire qui croît entre les lamelles cristallines. Le PEKK 6002 présente la température de cristallisation la plus faible (environ 305°C) et cristallise beaucoup plus lentement que les PEKK 7002 et 8002. Il a également le taux de cristallinité final le plus faible (Fig. 0.4).

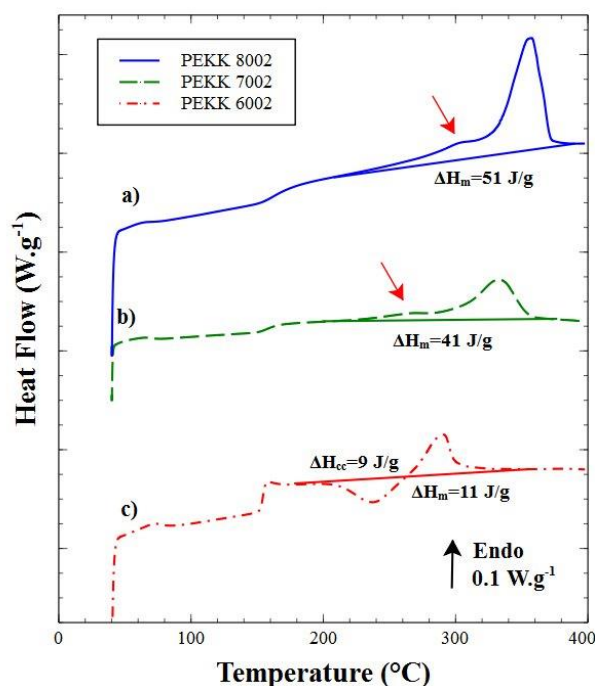


Fig. 0.4 : Scan DSC à 5°C.min⁻¹ pour les PEKK 8002, 7002 et 6002 refroidis à 10°C.min⁻¹ à partir de l'état fondu

La modélisation des cinétiques de cristallisation des PEKK a été difficile dû à la cristallisation secondaire qui doit être prise en compte dans les modèles et au fait que le début des pics de cristallisation isotherme mesurés par DSC soient tous tronqués ce qui gêne l'intégration des pics et l'identification des modèles de cristallisation avec les courbes expérimentales. Pour résoudre ce problème, une nouvelle méthode a été développée à partir de la dérivé du modèle de cinétique de cristallisation isotherme d'Hillier qui permet d'ajuster le modèle directement avec le flux de chaleur de cristallisation isotherme mesuré par DSC (Fig. 0.5).

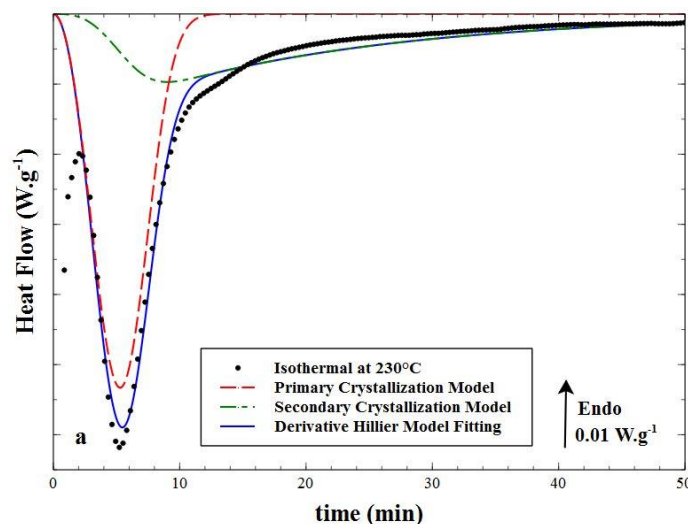


Fig. 0.5 : Comparaison d'un thermogramme DSC d'un PEKK 6002 cristallisé à 230°C à partir de l'état fondu avec le modèle d'Hillier dérivé et la modélisation de la cristallisation primaire et secondaire associée

Les cinétiques de cristallisation isotherme des PEKK 6002 et 7002 cristallisé à partir de l'état vitreux et fondu ont été modélisées avec cette méthode. Il a été montré que la cinétique de cristallisation associée à la cristallisation froide est plus rapide que celle à partir de l'état fondu dû à des taux de cristallinité plus faible pour la cristallisation froide. Le PEKK 7002 cristallise beaucoup plus rapidement que le PEKK 6002 avec une cinétique de cristallisation maximale aux alentours de 240°C. A partir de la modélisation du facteur de poids de la cristallisation primaire w_1 , il a été montré que la cristallisation secondaire est favorisée pour des faibles degrés de surfusion dû à des mécanismes de diffusion importants. Enfin, des diagrammes Temps Température Transformation (TTT) ont été établis pour le PEKK 6002 et 7002 constituant des outils très utiles pour la mise en œuvre des PEKK (Fig. 0.6).

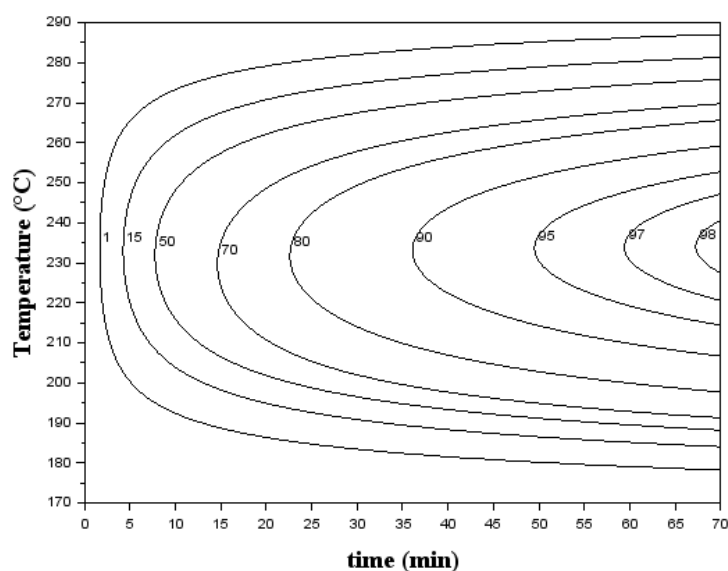


Fig. 0.6 : Diagramme TTT de la cristallinité relative du PEKK 6002 cristallisé à partir de l'état fondu

La dérivée du modèle de cinétique de cristallisation isotherme d'Hillier a été établie pour pouvoir prédire la cristallisation anisotherme du PEKK. Il a été montré que ce nouveau modèle surestime les résultats expérimentaux. Ce phénomène a été supposé être associé

au non-respect des hypothèses iso-cinétiques lors de cristallisations anisothermes. Pour remédier à cela, les paramètres cinétiques de cristallisation ont été légèrement modifiés pour prendre en compte ce phénomène. De cette manière, une bonne corrélation entre la modélisation et les expériences a été établie (Fig. 0.7).

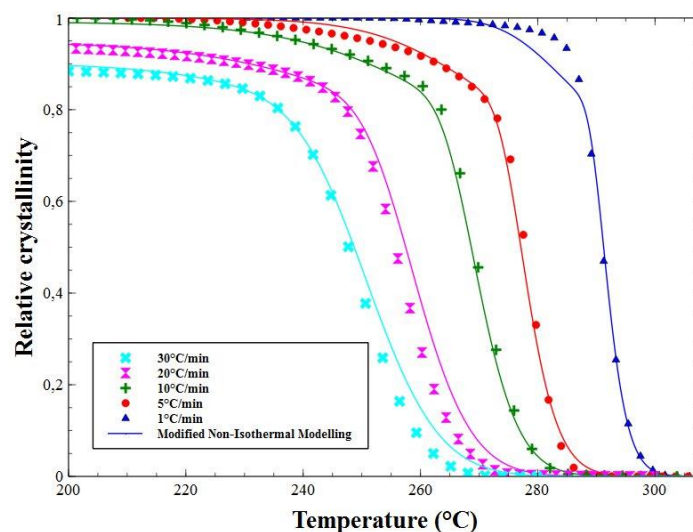
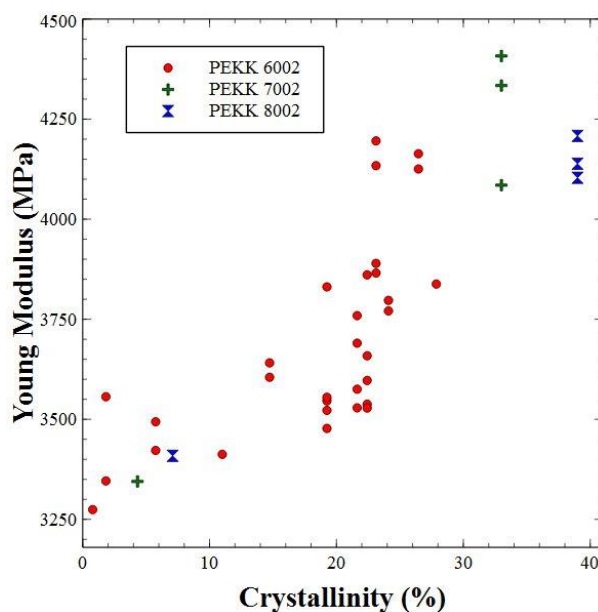


Fig. 0.7 : Evolution de la cristallinité relative en fonction de la température pour un PEKK 6002 cristallisé à partir de l'état fondu pour différentes vitesses de refroidissement avec le modèle cinétique anisotherme de cristallisation

Comme pressenti, il a été montré que le module d'Young et la contrainte au seuil de plasticité augmente avec la cristallinité alors que c'est l'inverse pour la déformation à la rupture (Fig. 0.8). Ce comportement est accentué pour des températures d'essai (180°C) au-dessus de la température de transition vitreuse puisque pour ces températures la phase amorphe est à l'état caoutchoutique et que les propriétés mécaniques du polymère dans ces conditions dépendent essentiellement de la phase cristalline.



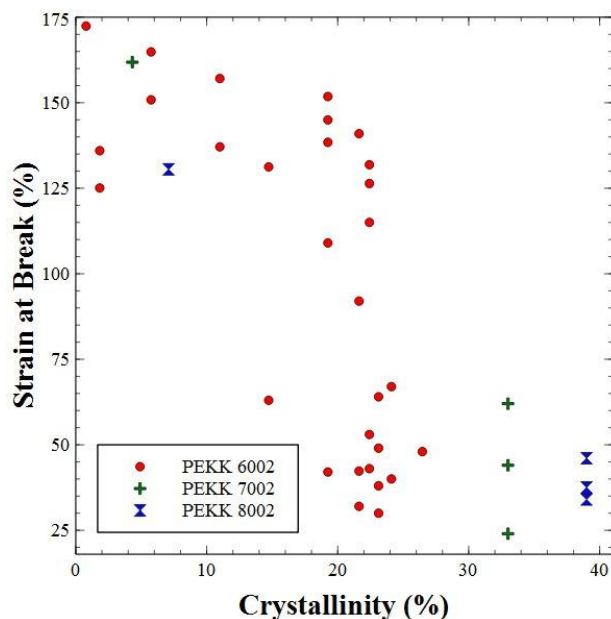


Fig. 0.8 : Evolution du module d'Young et de la contrainte à la rupture en fonction de la cristallinité du PEKK 6002 cristallisé à 230°C et testé à température ambiante

Enfin, il a été observé des modules d'Young et des contraintes au seuil de plasticité plus élevés pour des échantillons cristallisés à faible température (200°C) favorisant la formation de petites sphérolites ce qui a été attribué à une structure cristalline plus homogène comparé à des sphérolites plus grandes (Fig. 0.9).

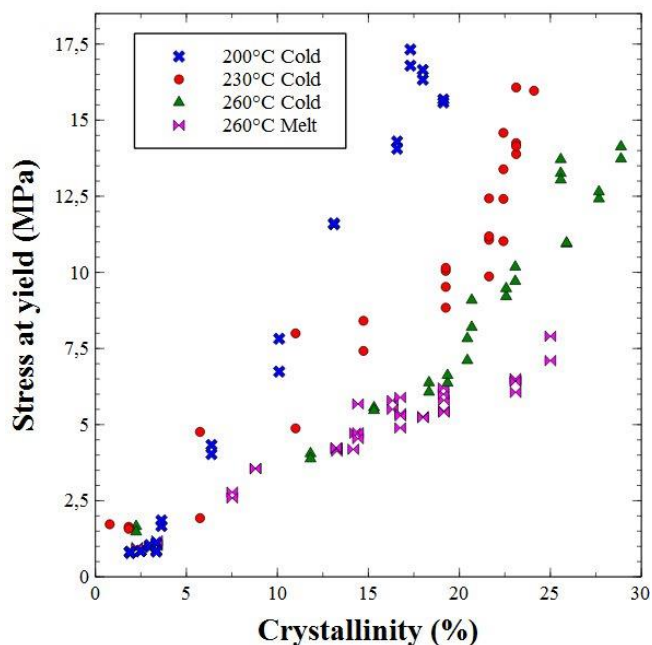


Fig. 0.9 : Comparaison de la contrainte de plasticité au seuil en fonction de la cristallinité à 180°C pour des échantillons PEKK 6002 cristallisés avec différentes conditions de cristallisation

IV. IMPACT DES PARAMETRES TEMPS/TEMPERATURE SUR LA FENETRE DE MISE EN OEUVRE

A partir d'essais ATG, rhéologiques, GPC et DSC sous air et sous azote, il a été montré que la matrice PEKK 6002 est modifiée au-dessus de 320°C associé à l'apparition de pertes de masses, d'une augmentation de la masse molaire moyenne en poids M_w et d'une augmentation de la température de transition vitreuse T_g . Tous ces phénomènes sont typiques de l'apparition de mécanismes de réticulation. De plus, à partir de l'approche de Saito et des résultats GPC, un mécanisme de coupures de chaîne ayant lieu en parallèle du mécanisme de réticulation a également été mis en évidence.

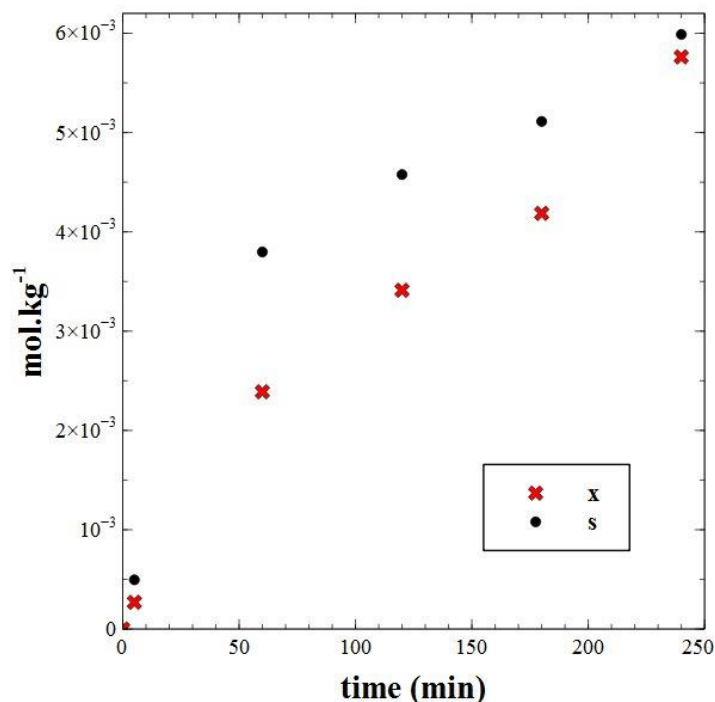


Fig. 0.10 : Evolution du nombre d'actes de réticulation (x) et de coupures de chaîne (s) en fonction du temps d'exposition à 400°C sous air pour le PEKK 6002

Il est apparu clairement que le mode de dégradation est essentiellement thermique et a principalement lieu car le mécanisme d'oxydation est seulement confiné à la surface (environ 10 nm de profondeur) en contact avec l'air pendant la mise en œuvre dû au fait que la cinétique d'oxydation est très rapide par rapport à la diffusion de l'oxygène. Des mesures rhéologiques réalisées sous azote pour différentes isothermes compris entre 320°C et 400°C ont permis, à travers les évolutions de viscosité, de suivre la cinétique de réticulation (Fig. 0.11). Il a été montré que ces mécanismes conduisant à la réticulation sont thermiquement activés et suivent une loi d'Arrhenius. A partir d'un schéma mécanistique conduisant à la réticulation du polymère, la cinétique de réticulation a été modélisée avec un modèle linéaire pour des faibles temps d'exposition ($t < 20$ min) (Fig. 0.11).

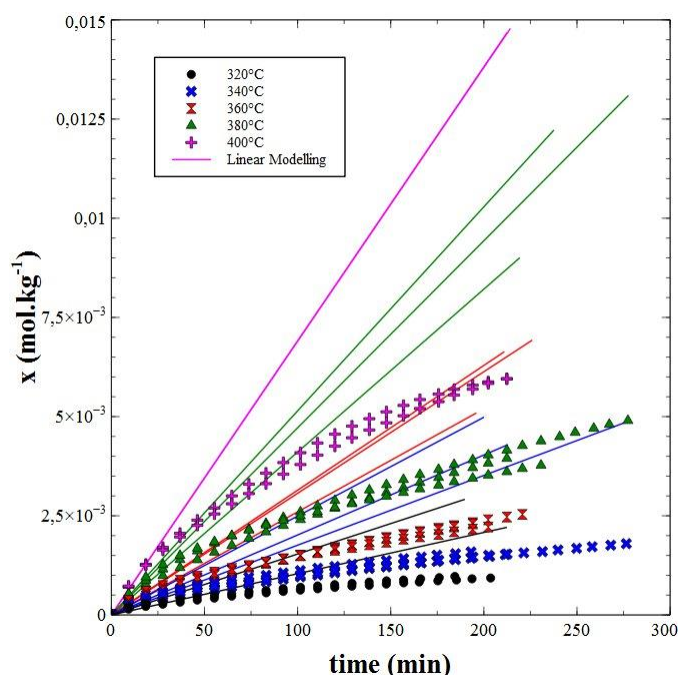


Fig. 0.11 : Nombre d'actes de réticulation x en fonction du temps d'exposition du PEKK 6002 pour différentes températures sous azote avec le modèle linéaire

Il a été montré que la réticulation qui a lieu à l'état fondu diminue le taux de cristallinité final et la cinétique de cristallisation, se traduisant par une diminution des paramètres cinétiques de cristallisation K_1 et K_2 . Il a également été observé du point de vue de la modélisation que le facteur de poids de la cristallisation primaire w_1 diminue avec la réticulation ce qui a été expliqué par une cristallisation moins parfaite dû à un branchement des chaînes macromoléculaires laissant plus de place pour la croissance de la cristallisation secondaire.

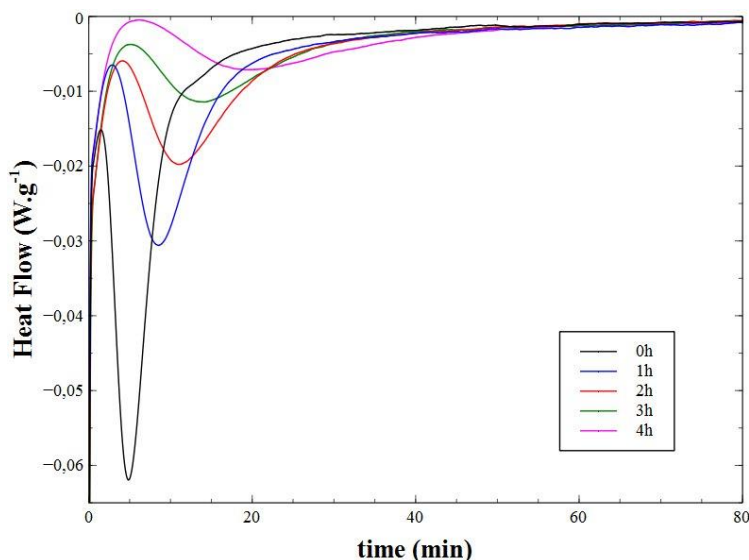


Fig. 0.12 : Thermogramme DSC du PEKK 6002 cristallisé à 230°C à partir de l'état fondu après différent temps d'exposition à 400°C sous azote

Enfin, il a été établi le fait que les propriétés mécaniques diminuent avec la réticulation (Fig. 0.13). Cette diminution des propriétés mécaniques est principalement due à la diminution du taux de cristallinité par la réticulation (Fig. 0.14). Ce résultat est cohérent avec les résultats du chapitre précédent qui a établi le lien entre la cristallinité et les propriétés mécaniques.

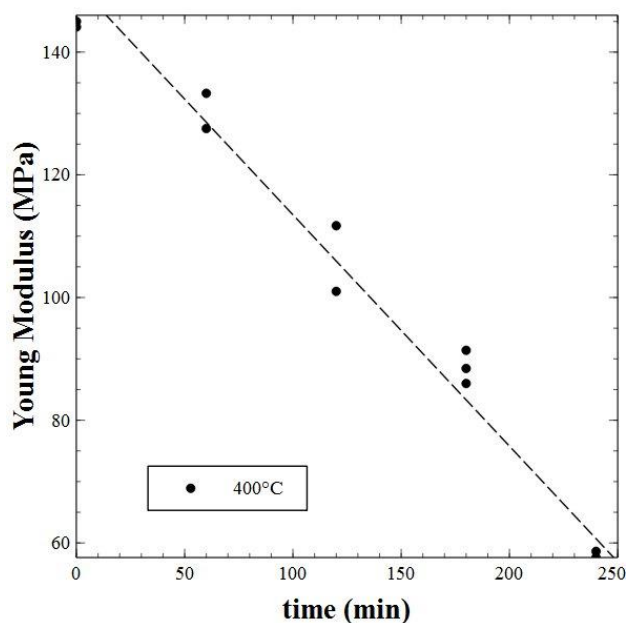


Fig. 0.13 : Evolution du module d'Young en fonction du temps d'exposition à 400°C sous air du PEKK 6002 cristallisé à 260°C à partir de l'état fondu et testé à 180°C

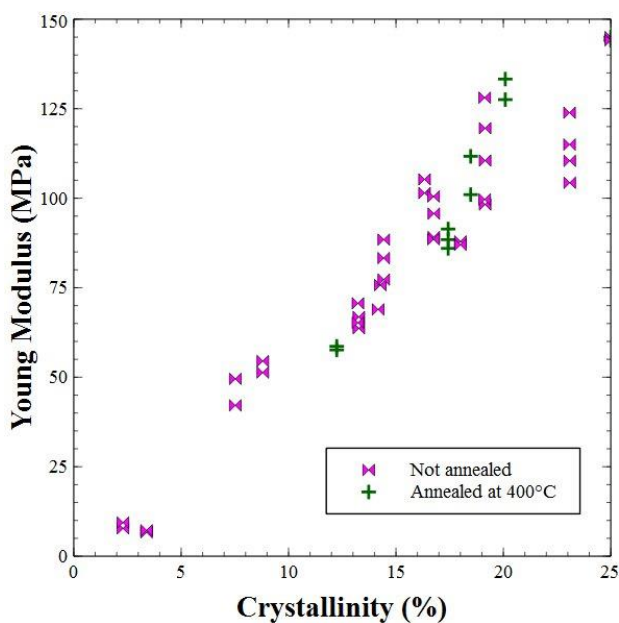


Fig. 0.14 : Evolution du module d'Young en fonction du taux de cristallinité pour le PEKK 6002 non exposé et exposé à 400°C sous air cristallisé à 260°C à partir de l'état fondu et testé à 180°C

V. APPLICATION AUX COMPOSITES STRUCTURAUX PEKK

Il a été montré que les fibres de carbone modifient les morphologies cristallines et les cinétiques de cristallisation des matrices PEKK. En effet, il a été observé par microscopie optique pour des températures de cristallisation élevées, une nouvelle phase cristalline en parallèle de la phase sphérolitique identifiée précédemment. Cette phase est appelée phase transcristalline et croît perpendiculairement à la surface des fibres de carbone. En effet, les fibres de carbone jouent le rôle d'agent nucléant à partir desquels les entités cristallines croissent. Comme les germes cristallins à la surface des fibres sont proches, les entités cristallines voisines se touchent lors de leur croissance ce qui les force à croître perpendiculairement aux fibres. Si ce phénomène est largement connu dans les polymères

semi-cristallins (PP...) en présence de fibres, on le reporte ici pour la première fois pour le PEKK.

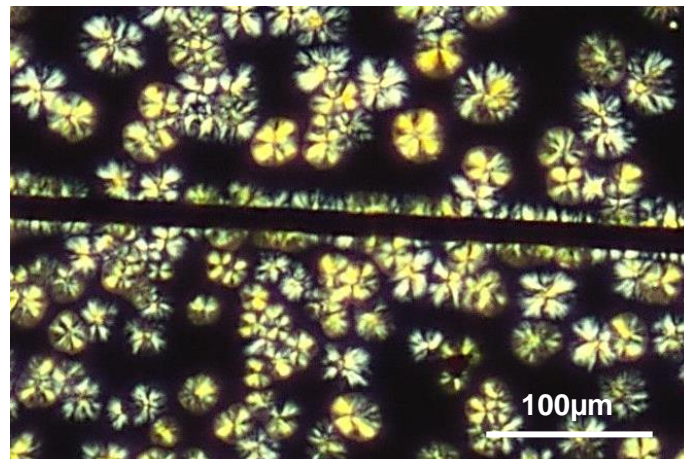
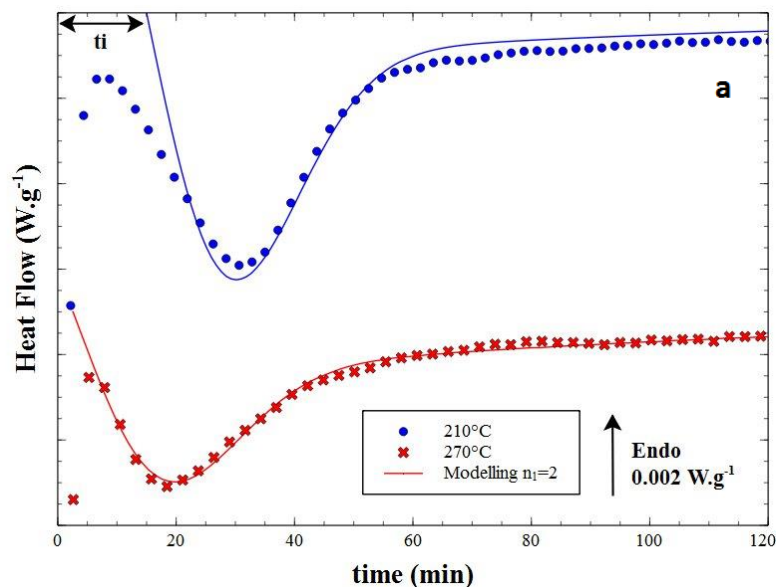


Fig. 0.15 : Micrographie d'un PEKK 6002 cristallisé à 270°C pendant 2h à partir de l'état fondu en présence de fibres de carbone

Il a été observé que si le modèle de cristallisation isotherme d'Hillier dérivé établi dans le CHAPITRE II décrit mieux les données expérimentales pour un exposant d'Avrami $n_1=3$ (croissance en 3D) pour des températures de cristallisation faibles, le modèle décrit mieux les données expérimentales avec un $n_1=2$ (croissance en 2D) pour des températures de cristallisation élevées (Fig. 0.16). En effet, vu que la surface des fibres de carbone et les germes dans le fondu sont en compétition pour la croissance cristalline, la croissance de larges sphérolites est facilitée pour des températures de cristallisation faibles puisque la cinétique de germination dans le fondu est élevée. Au contraire, pour des températures de cristallisation élevées, la cinétique de germination est faible diminuant le nombre de sphérolites formées et facilitant ainsi la croissance de zones transcristallines.



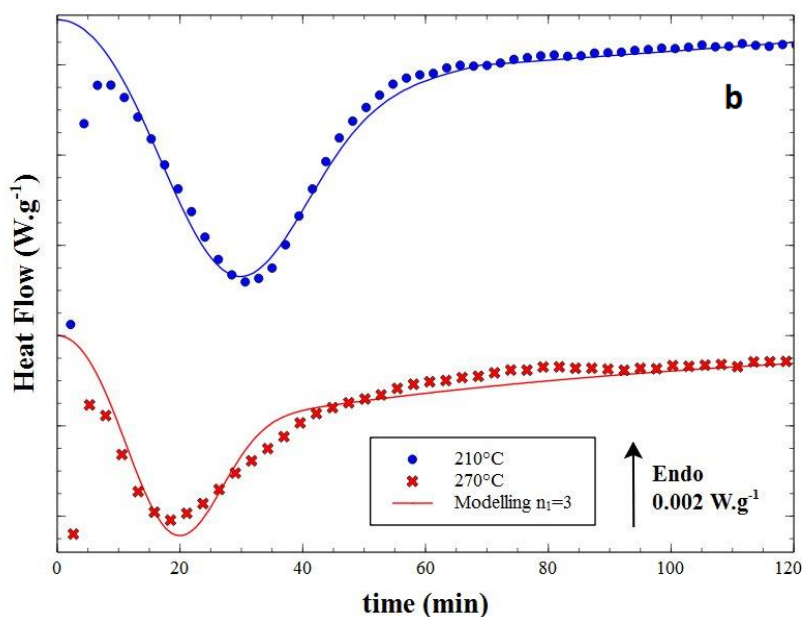


Fig. 0.16 : Thermogramme DSC d'un prepregs PEKK 6002 cristallisé à 210°C et 270°C à partir de l'état fondu avec le modèle d'Hillier dérivé pour un $n_1=2$ (a) et un $n_1=3$ (b)

Il a été enfin montré que la cinétique de cristallisation des matrices renforcées par des fibres de carbone est accélérée par rapport à la matrice seule ce qui est probablement dû à la formation des nouveaux germes à la surface des fibres de carbone qui amorcent plus tôt la cristallisation. Cependant, pour des températures de cristallisation faibles, l'inverse a été observé ce qui pourrait être expliqué par le fait que les fibres de carbone gênent la mobilité des chaînes macromoléculaires sachant qu'elle ne peuvent pas être considérées comme confinées par les fibres. Il a également été montré que le facteur de poids de la cristallisation primaire w_1 est plus faible pour le prepregs que pour la matrice seule ce qui peut être associé au fait que les entités cristallines sont sans doute moins parfaites augmentant ainsi la cristallisation secondaire.

Des plaques composites unidirectionnelles et orientés à $\pm 45^\circ$ ont été fabriquées sous presse et sous autoclave avec différents cycles thermiques pour obtenir des échantillons avec différents taux de cristallinité et morphologies cristallines. De la même manière que pour la matrice seule, il a été observé une chute du module d'Young et du module de cisaillement des composites PEKK pour des températures au-dessus de la température de transition vitreuse. Le module d'Young et de cisaillement augmente avec la cristallinité (Fig. 0.17) pour une condition de sollicitation donnée. Ce comportement est accentué pour des températures d'essai au-dessus de la température de transition vitreuse puisque pour ces températures la phase amorphe est à l'état caoutchoutique et les propriétés mécaniques du polymère ne dépendent que de la cristallinité.

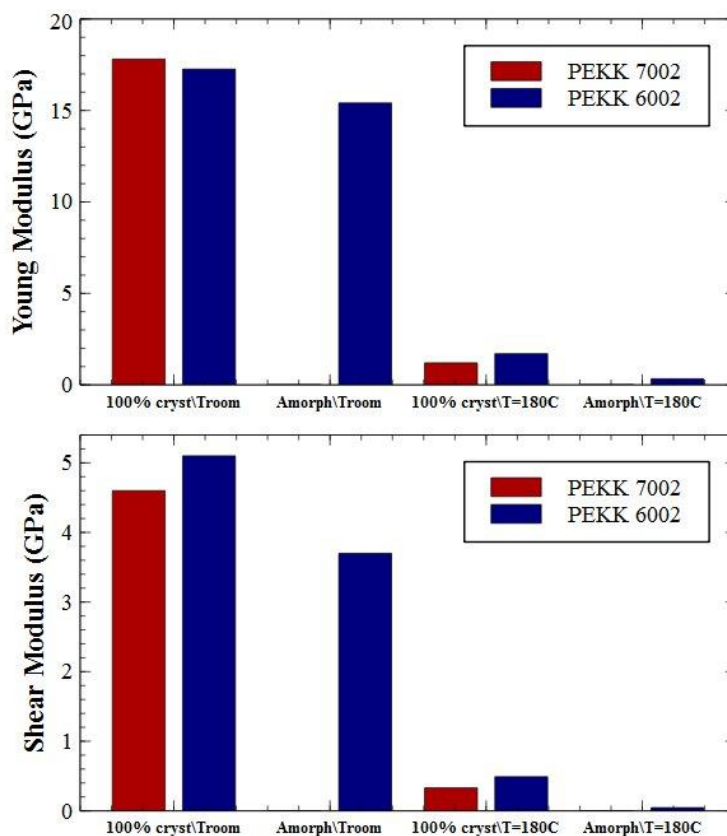


Fig. 0.17 : Evolution du module d'Young et de cisaillement de composites PEKK orientés à $\pm 45^\circ$ totalement cristallisés à 230°C à partir de l'état fondu et amorphes fabriqués sous presse, testés à température ambiante et à 180°C

Comme escompté, il a été observé que les propriétés mécaniques des composites orientés à $\pm 45^\circ$ sont plus sensibles aux propriétés de la matrice que celles des composites unidirectionnels. Les composites consolidés sous autoclave ont semblé avoir des propriétés mécaniques supérieures à ceux consolidés sous presse ce qui pourrait être associé au fait que les plateaux de la presse ne soient pas parfaitement parallèles ne permettant pas une pression uniforme à la surface du composite pendant la consolidation. Enfin, il a été montré que les composites cristallisés à hautes températures à partir de l'état fondu favorisant la croissance de la phase transcristalline semblent présenter des modules d'Young et de cisaillement plus élevés que les composites cristallisés à faibles températures à partir de l'état vitreux (Fig. 0.18). Ce phénomène a été associé à l'amélioration de l'efficacité du transfert des contraintes entre les fibres et la matrice grâce à la phase transcristalline.

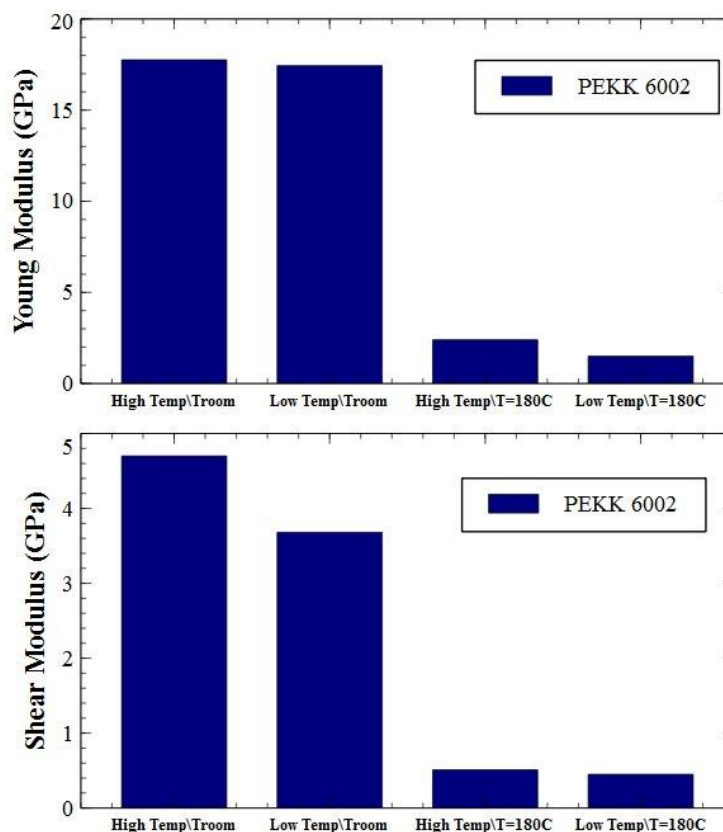


Fig. 0.18 : Evolution du module d'Young et de cisaillement de composites PEKK orientés à $\pm 45^\circ$ totalement cristallisés à 260°C à partir de l'état fondu sous autoclave et cristallisés à 200°C à partir de l'état vitreux sous presse, testés à température ambiante et à 180°C

VI. PERSPECTIVES

Dans le futur, du point de vue de la dégradation thermique à l'état fondu, il serait intéressant de modéliser les modifications macromoléculaires pour des temps d'exposition plus longs en résolvant le schéma cinétique du mécanisme de réticulation. Il a été montré que les coupures de chaînes qui sont à l'origine des mécanismes de réticulation peuvent avoir lieu au niveau des liaisons éthers ou carbonyles. Pour identifier où ces coupures de chaînes sont privilégiées, la même étude pourrait être faite sur du PEEK qui a un nombre différent d'entités éthers et cétones que le PEKK. Par ailleurs, l'impact du ratio entre les entités isophthaloydes et terephthaloydes sur les modifications macromoléculaires qui ont lieu aux hautes températures pourrait être étudiée en comparant la cinétique de dégradation des séries 8002, 7002 et 6002.

A partir des mesures DSC, il a été avancé l'apparition d'une cristallisation secondaire entre les lamelles cristallines lors des cristallisations isothermes. Il serait intéressant de confirmer la présence de cette phase cristalline supplémentaire et sa nature. De plus, à partir de la modélisation de la cristallisation, il a été montré que la proportion de cristallisation secondaire augmente avec la température de cristallisation. Des essais SAXS in-situ pourrait être mis en place pour identifier la cristallisation secondaire et sa cinétique d'apparition. De même, les essais WAXS ont montré une morphologie cristalline supplémentaire pour le PEKK favorisé pour les copolymères avec des taux d'entités isophthaloyles importants et pour des cristallisations froides. Des essais WAXS in-situ pourraient être également effectués pour identifier sa cinétique d'apparition. Enfin comme pour le taux de cristallinité, il

serait intéressant d'étudier l'impact de la cristallisation secondaire et de la deuxième morphologie cristalline sur les propriétés mécaniques.

Il a été supposé qu'en présence de fibres pour des températures de cristallisation élevées seule la phase transcristalline croît avec un exposant d'Avrami $n_1=2$ alors que pour des températures de cristallisation faibles, seule la phase sphérolitique croît avec un $n_1=3$. Ces hypothèses pourraient être confirmées par d'autres observations microscopiques. Pour des températures intermédiaires, ces deux mécanismes ont lieu en parallèle avec différentes cinétiques de cristallisation. Le modèle d'Hillier établi ne peut pas prendre en compte ces deux mécanismes qui ont lieu en même temps. Il serait donc intéressant de pouvoir établir un nouveau modèle capable de prendre en compte ces deux cristallisations distinctes. Une autre manière serait de pouvoir étudier des échantillons ne comportant que de la phase transcristalline pour différentes températures de cristallisation pour identifier ses cinétiques de cristallisation comme cela a été fait pour la résine seule.

Concernant les composites, seules des plaques composites totalement cristallisés ou amorphes ont été fabriquées. Des plaques composites avec différents taux de cristallinité pourraient être mises en œuvre pour étudier l'évolution des propriétés mécaniques avec le taux de cristallinité. De même, il serait intéressant de confirmer l'impact de la phase transcristalline sur les propriétés mécaniques.

Enfin, les modèles cinétiques de cristallisation établis dans cette étude pourraient être couplés avec l'équation de la chaleur et implémentés dans un code d'éléments finis pour simuler l'évolution de la cristallinité dans l'épaisseur d'une pièce composite PEKK pendant son cycle de mise en œuvre.

MECHANICAL PERFORMANCES OF PEKK THERMOPLASTIC COMPOSITES LINKED TO THEIR PROCESSING PARAMETERS

ABSTRACT

Poly(ether-ketone-ketone) (PEKK) high performance thermoplastics are currently studied with a great interest by the aeronautic industry as matrix for carbon fiber reinforced structural parts. In fact, PEKK composites can be consolidated out of autoclave and they have lower processing temperatures than PEEK composites.

The aim of the study was to investigate and predict the evolution of PEKK composite mechanical properties depending on the processing thermal cycle to determine the best processing parameters for PEKK composite part manufacturing regarding processing times and final mechanical performances.

A first part investigates the crystallization kinetics modelling of PEKK matrices and the influence of crystallinity and crystalline morphologies on PEKK matrix mechanical properties. A second part focuses on the macromolecular modifications of PEKK matrices at high processing temperatures under air and nitrogen and their impact on PEKK matrices crystallization and mechanical properties. A last part presents the influence of carbon fibers on crystalline morphologies and crystallization kinetics, the manufacturing of unidirectional and $\pm 45^\circ$ PEKK composites under press and autoclave and finally the impact of crystallinity and crystalline morphologies on PEKK composite mechanical properties.

Key words: Thermoplastics, Composites, PEKK, Crystallization, Crosslinking, Modelling

PERFORMANCES MÉCANIQUES DE COMPOSITES THERMOPLASTIQUES PEKK EN RELATION AVEC LEURS PARAMÈTRES DE MISE EN ŒUVRE

RÉSUMÉ

Les thermoplastiques hautes performances poly(éther-cétone-cétone) (PEKK) sont actuellement étudiés avec un grand intérêt dans l'industrie aéronautique comme matrice pour la fabrication de pièces de structure composites renforcées par des fibres de carbone. En effet, les composites thermoplastiques PEKK ont l'avantage d'être consolidables hors autoclave et ont des températures de mise en œuvre plus faibles que les composites PEEK. L'objectif de cette étude est de comprendre et prédire l'évolution des propriétés mécaniques des composites PEKK suivant le cycle thermique de mise en œuvre pour déterminer les paramètres de mise en œuvre optimaux pour la fabrication des pièces composites PEKK concernant les temps de mise en œuvre et les performances mécaniques finales.

Une première partie traite de la modélisation des cinétiques de cristallisation des matrices PEKK ainsi que l'influence de la cristallinité et des morphologies cristallines sur les propriétés mécaniques des matrices PEKK. Une deuxième partie se concentre sur les modifications macromoléculaires des matrices PEKK pour des hautes températures de mise en œuvre sous air et sous azote et leurs impacts sur la cristallisation et les performances mécaniques des matrices PEKK. Enfin une dernière partie présente l'influence des fibres de carbone sur les morphologies cristallines et les cinétiques de cristallisation, la fabrication de composites PEKK unidirectionnels et orientés à $\pm 45^\circ$ sous presse et sous autoclave et enfin l'impact de la cristallinité et des morphologies cristallines sur les performances mécaniques finales des composites PEKK.

Mots clés : Thermoplastiques, Composites, PEKK, Cristallisation, Réticulation, Modélisation